National Technical University of Athens
School of Naval Architecture and Marine Engineering
Shipbuilding Technology Laboratory

Diploma Thesis

Static Torsional Tests of Composite Driveshafts

Dimitrios Vavatsikos

Thesis Supervisor: Professor N. Tsouvalis

June 2020

National Technical University of Athens
School of Naval Architecture and Marine Engineering
Shipbuilding Technology Laboratory

Diploma Thesis

Static Torsional Tests of Composite Driveshafts

Dimitrios Vavatsikos

Thesis Supervisor: Professor N. Tsouvalis

Committee member: Assist. Professor K. Anyfantis

Committee member: Assist. Professor G. Papalambrou

June 2020

Thank you mother for your persistence

Thank you father for your morality

Thank you both for teaching me decency

Acknowledgements

The work for the present thesis was carried out at the Shipbuilding Technology Laboratory of the School of Naval Architecture and Marine Engineering of the National Technical University of Athens under the supervision of Professor N. Tsouvalis.

First of all, I want to express my gratitude to my supervisor Professor Nicholas Tsouvalis for his trust in assigning me the specific issue. His scientific guidance, his suggestions, his perseverance and his undiminished interest, contributed in carrying out the present thesis.

Also, I would like to thank Assistant Professors K. Anyfantis and G. Papalambrou for being members of the supervision committee.

Furthermore, I want to thank Elias Bilalis, PhD student at the Shipbuilding Technology Laboratory, for his enlightening comments and his invaluable help in carrying out the experiments.

At this point, I want to thank B&T Composites and Mr. Kosmas Tiriakidis for providing valuable technical and experimental information, as well as their facilities for the conduction of the experiments.

Last but not least, I want to thank my family for supporting me throughout my university studies. Without them I would never accomplish my goals as a student in the School of Naval Architecture and Marine Engineering. I want to specially thank my grandfathers who both passed away just before the end of the present thesis.

Abstract

The power transmission is one of the most important issues in the field of engineering. The power transmission shaft, called driveshaft, is the main component that transmits torque from the engine of a ship to the propeller and it has been a subject of study in marine engineering for years.

While the driveshafts are mainly made of metal (steel), in recent years, due to the gradual introduction of composites in shipbuilding, the composite materials and mainly carbon fiber, are gaining more and more interest in driveshaft manufacturing.

An important area of study in the domain of composite shafts is their resistance in torsion. Determining a driveshaft's resistance in torsion is one of the subjects covered in the present thesis.

The main purpose, therefore, is the study of the type testing of a power transmission shaft, according to the existing standards and regulations of the class registers. After the analysis of these standards, the research focuses on the study of two existing torsion test devices.

The first torsion test machine is located in the Strength of Materials of Materials Laboratory of the School of Applied Mathematics and Physical Sciences of NTUA. After listing every individual component of the machine and its main dimensions, it was investigated whether it is possible to perform an experiment that complies to the specifications set by DNV-GL register.

The second torsion test machine is located at the B&T Composites facility in Florina, Greece. At this machine, experiments were performed on three driveshafts made of Carbon Fiber Reinforced Polymer (CFRP). A part of the experiment preparation took place in Shipbuilding Technology Laboratory of the School of Marine Architecture and Marine Engineering, where the recording systems (Spider) were adjusted and the torque and angle measuring devices were calibrated. The next phase of preparation took place at the B&T Composites facility where Strain Gage sensors were glued on the shafts in order to record the deformations. The results of the experiments were very interesting. The shafts failed in the area where the composite and the flange are connected, while the deformations recorded show that the shaft operated in the elastic area. By using the recorded data, an attempt was made to predict the form of torsional buckling that would occur on the shafts. Finally, the various problems of the process were presented. Some solutions were suggested in order to improve the torsion test machine. The objective of these suggestions was the conduction of a smoother experimental process in the future.

Περίληψη

Το ζήτημα της μετάδοσης της ισχύος που παράγει μια μηχανή, αποτελεί ένα από τους σημαντικότερους τομείς στον κλάδο της μηχανολογίας. Ο άξονας μετάδοσης ισχύος αποτελεί το βασικό εξάρτημα που μεταδίδει τη ροπή από τη μηχανή ενός πλοίου στην προπέλα και είναι αντικείμενο μελέτης της ναυπηγικής εδώ και χρόνια.

Ενώ οι εν λόγω άξονες, κατασκευάζονται κατά κύριο λόγο από μέταλλο (χάλυβα), τα τελευταία χρόνια και λόγω της σταδιακής εισχώρησης των σύνθετων υλικών στη ναυπηγική, η κατασκευή τους από σύνθετα υλικά και κυρίως από ίνες άνθρακα, συγκεντρώνει ολοένα και περισσότερο ενδιαφέρον.

Σημαντικό πεδίο μελέτης στο κομμάτι των αξόνων από σύνθετα υλικά αποτελεί η αντοχή τους σε στρέψη. Η διαπίστωση της αντοχής τους σε στρέψη, είναι ένα από τα αντικείμενα τα οποία πραγματεύεται η παρούσα διατριβή.

Βασικό σκοπό κατ' επέκταση αποτελεί η μελέτη της τυποποιημένης δοκιμής σε στρέψη (type testing) των αξόνων μετάδοσης ισχύος, σύμφωνα με τους υπάρχοντες κανονισμούς των νηογνωμόνων. Αφού συγκεντρώθηκαν και αναλύθηκαν, η έρευνα εν συνεχεία επικεντρώθηκε στη μελέτη δύο υφιστάμενων πειραματικών διατάξεων επιβολής στρέψης.

Η μία διάταξη είναι μια μηχανή στρέψης η οποία βρίσκεται στο Εργαστήριο Αντοχής Υλικών της Σχολής Εφαρμοσμένων Μαθηματικών και Φυσικών Επιστημών. Αφού καταγράφηκαν τα επιμέρους στοιχεία της μηχανής και οι απαραίτητες διαστάσεις της, έγινε διερεύνηση για το αν είναι δυνατή η εκτέλεση πειράματος σύμφωνα με τις προδιαγραφές που ορίζει ο νηογνώμονας DNV-GL πάνω στις δοκιμές αντοχής σύνθετων αξόνων μετάδοσης ισχύος.

Το επόμενο μέρος ασχολήθηκε με τη μηχανή στρέψης που βρίσκεται στις εγκαταστάσεις της εταιρίας B&T Composites στη Φλώρινα. Στη συγκεκριμένη μηχανή εκτελέστηκαν πειράματα πάνω σε τρεις άξονες κατασκευασμένους από σύνθετο υλικό, ενισχυμένο με ίνες άνθρακα (CFRP). Η προετοιμασία των πειραμάτων ξεκίνησε από το Εργαστήριο Ναυπηγικής Τεχνολογίας της Σχολής Ναυπηγών Μηχανολόγων Μηχανικών όπου και έγινε προετοιμασία των καταγραφικών συστημάτων (Spider) και ρύθμιση των συσκευών μέτρησης της ροπής και της γωνίας στρέψης. Η συνέχεια έγινε στις εγκαταστάσεις της B&T Composites όπου αισθητήρες Strain Gage κολλήθηκαν πάνω στους άξονες για την καταγραφή των παραμορφώσεών τους. Τα αποτελέσματα των πειραμάτων ήταν πολύ ενδιαφέροντα. Η κατάρρευση των αξόνων συνέβη στην περιοχή της σύνδεσης μεταξύ σύνθετου υλικού και φλάντζας, ενώ οι παραμορφώσεις που καταγράφηκαν δείχνουν ότι οι άξονες λειτούργησαν στην ελαστική περιοχή. Πάνω στα συγκεκριμένα δεδομένα έγινε μια προσπάθεια πρόβλεψης της μορφής του στρεπτικού λυγισμού που θα συνέβαινε στους άξονες. Τέλος, τα διάφορα προβλήματα της διαδικασίας καταγράφηκαν και προτάθηκαν λύσεις για τη βελτίωση της πειραματικής διάταξης, με σκοπό την ομαλότερη διεξαγωγή πειραμάτων στο μέλλον.

Contents

CHAPTER 1

STATE OF THE ART OF COMPOSITE SHAFTS AND RELATED REGULATIONS

1.1 Introduction

A material that consists of two or even more components or phases is considered a composite material. Nowadays, composites are considered those materials, whose, each component has significantly different mechanical and physical properties from the others, so that the composite material itself has significantly different properties than those of its components (Tsouvalis, 1998).

Composite materials are widely used in marine and automotive industries, aerospace, aircrafts, buildings and sport equipment for many years. The technological progress and the considerable cost reduction of the raw materials and fabrication proecesses, contributed to the use of composites on a larger scale in marine industry. According to a market report on the website marketsandmarkets.com, the total value of the marine composite market was 3,637.2 million USD in 2017 while it is estimated that it will reach the amount of 5,037.5 million USD by 2023 at a compound annual growth rate (CAGR) of 5.6%. The use of composites provides a big variety of benefits:

- Reduction of the weight of a structure compared with the metal structure which leads to other benefits such as better fuel efficiency, operating costs and reduced gas emissions.
- Greater design freedom.
- Lower maintenance cost.

On the other hand, there are some disadvantages to consider:

- More expensive materials due to the cost of glass and carbon fibres, foam cores and resins.
- Very poor recyclability.

A major application that the composites are used, is the shafting systems in ship propulsion systems and vehicles. Carbon Fibre shafts, in combination with couplings, as demonstrated in Figure 1.1, were first introduced in fast ferries (Jaure, 2017). They are now making inroads on other types of vessels such as dredgers, supply vessels, commercial and cruise ships. A driveshaft is the component that transmits torque and rotation from the main engine to the propeller of a ship. It may consist of more than one sections. Usually, they are made of high strength steel. In automotive and marine driveshafts, the composites, such as carbon fibers with suitable resins, are preferable due to benefits that are described later on. A main drawback of steel shafts, except of the higher specific weight compared to the composite shafts, is the length limitation. In automotive industry a vehicle shaft over the length of 1500 mm must be constituted by two pieces of metal shafts in order to increase the fundamental bending natural frequency of the shaft. The bending moment is inversely proportional to the

square of beam length and proportional to the square root of specific modulus, demanding more universal joints (three) and a cross centre bearing and bracket, thus increasing the total weight and complexity of the shafting system (Nadeem et al, 2016). This problem can be solved by using composite materials enabling the replacement by a single piece shaft due to the high specific elastic modulus and higher specific strength and stiffness of the composites.

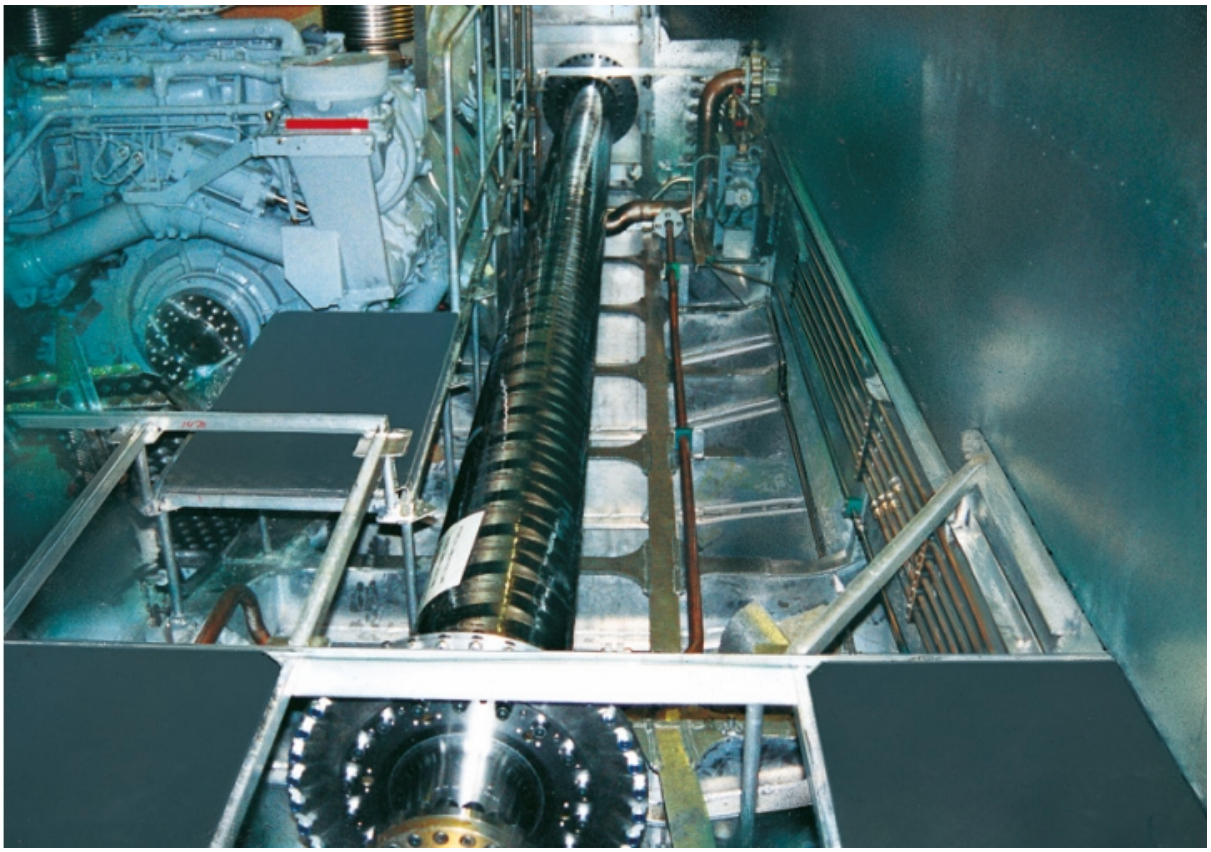

Figure 1.1: CFRP driveshaft on ship (Centa)

Carbon fibres are mainly used in marine composite shafts due to their numerous advantages (Jaure, 2017):

- High specific elastic modulus and strength.
- Weight reduction: depending on the configuration, the metal shafting system is almost 50-70% heavier than the same composite configuration
- Less vibration and noise due to high damping capacity
- Good corrosion resistance, no wear, non-magnetic, no maintenance is required and service life is longer.
- Greater torque capacity than metal drive shafts.
- Longer fatigue life than metal shafts.
- Temperature stability which results in no misalignment in longer shafts.
- Longer distance between bearings which results in less bearings and simpler layouts.
- Greatly enhanced safety. Composites absorb energy upon impact (Leslie et al, 1996).

There are many parameters on which the characteristics of a composite drive shaft depend. Such parameters are the main dimensions. These are the diameter and the length of the shaft,

which determine the critical speed of the shaft line. In order to increase the critical speed, which is one of the main objectives when designing a driveshaft, the diameter must be as large as possible while the length as short as possible (Prasad et al, 2016). Another designing issue is whether the shaft will be solid or hollow. The hollow design is preferable due to better stress distribution. In solid shafts the material in the centre is not fully utilised because the stress in that point is zero (Nadeem et al, 2016). One more factor that must be considered is the angle of orientation of the fibres while another is the stacking sequence. Regarding the angle with respect to the longitudinal axis, 0° offers maximum bending stiffness leading to maximum bending moment, ±45° offers maximum shear strength, while 90° offers the greatest buckling strength (Ghatage et al, 2012).

A composite driveshaft can be manufactured by using several techniques. The most frequent is filament winding. The main disadvantage of this technique is the low interlaminar strength which leads to easier delamination between the plies of the composite. Another way to build a driveshaft is braiding. Braided shafts overcome these drawbacks and combine good impact and fatigue resistance (Hao et al, 2020). In figure 1.2 a schematic view of a 3-D braided shaft section is demonstrated. These processes are described in the following chapters.

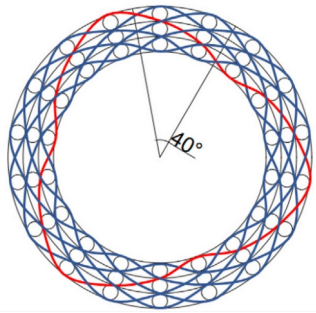

Figure 1.2: 3-D circular knitted yarn layout

1.2 Filament winding process

The most common process to produce hollow tubular-cylindrical composite shafts is the filament winding. Most shapes generated through this process are surfaces of revolution, such as pipes, cylinders and spheres. Filament winding is the process in which resin impregnated fibers are wound over a rotating mandrel at a desirable angle. Continuous reinforcements, such as rovings, are wound onto the mandrel until the surface is covered and the required thickness is achieved. The process uses raw materials, fiber and resin, in a fairly automated process with low labour, thus contributing to a low production cost. The preprogrammed rotation of the mandrel and horizontal movement of the delivery eye produce the helical pattern, which is the simplest mode of operation of a helical winding machine.

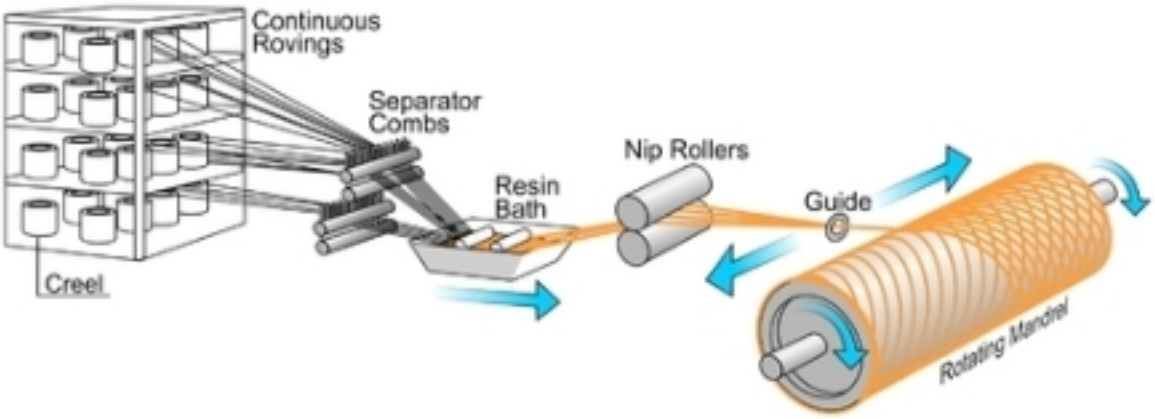

Figure 1.3: Schematic view of filament winding process

There are two types of winding machines: helical and polar. The helical process is the one of the most interest in the case of composite shafts as soon as polar winders are used to produce spherical vessels or cylindrical vessels with length/diameter ratio less than 2.0. In helical machines the mandrel rotates continuously while the delivery eye (the Guide in Figure 1.3) moves back and forth. The rotational speed of the mandrel and the linear speed of the delivery eye can be adjusted to produce any fiber orientation between 5 and 90 degrees, the latter called hoop winding. Several back-and-forth travels of the carriage are needed to complete a lamina covering the mandrel. Such a lamina is always a two-ply balanced laminate at $\pm\theta$. The fibre reinforcements are delivered from creels and tape racks, and through a tensioning device or brake (Separator Combs in Figure 1.3) that can be adjusted to control the tension in the reinforcement. Next, the reinforcement goes through a resin bath where it picks up resin. Next goes through the nip rollers in order to remove the excess resin from the fibers. Then, the wet reinforcement is delivered through the delivery eye that is mounted on a carriage. In addition to the spindle rotation, the carriage and delivery eye can move in a number of ways designed to place the reinforcement along complicated contours (Barbero, 2010).

1.3 Braiding processes

1.3.1 The 2-D braiding

The 2-D braiding technique, which is demonstrated in Figure 1.4, is based on the counter rotation of two yarn carriers around a circular frame. The yarn movement is achieved by the use of “horn gears”. By this way the yarn is transferred from the one gear to the next. The produced geometry is highly compact in a tubular form.

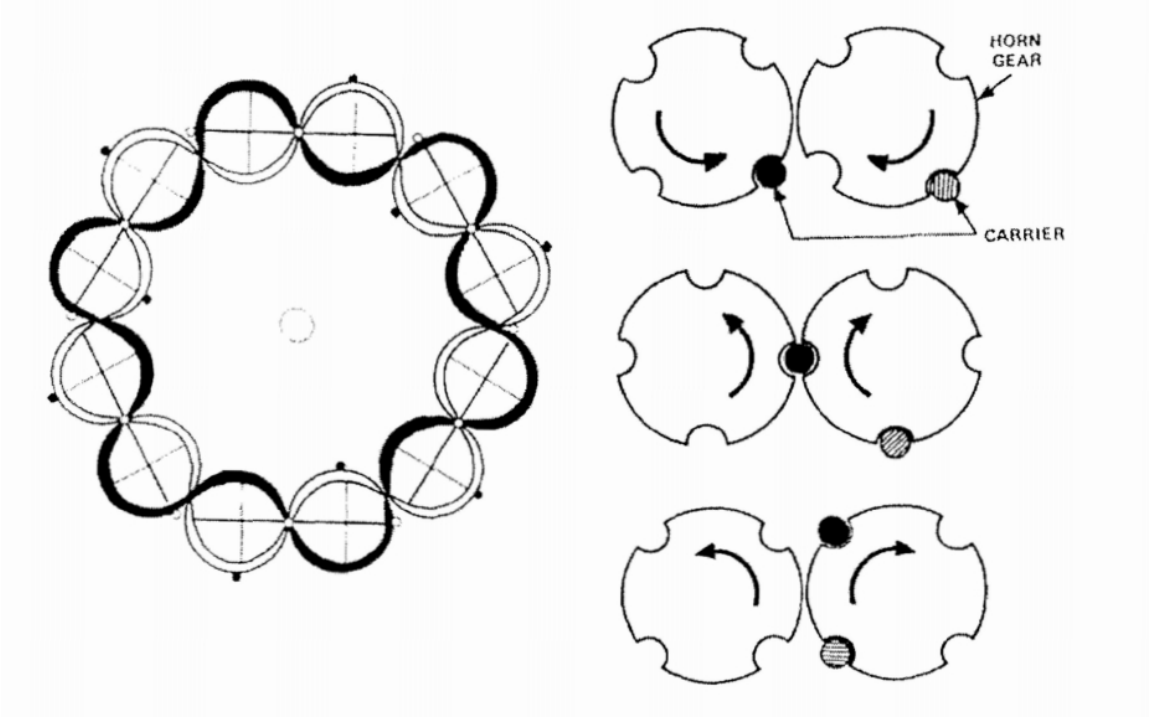

Figure 1.4: The rotation of the “horn gears”.

A 2-D braided tubular geometry is shown in Figure 1.5. The number of braiding yarns, the length of the yarns and the braiding angle are some of the factors affecting the braiding architecture, the final form of the produced component and the production rate. However, the technique is suitable for narrow width geometries and tubular objects. A typical braiding machine consists of 144 yarn carriers, while, larger machines may consist of approximately 800 carriers.

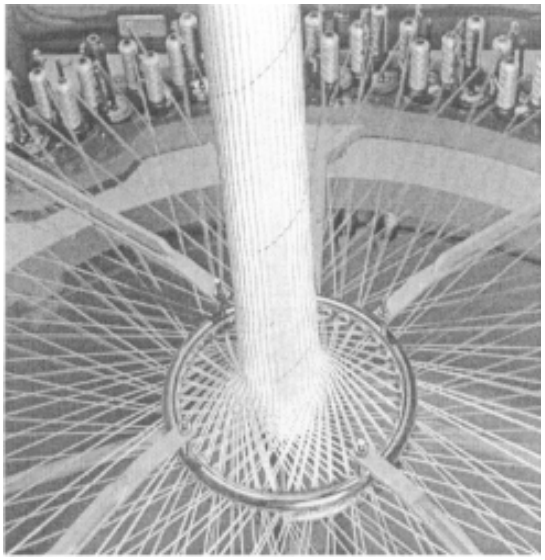

Figure 1.5: Standard braided tubular fabric

More complex fabric architectures may be accomplished, by using mandrels during the process as shown in Figure 1.6. In this way, multi sectional components can be made, i.e. objects with different shaped sections along their length. Preforms with attachment points and holes can also be braided. In this way, the final object's mechanical properties are improved, due to the fact that no breaking can occur on the fibers beacause the composite piercing is avoided. Unlike other weaving techniques, angles like ± 45 deg and 0 deg are possible for the fiber orientation, while, 90 deg orientation is not possible with the standard braiding process.

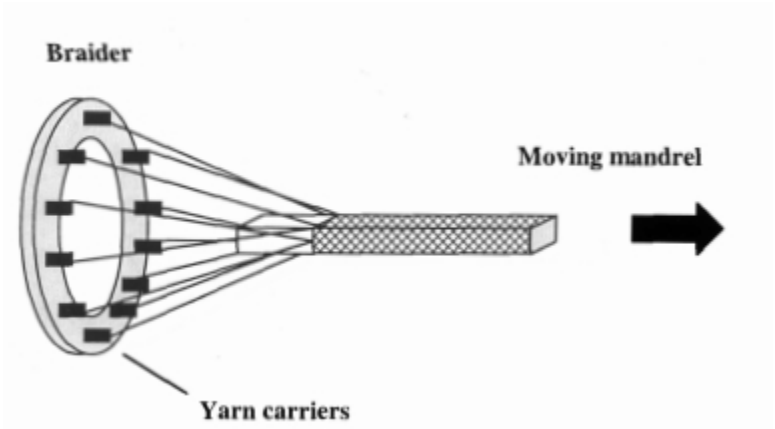

Figure 1.6: Schematic view of braiding over a moving mandrel

A basic problem of this process is the difficulty in achieving thick-walled architectures. This can be accomplished by repeatedly braiding over the mandrel, but, components made by this method lack in through-the-thickness reinforcement (Tong et al, 2002).

1.3.2 The 3-D braiding

The 4-step braiding process (or row-and-column) uses a flat-bed which consists of rows and columns. The role of these rows and columns is to direct the yarns in order to create the preform's geometry. The moving sequence consists of 4 different steps as shown in figure 1.7. The purpose of the moving sequence is to interlock the yarns by mechanically forcing them into the structure just like the reed in weaving. The row and column movement can be changed, depending on the desired mechanical characteristics and the preform geometry.

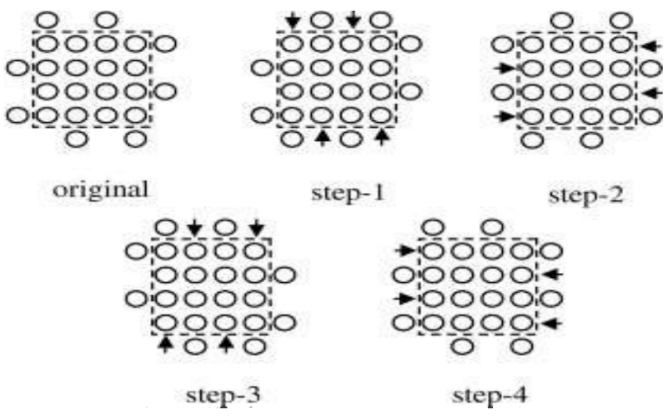

Figure 1.7: The 4-step moving sequence

A 4-step braiding technique is the through-the-thickness braiding, which uses a cylindrical equipment configuration. As shown in Figure 1.8, the equipment consists of a number of identical rings, placed side by side in an axial arrangement. On the rings there are troughs that guide the yarns from the one ring to the next in the axial direction. At the same time the yarns are circumferentially twisted due to the rotation of the rings, accomplishing in this way, the braiding architecture.

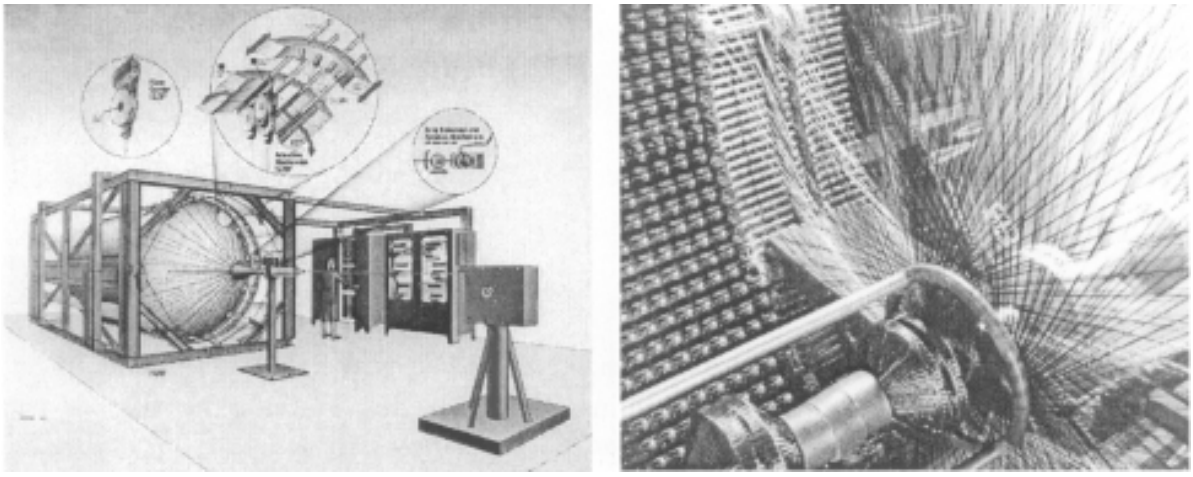

Figure 1.8: ”Through-the-Thickness” equipment developed at Atlantic Research Corporation (courtesy of Atlantic Research Corporation)

The through-the-thickness equipment configuration is more space efficient than the flat-bed configuration. Both configurations can be expanded by adding more rings or tiles of rows and columns (Tong et al, 2002).

There is another process of 3-D bed-braiding called 2-step. In this process a big number of yarns is fixed on the axial direction, while, some yarns are fixed on braiding carriers. The axials shape the desired geometry of the preform, while, the braiding carriers are distributed around the perimeter of the axial array. The process is shown in figure 1.9.

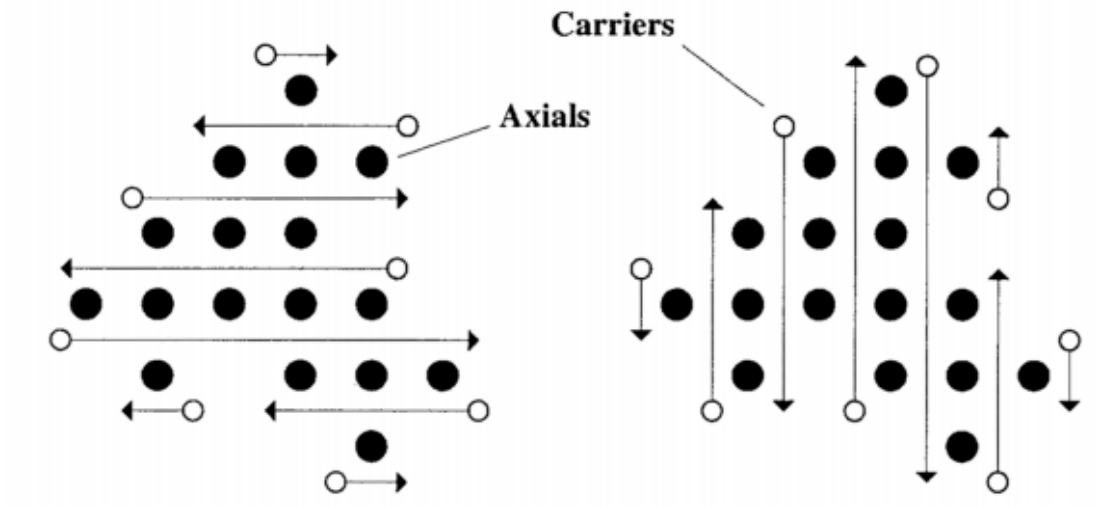

Figure 1.9: Schematic view of the 2-step process

There are two steps in which the braiding carriers move completely through the structure between the axials. In this way, any geometry can be accomplished even circular and hollow-circular. The 2-step process does not require mechanical tightening as the 4-step, due to the fact that the braid can be pulled tight by yarn tension (Tong et al, 2002).

1.4 Couplings and end fittings

Usually, the composite drive shaft is connected to the propeller system by a configuration of a flexible coupling system in order to deal with possible misalignments during the installation, as shown in Figure 1.10. For that purpose, in each end of the composite shaft a metallic flange (end fitting) is put, in order to be bolted to the power transmission system of the ship. The geometry of the end fitting depends on the mechanical properties needed for the application and the couplings which are used.

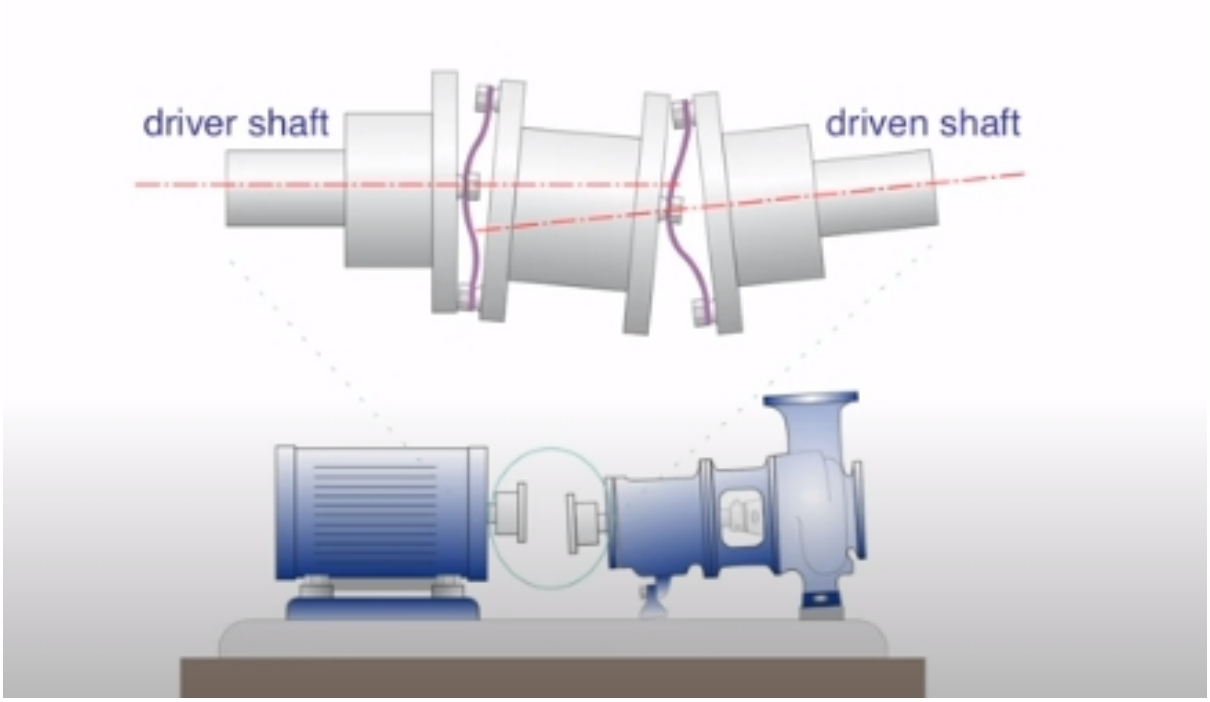

Figure 1.10: Schematic view of a coupling

For hollow tubular shafts the standardization of the end fittings is not common. After all, there is a big number of different coupling structures each requiring a different structure of end fitting. A good example is the coupling configuration of “Roba ds”, shown in Figure 1.11, and the geometry of the flange used. A flange compatible with this coupling was put on two of the shafts that were tested in the torsion experiments carried out, in chapter 3 of the present thesis.

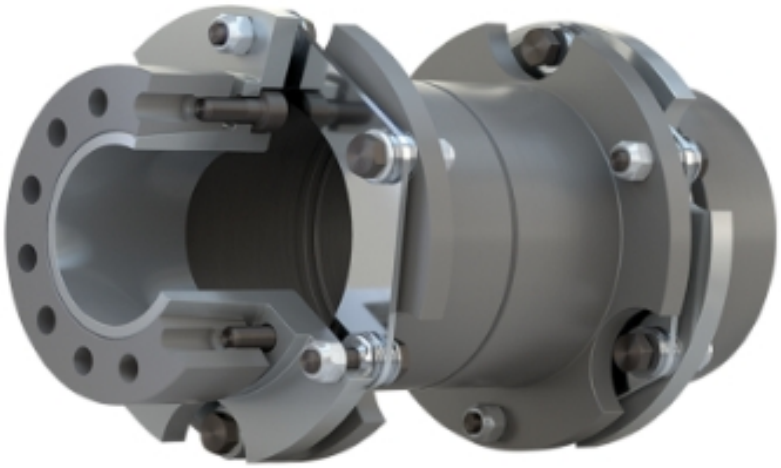

Figure 1.11: “Roba ds” coupling

The coupling can be made of metal or composite material. The manufacturers that make composite shafts offer a vast list of different type of flexible couplings and coupling disks made of metal or composite.

There are occasions that the flange is integral with the shaft and is made of composite (see Geislinger in section 1.5). In the majority of the applications, the end fitting is metallic. The join between the metallic flange and the composite shaft is usually done with the use of adhesives. Also, there are many occasions where the connection is additionally supported with bolts as it is shown in figure 1.12.

Figure 1.12: End fitting flange with bolts

After a search on class regulations the common requirements have to do with the thickness of the flange and are stated on the sequence.

DNV-GL- Part 4 Systems and components, Chapter 4 Rotating machinery – Power transmission

$$t = \frac{d}{4\left(1+2\frac{r}{d}\right)^2} \tag{1.1}$$

where

d = the required plain, solid shaft diameter (the parameter d is referred to as the required shaft diameter for a plain shaft without inner bore, meaning the necessary diameter for fulfilling whichever shaft dimensioning criteria are used).

r = flange fillet radius.

For multi-radii fillets the flange thickness shall not be less than 0.2 d.

In addition, the following requirement applies:

- recesses for bolt holes shall not interfere with the flange fillet, except where the flanges are reinforced correspondingly
- for flanges with shear bolts or shear pins:

$$t \geqslant \frac{1}{2} \cdot d_b \cdot \left(\frac{\sigma_{y,bolt}}{\sigma_{y,flange}}\right) \tag{1.2}$$

where:

d_b = diameter of shear bolt or pin

$\sigma_{y,bolt}$ = yield strength of shear bolt or pin

$\sigma_{y,flange}$ = yield strength of flange.

1.5 Manufacturers

There are many manufacturers that shape the state of the art in the field of composite shafting systems. After a thorough research on the internet many were found and they are presented afterwards:

Geislinger GmbH

Geislinger develops and produces torsional vibration dampers, torsional elastic, high-damping couplings, misalignment couplings, and torsional vibration monitoring systems for large engines and wind turbines. The company has developed the Gesilco shaft lines based on a 25-year experience in the domain of driveshafts. A Gesilco shaft is demonstrated in Figure 1.13. It is produced by the filament winding technique by using carbon fibres and epoxy

resin. The one-piece shaft with the fibre flange connection integrated on the main body of the shaft offers almost 50% weight reduction. The shaft can be adjusted for the application needed, depending on the power transmission, length, bending and torsional stiffness, by changing the angle of fibre orientation. The in-house manufacturing procedure reserves high quality products. The shaft can be supplied with a special fire resistant outer layer in combination with a sprinkler system mounted above the shaftline. SOLAS fire resistance requirements can be met without the need of an additional housing.

Figure 1.13: The one-piece Geisilco Shaft line

Standardized technical data:

- Torque range: 1 kNm – 700 kNm
- Ambient temperature: -45 ºC to 100 ºC
- Diameters: 80 mm – 1200 mm
- Length up to 12 m

DYNEXA

DYNEXA is specialized in the design and manufacture of tubes and profiles made of high-quality fiber-reinforced composites. Since mid-1990 the company has been manufacturing carbon fibre shafts installed in many fast ferries (mono-hull and catamaran), luxury yachts, marine and cruise ships, as well as for tugs, pilot and hydrofoil boats as well as many others. A ship using Dynexa driveshaft is shown in Figure 1.14.

Figure 1.14: A ferry using DYNEXA composite shaft

Standardized technical data:

- Torque range: up to 800 kNm
- Diameter: up to 800 mm
- Length up to 12 m

The X-SHAFT developed by Dynexa is 70% lighter than a conventional shaft. It has achieved high critical speed without the need of intermediate bearing or less bearings than usual. The torque and bending stiffness can be achieved by adapting the shaft's architecture to the application needed. The model meets the requirements of BV and DNV-GL registers.

REXNORD-CENTA

Rexnord acquired CENTA Power Transmission in 2018. The company designs and builds mechanical components for many applications. Marine industry is one of them. The composite shaft model manufactured is CENTA CARBON, a low-weight CFRP shaft, appropriate for high-speed drive machines. It has been installed in a vast list of ships such as ferries, naval ships, hydrofoils, yachts etc.

Standardized technical data:

- Torque range: 0.1-650 kNm
- Temperature: -40ºC to 90ºC
- Length up to 10 m
- Diameter: 162 mm to 725 mm

It is a cost-effective shafting system because of the small amount of additional components, such as bearings and foundations. Another benefit, except the extreme durability, noise damping and low thermal expansion, is that CENTA offers a big variety of couplings and connecting elements that can be combined with the shaft. In figure 1.15 various ships are shown that use CENTA CFRP driveshaft.

Figure 1.15: Ships using CENTA CFRP driveshaft

VULKAN

For more than 125 years VULKAN Couplings, as a division of the globally active VULKAN Group, has been developing, producing and marketing innovative system solutions for marine driveshaft technology. One of the Composite shafting models (CS-System) is VULKAN COMPOSITE SHAFTS with steel end fittings. The driveshaft is manufactured by the filament winding technique using epoxy resins combined with carbon or glass fibres.

Standardized technical data:

- Torque range: 5-800 kNm
- Diameter: 170 mm to 670 mm
- Length up to 12 m

VULKAN COMPOSITE SHAFTS are available in high torque capacity (T model) or in high bending stiffness (B model) execution. Shafts with diameter up to 1500 mm and length up to

20 m can be built, while, in special projects the capacity torque can reach the value of 5000 kNm.

JAURE

JAURE provides driveshafts for marine propulsion made by carbon fibres (JCFS). JCFS composite shaft is standardized in two available series depending on the application:

- L series: Suitable for long distance between bearings and high speeds
- T series: Developed for high torques (above 65 kNm)

Standardized technical data:

- Torque: up to 900 kNm
- Diameters: 168mm to 752 mm
- Length up to 14 m

It is mentioned that the standardized maximum torque is 900 kNm but there are no restrictions for higher rates.

In Table 1.1 the maximum standard values are summarized for each manufacturer's shaft mentioned.

Table 1.1: Maximum standard values of each manufacturer's shaft

	Torque (kNm)	Diameter (mm)	Length (m)	Range of temperature (°C)
GEISLINGER	700	1200	12	-45 to 100
DYNEXA	800	800	12	-
CENTA	650	725	10	-40 to 90
VULKAN	800	670	12	-
JAURE	900	752	14	-

After the research on the manufacturers' websites we have come in certain conclusions. All the manufacturers offer a big list of standardized products in a big range of torque and principal dimensions (length and diameter). However, there are some that can build shafts for special applications with no restrictions, for demands higher than the standardized ranges (ex. JAURE, VULKAN). The main technique used is filament winding and the most commonly used fibres are those made of carbon with epoxy resin. All the suppliers in their technical brochures mention the benefits of their CFRP shaftlines over the traditional steel shafts (low weight, fatigue life, vibration damping, thermal expansion) confirming the advantages mentioned in the beginning of the present chapter.

1.6 Composite shafting rules & regulations

The composite materials are gaining more space in the domain of the marine industry. The need for rules and regulations, which will determine clearly the procedural and technical demands of the structures made by composite materials, has been answered by some of the

major shipping registers. Unfortunately, only DNV-GL and Bureau Veritas (BV) include in their rules a complete set of regulations, concerning the composite drive shafts, while others such as Lloyd's, offer general rules for metal shafting systems and some other rules for the manufacture testing and certification for composite materials, which will not be presented here. After a detailed study of the DNV-GL and BV regulations, it is noticed that, there are some common issues on how they deal with the solution of the problem, however, there are differences between the equations used for the main parameters which describe the problem.

DNV-GL class programme 0093 and BV NR 546 Section 10 set of rules

1.6.1 General

DNV-GL register offers a detailed class programme (from now on it will referred to as CP) named: 'Composite drive shafts and flexible couplings - Non-metallic materials. The objective is to determine the criteria by which, composite drive shafts and flexible couplings will be approved by the class. It also describes the requirements related to the documentation, design and type testing applicable for type approval. In general, it covers FRP drive shaft section(s) joined by metallic couplings in both ends to a metallic flange, however the type approval is given for a specific set of raw materials, method of fabrication and bonding between central section and the flanges (adhesives, couplings etc).

Concerning the documentation, the CP provides a list of demands that must be fulfilled for the type approval. These demands cover topics such as the product details which include the name, various specifications and descriptions (design, laminate lay-up, material specifications etc.), and information for marking and packaging. The documentation is also demanded to refer to the manufacturer's details (production places, name, phone, mail etc). Also, the construction procedures, the operational conditions, the adopted quality system and the quality tests carried out with the results and the list of the measuring systems and calibration certificates must be included. Summarizing, the basis of approval will be counted on the design analyses, a small scale and a full scale testing and the specification of the materials used and the fabrication procedure which was followed.

On the other hand, BV register offers a more comprehensive and compact set of rules, named Composite Shaft Line, in order to classify composite shafting systems and it constitutes the tenth section of NR 546 rule publication. The main objective of these rules is the scantling check of composite shafting systems used in main propulsion. These rules are supplementary and specific for composite shaft lines. In general, we meet many references in other sections of NR 546 publication in order to supplement extra elements already mentioned in the rule publication for other objectives. Requirements such as installation arrangement, alignment and durability of some components are specified by other set of rules (Classification of Steel Ships, NR467). Just like DNV class programme, BV rules set the operational conditions (temperature and humidity) and the demands of the raw materials used. Lastly, the submitted documentation is determined concerning the arrangement, the laminate composition (sequence, lamination, materials), raw materials technical data, the procedure, design analysis information and the mechanical test results.

1.6.2 Design Input

In section 2 the CP defines the design and operational (functional, loading, environmental) requirements and condition of the composite shafting system (drive shaft and flexible couplings).

Functional requirements:

(i) torsional static strength – transfer of engine torque
(ii) torsional fatigue strength – sustain normal operational load cycles and induced vibrations
(iii) bending fatigue strength – sustain permanent and variable shaft misalignments
(iv) angular misalignment – accommodate shaft misalignments under given maximum bending moments (applies to flexible couplings
(v) axial offset – accommodate axial offset of shaft under given maximum reactions forces (applies to flexible couplings)
(vi) radial offset – accommodate radial offset of shaft under given maximum reaction forces (applies to flexible couplings)

Load conditions the shaft must be analysed:

(i) start-stop cycles: start – max. load – reversing (if relevant) – stop. Dynamic effects shall be included.
(ii) rare peak torques, e.g. due to synchronization problems with a generator or other rare disturbances of nominal operation.
(iii) transient operation, e.g. passing through a speed range barred from normal operation, ice shock loads etc.
(iv) steady state torsional vibrations.
(v) bending induced by shaft misalignment.
(vi) angular misalignment (for flexible couplings).
(vii) radial offset (for flexible couplings).
(viii) axial offset (for flexible couplings).

The different parameters are described in figure 1.16.

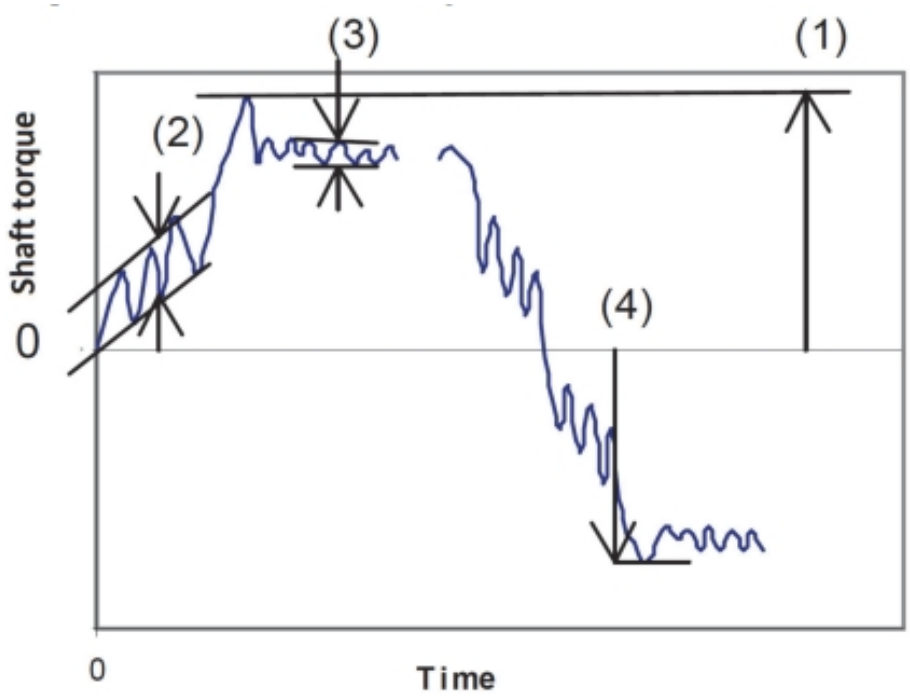

Figure 1.16: DNV-GL parameter description

The graph indicating parameters are listed below:

(1) peak torque: start - max. load - stop-cycle, rare peak torques

(2) 2 x Tv(transient): transient operation vibrations

(3) 2 x Tv(continuous): steady state torsional vibrations

(4) peak torque: reversing

In BV set of rules the load conditions are divided in Sec 10, [3] in 4 general categories, according to the kind of the load which correspond to the functional requirements of DNV-GL CP:

(i) Static loads (Article [4])
- torsional moments due to the peak torque
- axial force and bending moment by relative movements of the shaft line and hull structure deformation
  - Tensile and compressive axial force induced by axial relative movement
  - Bending moment induced by angular relative movement
- hydrodynamic horizontal force by the propeller

(ii) Buckling loads (Article [5])

(iii) Vibratory loads (Article [6])

(iv) Fatigue (Article [7])

These loads are further analysed on how they occur in each article mentioned.

DNV-GL environmental conditions:

(i) Temperature within the range +5 to +55 ºC.
(ii) A relative humidity within the range 0 to 96%.
(iii) No exposure to liquids or gases with a possible detrimental effect on the properties of the shaft.

The same conditions are also accepted by BV in Sec 10.

1.6.3 Materials

According to section 3 of the CP 0093 of DNV-GL the only types of fibres accepted are **glass** and **carbon** while others will be accepted under consideration. Additionally, the only type of resin that is accepted is **epox**y, while, others will be accepted under consideration. On adhesives, the society refers that they should be chosen according to the environmental conditions which are described in the previous section.

Some suggestions are made also, in order to prevent the delamination of the drive shaft which concern the stacking sequence of the plies, the angles and the shafts which are not fabricated by the filament winding method.

BV register, in NR546 Sec10, Article [1] Par [3] also refers to the raw materials approved by its set of rules. They are determined on a different section of NR546 (Section 4 App 1). BV accepts more types of raw materials than DNV: **polyester**, **vinylester** and **epoxy** resin systems and **glass**, **carbon** and **pararamid** fibres. The adhesives must be chosen according to the conditions, also, technical data must be submitted concerning shear stress curves and corrosion.

1.6.4 Failure mechanisms and criteria

According to Sec 4 of the CP the composite shafting system must be analysed as a minimum for some mechanical failures such as: **fibre failure**, **matrix cracking**, **delamination**, **buckling** and **fatigue failure** for the FRP central sections plus **shear failure** of the bond line and **bearing pressure** for the bond between FRP central sections and the flanges.

Last but not least, failure criteria are set for the FRP sections and bearing pressure based on a maximum stress criterion. For buckling and adhesive bonds a maximum shear stress condition is stated that must be set.

This type of analysis is not required in this section for BV approval.

1.6.5 Material Properties

The most important property of the shaft line is to confirm that the characteristic values must exceed the nominal with a 97.5% probability. In section 5, the CP states that the tests, that are described at the seventh section, must be taken into consideration for the static strength confirmation. The necessary tests, in order to generate the fatigue strength data of the

composite laminates and the adhesive bonds, are also described. They must be presented on a double logarithmic scale.

1.6.6 Design analyses

The sixth section of the CP is dedicated to the static and fatigue strength calculation analyses. For the static strength calculation, the mechanical properties must be defined for every failure mechanism described in the fourth section of the present CP.

The directions state that the loading case studied must be a combination of peak torque and bending moment (the worst case combination) for the shaft and couplings.

The issue is analysed with the use of the ratio "SF" for the characteristic strength to the local stress or strain due to the load case studied and it is set for every part of the shafting system (central section, joint, adhesive bond and pin/bolt connection) and every failure mechanism quoted on the corresponding section.

Table 1.2: The ratio "SF" of characteristic strength to the local stress or strain corresponding to the design load

Part	*Failure mechanism*	*SF*
Central section Joint	Fibre failure	3.0 - 4.0[1)]
Central section Joint	Matrix cracking	1.5
Central section Joint	Delamination – shear Delamination – through-thickness stress	[2)] 4.0
Central section	Buckling	3.0
Joint: adhesive bond	Shear of adhesive bond-line	6.0[3)]
Joint: pin/bolt connection	Contact pressure	5.0[3)]

1) for designs with SF ≥4.0 design against fatigue due to torsion will normally not be required, see [3]. For designs with 3.0 ≤ SF < 4.0 documentation of the slope "m" of the fatigue curve of the material will be required for design against torsion fatigue, see [3]. For fatigue wrt other load conditions (e.g. deformations in flexible couplings) other requirements apply, see [3]

2) to ensure an adequate safety against delamination the through thickness shear stress in the laminate including residual stresses shall not exceed 5 MPa at any location

3) the capacity of the joint will be based on static tests in addition to the design analyses, see Sec.7. The manufacturer shall provide a calculation procedure for applying the test results to other shaft designs included in the type approval to the satisfaction of the Society

The equations of the critical buckling stress in torsion (τ_{crit}) and bending (σ_{crit}) are also presented. For long cylindrical cross sections the critical buckling stress in torsion can be calculated according to the following equation as an alternative to FEM-analyses or tests:

$$\tau_{crit} = \frac{E}{1-v^2} \cdot \left(\frac{t}{l}\right) \cdot \left(-2.39 + \sqrt{96.9 + 0.605\, H^{1.5}}\right) \qquad (1.3)$$

$$H = \sqrt{1-v^2}\,\frac{l^2}{r \cdot t}$$

For long cylindrical cross sections the critical buckling stress in bending can be calculated according to the following equation as an alternative to FEM-analyses or tests:

$$\sigma_{crit} = \frac{E}{\pi\left(1-\nu^2\right)} \cdot \left(\frac{t}{r}\right) \qquad (1.4)$$

τ_{crit} = critical shear stress due to torsion
σ_{crit} = critical bending stress
r = inner radius of cylindrical section
t = minimum thickness of laminate in central section
l = length of central section between flanges
E = the lowest of the engineering moduli in longitudinal and circumferential direction of the central section
ν = the lowest of the Poison ratios of the central section.
The equations are valid for r/t > 10.

The combined loading must fulfil the following condition:

$$\tau_{crit}/\tau + \sigma_{crit}/\sigma \geq SF. \qquad (1.5)$$

The fatigue endurance, in torsion and other load cases, of the drive shaft and couplings must be calculated too. According to the CP the study is based to the SF that is chosen previously in strength assessment. The requirements set, are based on the selection of the SF and the slope "m" of the fatigue curve of the FRP material. The fatigue strength can be demonstrated also, by full scale tests described on the next section.

BV follows a different root, with some similarities, for the scantling check of the shafting system by analysing and checking every load case separately. Generally, the tactic followed by the register is to establish the equations of the main forces induced to the shaft then the strain and stresses and then the scantling criteria by a Safety Factor analysis by using coefficients for each load case examined. The register also dedicates an article for shaft line coupling check. A review is written afterwards:

Design check of line under static loads

The static design loads are analysed here along with the strain and stresses in the laminate shaft line and the scantling criteria.

As already said, the torsional load must be considered at least 1.3 of the nominal, while, the axial forces are determined by simple equations. The propeller load is to be defined by the designer. Equations are also given in order to calculate strain and stresses for the whole shafting line while the calculation in the individual layers is determined by other section of NR546 rule publication (Sec 6, [3.2.3]). The scantling criteria under static loads are analysed. It is based on a safety factor and coefficient description and they are chosen according to the conditions applied.

Buckling analysis

The same tactic as previously is followed for the buckling check and analysis. The equations of the compression, shear and critical buckling stresses are given and the scantling check coefficients are described.

Design check of shaft vibration

A method describedinNR467, Pt C, Ch 1, Sec 9, is used to carry out the calculations needed for propulsion systems over 220 kW and for internal combustion systems over 110 kW. For other installations, the equations for critical bending and torsional vibrations are given in order to be calculated. The checking rule applied is that the speed range limit should be at least 10% more and less than the critical vibration speed.

Design check under fatigue

Generally, if the coefficients are greater than the minimum values given in [4.3.1] by the static load calculation the fatigue check is not required. The base of the fatigue analysis is the S/N curves obtained for each ratio R (minimum stress divided by maximum stress). Stresses induced by bending moment because of angular relative movement can be taken into consideration but as a main rule, only stresses due to normal and continuous operation are estimated. At last, the total damage is calculated by Miner's damage accumulation rule.

Shaft line coupling

Lastly, the scantling criteria for the shaft coupling are determined. The equations are described for the shear force in the connection and the shear stress for bolted and bonding connections to end with the criteria that must be fulfilled.

1.6.7 Type testing

In section 7 of the DNV-GL CP, the tests needed to be carried out, in order to ascertain the capacity of the shafting system in static and fatigue loads, are described. The manufactured specimens must be made by the same materials and fabrication method as used for the normal parts. The torque applied in the test must be at least 30% of the maximum nominal torque which will be applied on the normal part in the domain which will be used. The properties of the specimens are also described, according to the properties of the normal parts that are used. Two types of tests are required:

(i) the test under static load
(ii) the full-scale fatigue testing.

The static load test is described. The demands of the instrumentation are determined (measuring acceptance criteria) and the environmental conditions (temperature and humidity). Then the test procedure follows, where the loading sequences are described and the graphs needed to be extracted at the end of the process. Lastly, it must be checked if the acceptance criteria are fulfilled. The following condition must be applied:

$$T_{fail} > 1.16 \cdot SF_{max} \cdot \text{Peak torque} \quad (1.6)$$

Otherwise another specimen must be made. The average value of the two specimens must exceed the value in condition (1.6).

The full scale fatigue testing is also described in order to verify the fatigue strength of the shaft according to the load cases set in the third section of the CP. Important values such as mean torque (Mi), torque amplitude and range (Ai, ΔTi) and the number of cycles (Ni), must be presented in a specific table. Safety margin factors (F_1,F_2) are also applied in order to ensure the reliability of the shaft in fatigue and to take into consideration the effects of the shaft's service history ($F_1 \cdot F_2 \geq 32$). Afterwards, values relative to the minimum required fatigue curves (m_i, C_i) fatigue damages (D_{Total}, di) and fatigue test conditions (ΔT_{Test}, N_{Test}) are presented. Furthermore, just like the static load test, the demands of the instrumentation are determined (measuring acceptance criteria) and the environmental conditions (temperature and humidity). Then the test procedure follows, where the loading sequences are described. Lastly, it must be checked if the acceptance criteria are fulfilled. The condition is: $N_{fail} > N_{Test}$. Otherwise another specimen must be made. The average value of the $\log(N_{fail})$ must exceed the value $\log(N_{Test})$. The test is unacceptable if

$$N_{fail} < N_{Test} / 10^{2 \cdot \log(\sigma)} \quad (1.7)$$

BV in Sec 10, [2] the "test and survey at works" is determined step by step on a general procedure described in another section of the NR546 publication. The main demand of the testing is that the shafting system (drive shaft and couplings) must be tested under static torsional load not less than the 1.3 of the nominal torque. Instrumentation is to be provided for continuously measuring the torque and the twist between the couplings.

1.6.8 Documentation required in each delivery

In Sec 8 of the CP, the documentation described in the first section, is analysed. The first orientation of the documentation concerns the proof of testing, then is the design documentation and last the requirements of production and the quality control arrangement.

The documentation required by BV is described in [1.4] of the set of rules. A more compact description demanding almost the same elements as DNV-GL.

1.6.9 Requirements for marking of product

(Extract directly from DNV-GL rules)

The pipes and fittings shall be marked. The marking shall at least include the following information:

- *manufacturer's name and/or logo*
- *type designation*
- *materials*
- *size/dimensions*
- *date of fabrication and/or serial number.*

The marking shall be carried out in such a way that it is visible, legible and indelible. The marking of product shall enable traceability to the Society's type approval certificate.

1.7 Objectives of the present thesis

Composite shafts are gradually gaining space in marine driveshaft applications. For such applications the main feature that needs investigation is the durability of the composite shaft in torsion.

The need of the Shipbuilding Technology Laboratory, to improve the already existing knowledge and experience on torsion experiments of composite shafts, was the main motivation of the present thesis.

The present thesis is experimentally oriented and has two main purposes. The first, is to study two existing torsion test devices and their equipment. One of them is located at the Strength of Materials Laboratory in the National Technical University of Athens. The machine parts, the electronics and the manufacturing standards were recorded. The machine was investigated whether it can carry out torsion tests that comply with the DNV-GL test standards presented previously. The main goal of this study is to prepare the device for future experiments. The other torsion test device is located at the B&T facilities in Florina where a series of torsion tests were carried out within the framework of the present thesis.

The other purpose of this thesis is the conduction of the aforementioned tests. Three CFRP shafts underwent torsion loading until failure. The main goal was to record the strain evolution on the shafts, in order to study the composite shaft's mechanical behaviour in torsion. The study resulted in many interesting conclusions about the failure mechanisms. Some valuable indications were extracted, about the buckling mode of each shaft.

CHAPTER 2

THE TORSION TEST MACHINE OF THE STRENGTH OF MATERIALS

An objective of the present thesis is to study the torsion test machine located in the Strength of Materials Laboratory of the School of Applied Mathematics and Physical Sciences. The specific machine was studied in order to find out, if composite shaft torsion tests could be conducted according to the rules and specifications of the Class Program of DNV-GL register, which were presented in Chapter 1 of the present thesis.

2.1 Machine overview

The machine is used by the Strength of Materials Laboratory for the testing of various small specimens.

Figure 2.1: Torsion test machine overview

As shown in figure 2.1 the machine consists of two ends and a railway. One end is fixed while the other can move on the rail in order to test specimens of various lengths.

2.1.1 Machine parts and specifications

In Figures 2.2 and 2.3 the inner sides of the two ends are shown. The plateau of the two sides can be noticed. Specific flanges are mounted, in order to carry out the torsion tests of various small specimens.

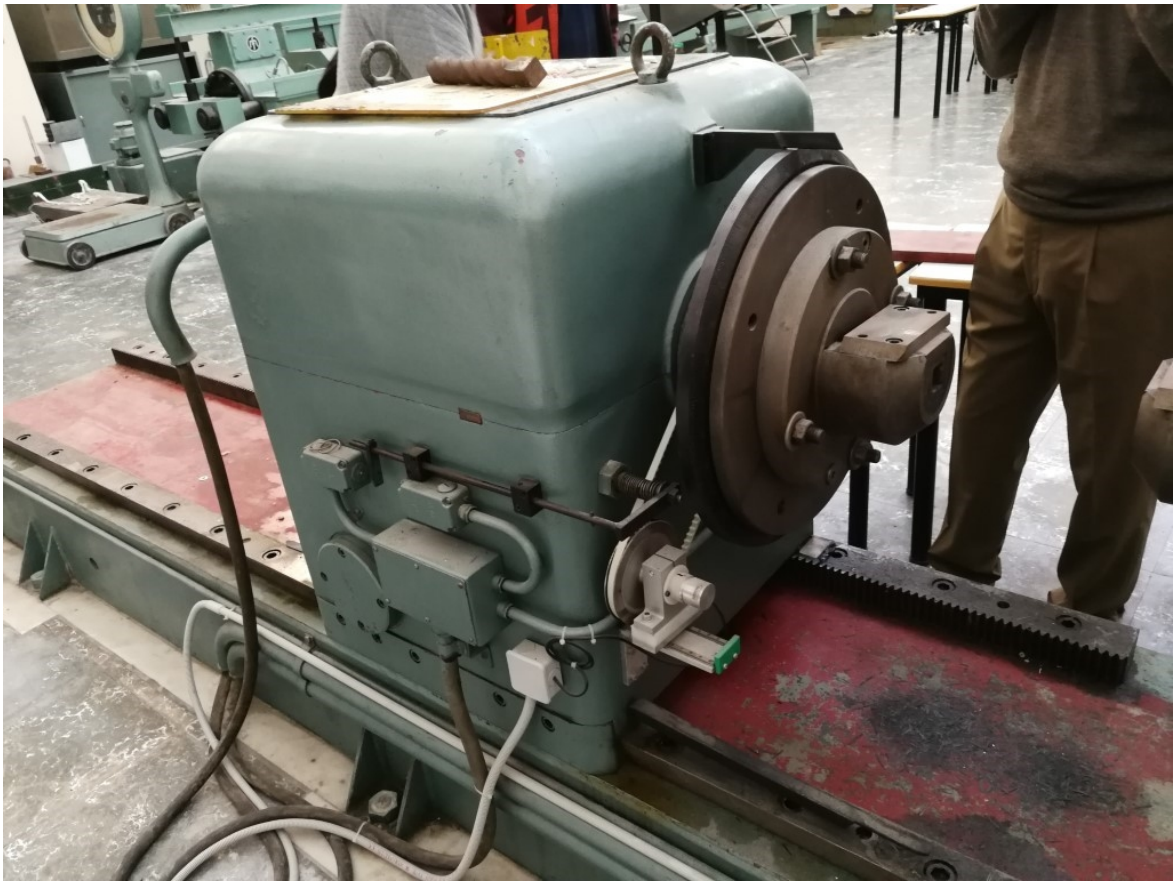

Figure 2.2: Free end (flange mounted)

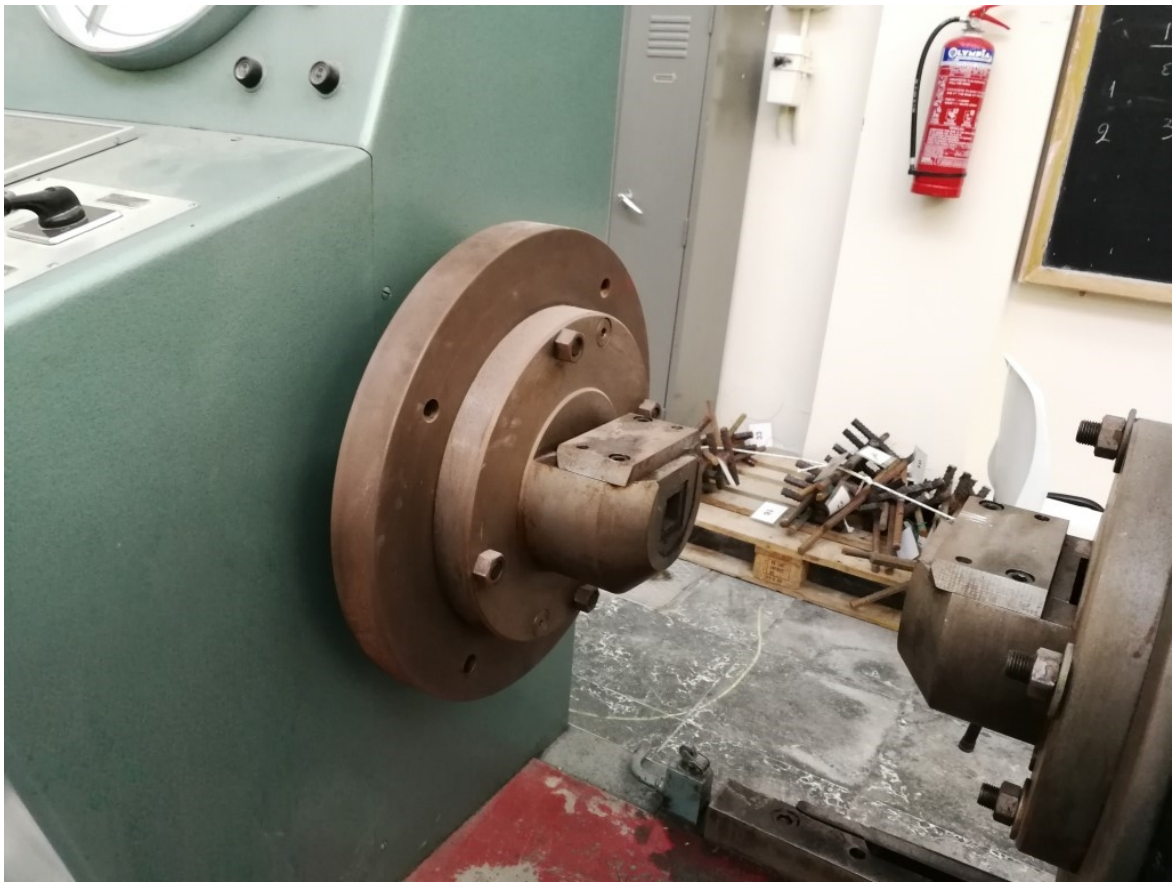

Figure 2.3: Fixed end (flange mounted)

The flanges, which are not needed for any torsion test of composite shafts, are removable. In Figure 2.4 the free end's plateau is shown with the flange removed. It must be noted that the plateau of the free end is the same with the plateau of the fixed end.

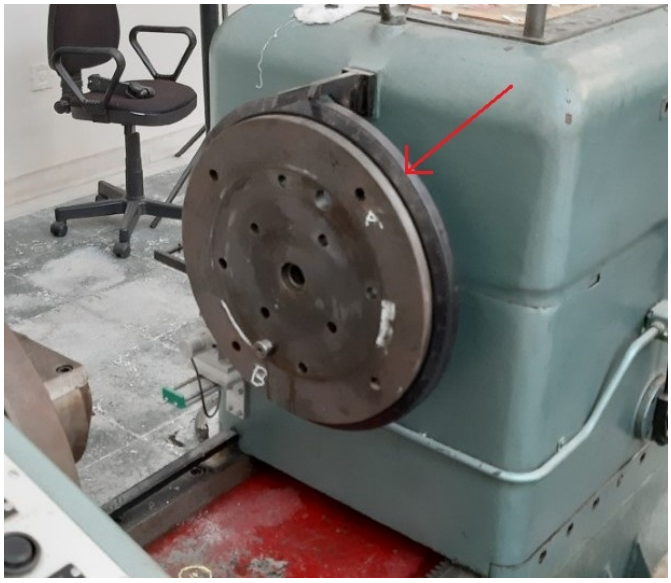

Figure 2.4: The plateau

The torque is imposed by the free end. The machine is equipped with analog measuring systems such as the angle measurement circular frame, around the free end's plateau, that is pointed in Figure 2.4 and the torque measuring system, to the fixed end, shown in Figure 2.5.

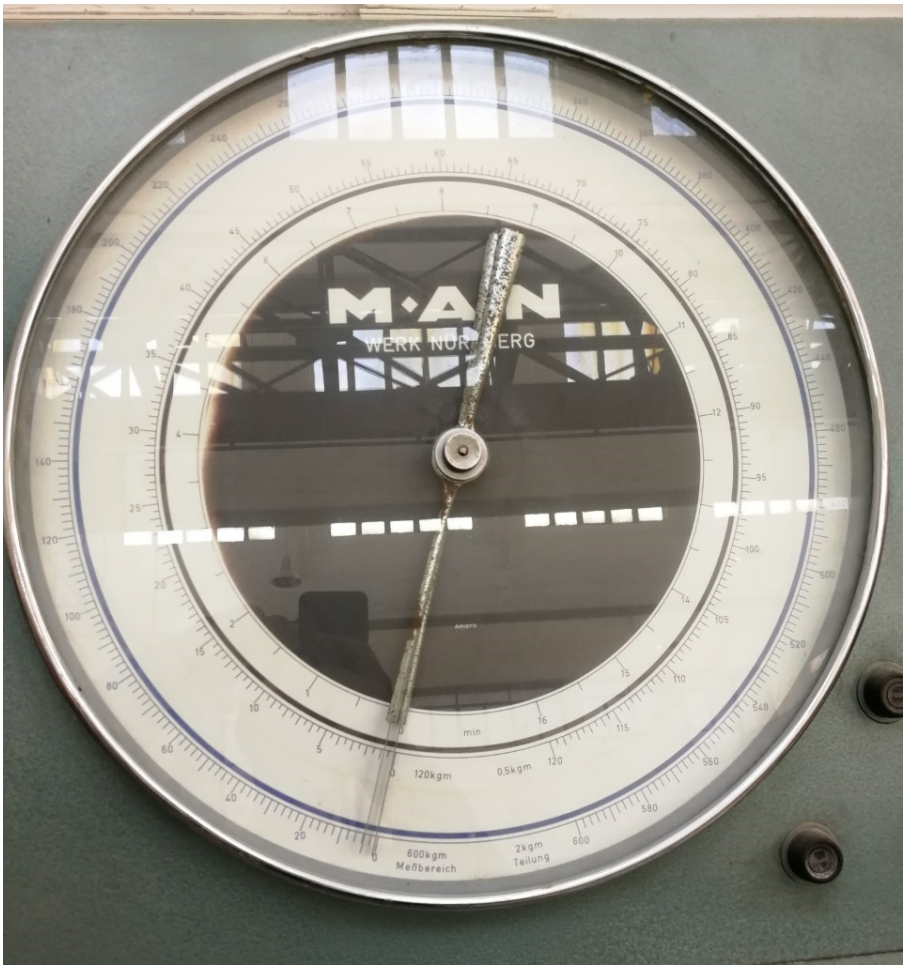

Figure 2.5: Analog torque measuring system

An effort was made in the past, to improve the machine and digitize the measuring systems. For this reason, an electronic system was installed in order to control the imposed torque and collect real-time data from the experimental procedure. The electronic system is described in the next section.

Figure 2.6: Control panel at fixed end

In Figure 2.6 the control panel of the torsion test machine is shown. On the right the control buttons are shown. On the left is the digital screen through which the real time data of the torque and angle are presented.

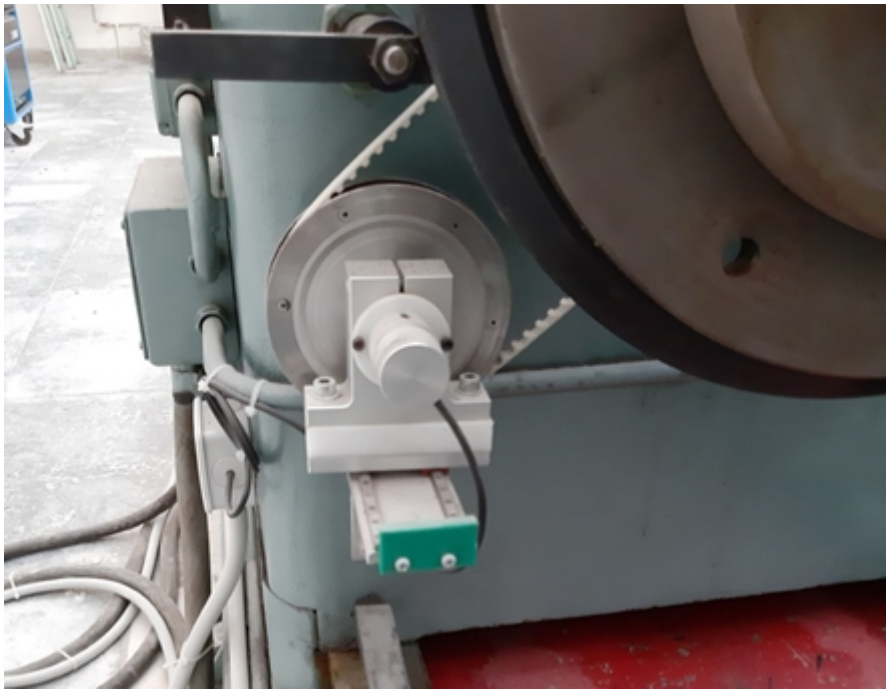

Figure 2.7: Digital clinometer (angle measurement)

Also, a digital angle measurement component is installed at the free end of the torsion test machine, as shown in figure 2.7.

2.1.2 Installed electronics

As already mentioned, some improvements were made on the machine in order to digitize the measuring devices. For that reason, an electronic system was installed in the machine. This system is a Programmable Logic Controller (PLC) which was developed by Unitronics. The system is capable of recording real time data of torque and angle through a software which is developed by Unitronics. The PLC is controlled by the digital screen (model: Vision 290) which is shown in Figure 2.6. The data are transferred to the computer via an ethernet socket. In figure 2.8, the screen Vision 290, in operation is shown.

Figure 2.8: Vision 290 operating

In order to be compatible with the Spider data recording system of the Shipbuilding Technology Laboratory, it was essential to add a socket to the PLC, by which, electrical signals can be sent to the Spider. The socket is shown in figure 2.9.

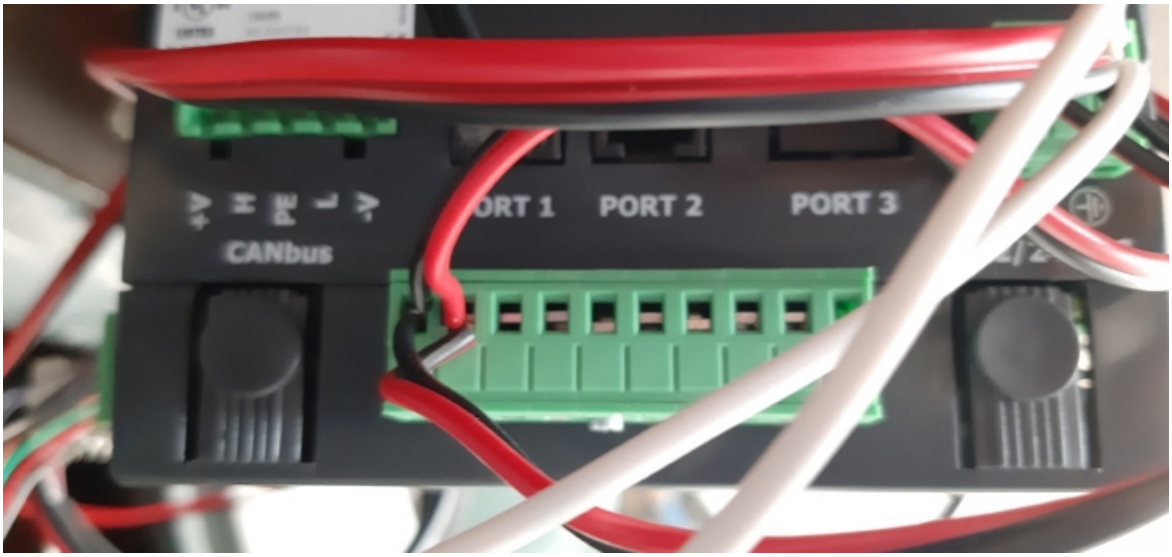

Figure 2.9: Electric signal sockets on Vision 290.

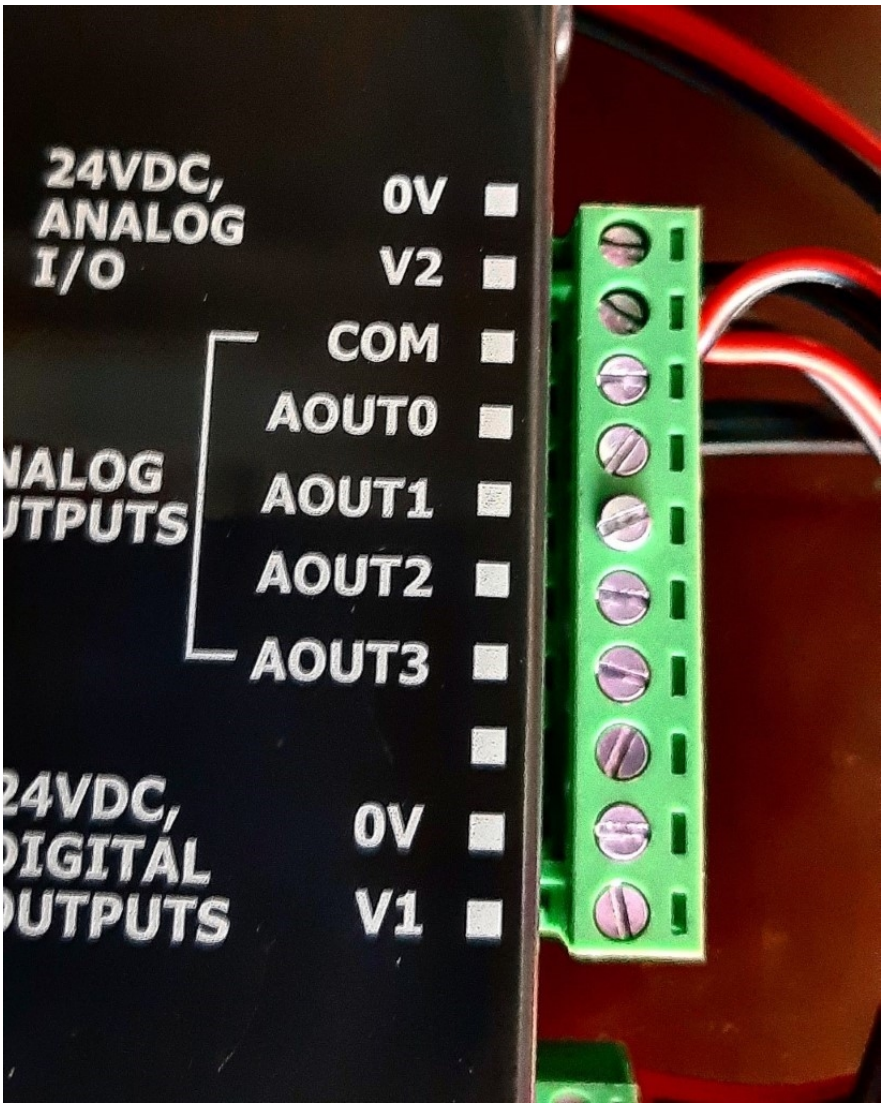

Figure 2.10: Socket configuration

In figure 2.10 the socket configuration is shown. The signal's voltage is 0-10 V for the angle measurement (0-360 deg). The same voltage range applies for the torque measurement (0-600 kgm). The negative electrode is connected to COM position while the positive electrode is connected to AOUT0 position in order to record the angle's signal. In order to record the torque signal, the positive electrode must be connected to AOUT1 position while connecting again the negative electrode to COM position.

2.1.3 Dimensions

Here, the principal dimensions are presented. After the flange removal from the free end, the plateau's dimensional characteristics were imprinted into a design as shown in Figure 2.11.

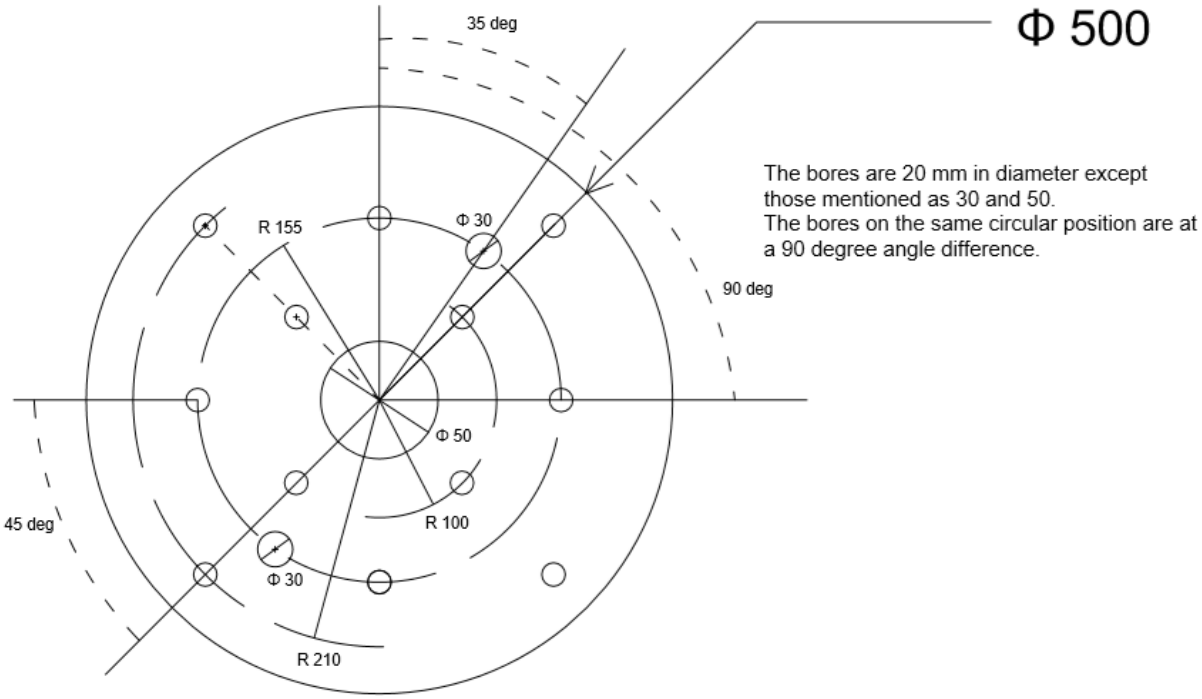

Figure 2.11: Plateau's principal dimensions

In Figure 2.11 there are three circular positions of threaded holes where a flange can be fitted: radius 100, 155 and 210 mm. In 155 mm radius position two extra holes are located as shown in the design. The holes of the inner and outer circular position are on the same angular position while the holes of the middle radius are at 45 degrees angle difference from the holes of the inner and outer circular position. The holes of the same circular position are placed on 90 degrees angle difference.

As already mentioned, the free end can be moved on the rails. The maximum plateau gap that can be reached, is 2.5 m according to the drawings provided by the manufacturer.

The maximum reachable torque is 600 kgm= 5886 Nm. The imposed torque is displacement controlled. There are three available speeds at which the torque can be imposed:

- High: 2.05 deg/s
- Mid: 1.00 deg/s
- Low: 0.52 deg/s

The speed can be controlled by the buttons shown in Figure 2.6. The sampling frequency can be controlled by the Unitronics software. Spider data recording system can control the sampling frequency of the electric signals of the socket configuration shown in Figures 2.9 and 2.10 as soon as the Unitronics system does not interact with the Spider data recording system.

2.2 DNV-GL standard type testing

In this section, the design data of the machine are studied, in order to find out the specifications by which the experiments can possibly comply with the DNV- GL standards of the type testing shown in the first chapter of the present thesis.

The machine can conduct static load tests. In the corresponding section of the DNV-GL class program, the safety factors table for each application are presented (see Chapter 1, 1.6.6 Design analyses) in addition with the critical shear stress due to torsion and critical bending stress equations (1.3), (1.4).

The acceptance criteria of the type testing under static loads are also mentioned (1.5), (1.6).

An investigation will be made in order to set the parameters for a destructive torsion test which will comply with the DNV-GL standards.

The following CFRP material properties were provided by experimental data of the Shipbuilding Technology Laboratory of NTUA. They are used as an example for our investigating procedure (Bilalis, 2016).

Table 2.1 Mechanical properties of the CFRP

E_1 (GPa)	143.7
E_2 (GPa)	9.2
E_3 (GPa)	9.2
G_{12} (GPa)	3.4
G_{23} (GPa)	1.7
G_{13} (GPa)	3.4
ν_{12}	0.32
ν_{23}	0.46
ν_{13}	0.32

In order to conduct an experiment which will exploit almost the full capacity of torque and geometrical dimensions of the torsion machine, the following values will be used in order to calculate the class program equations.

- Safety Factor (SF)= SF for joint: pin/bolt connection= 5.0
- Failure torque (T_{fail})= Machine's maximum torque= 5886 Nm
- CFRP shaft length (L)= A bit shorter than the machine's maximum gap (considering the end fittings) = 2 m
- CFRP shaft inner radius (r)= Same value as the radius of the circular position the end fitting will be bolted on the torsion machine = 0.210 m
- CFRP shaft mechanical moduli (E)= the lowest of the engineering moduli in longitudinal and circumferential direction (DNV-GL)= 9.2 GPa
- CFRP Poison ratio (ν)= the lowest of the Poison ratios of the central section (DNV-GL)= 0.32

Note that the shaft is theoretically designed in order to operate in the peak torque, but the maximum torque to which will be subjected during the test, in order to comply with the class program type testing, is the T_{fail} value (here T_{fail}= 5886 Nm): Peak Torque= 1014.8 Nm.

Now, a first assumption for the shaft thickness will be made. By taking into consideration the thickness of the shafts used in the experimental part of the present thesis we will assume that a common shaft thickness is approximately 0.005 m for a shaft radius similar to the one assumed above. The value complies with the acceptance criteria of the class program (r/t= 42>10).

By using these values, the shear stress due to torsion can be calculated by using the basic formula of torsion:

$$\tau = T \cdot (r+t)/ J_p = (\text{Peak Torque}) \cdot (r+t)/ J_p = 0.724 \text{ MPa}$$

Where:

$$J_p = \pi \cdot (R^4 - r^4)/2 = 301346781{,}3 \text{ mm}^4$$

R: outer radius

r: inner radius

t: shaft thickness

From the class program analysis τ_{crit} value can be calculated by using the (1.3) formula

$$\tau_{crit} = 18.577 \text{ MPa}$$

This is the critical buckling stress in torsion.

In order to comply with the specifications of the Class Program, (1.5) condition must be fulfilled where SF=5

From the above calculations the rate τ_{crit}/τ is calculated:

$$\tau_{crit}/\tau = 25.7$$

It can be easily noticed that the Safety Factor condition is already fulfilled by the τ_{crit}/τ ratio. For a most complete study an investigation on the bending stress ratio should be made, although for the specific example is not needed. Due to the fact that a bending moment value is not suggested by the class program, while an assumption for a real shaft application cannot be made with certainty, the bending stress rate investigation will not be carried out in this example.

From the previous example it is perceived that a big waste of material is made for the specific application. In order to set some standards on the tests that can be carried out to the specific torsion machine, the Table 2.2 is developed, showing, for various lengths and inner radii, the minimum essential thickness of the composite shaft in order to comply with the type testing of the DNV-GL register.

Table 2.2: Length, radius and thickness correlation

Length (m)	Inner radius (m)	Thickness (m)
2	0.210	0.0022
	0.155	0.0026
	0.100	0.0034
1.5	0.210	0.0021
	0.155	0.0025
	0.100	0.0032
1	0.210	0.0019
	0.155	0.0023
	0.100	0.0029

In table 2.2 the inner radii taken into consideration, coincide with the radii of the circular positions where the end fittings can be bolted on machine's plateau. This is not mandatory. The inner radius of the shaft can be lower or even sometimes higher than the radius of the circle where the end fitting will be bolted. The results in Table 2.2 are indicative of the dimensions and respective thicknesses of CFRP shafts that can be adequately tested in the testing machine of the Strength of Materials Laboratory of NTUA, taking into account the maximum capacity of the system. In any case, Table 2.2 is just a suggestion of dimensions for which the rate τ_{crit}/τ complies with the acceptance criteria without considering the bending stress rate (note that in the acceptance criteria, there is the rate of the bending stress which contributes in exceeding the SF value which is the main objective of the criterion (1.5)). For shafts of different dimensions, the path followed above is suggested in order to comply with the DNV-GL Class Program.

CHAPTER 3

B&T COMPOSITES TORSION TEST DEVICE AND RELEVANT SHAFT TESTS

3.1 Experimental set-up

A series of torsion tests on three Carbon Fiber Reinforced Polymer (CFRP) shafts were carried out within the framework of the present thesis. The tests took place at the facilities of B&T Composites in Florina, Greece, in February 2020. The torsion was applied to the shafts by a mechanical torsion in-house manufactured fixture which is presented in Figure 3.1. It consists of two blocks that constitute the two ends of the machine (the free and fixed end). They are both mounted on rails which allow the easy movement of the movable end, which imposes the torque. Thanks to this movement, shafts of different lengths can be tested on the fixture.

Figure 3.1: Shaft torsion test device

We can easily notice, in Figure 3.1, that a pair of hydraulic pistons is installed at the free end, in order to apply the desired torque. The pistons are set into motion by the hydraulic pump which is shown in Figure 3.1. The rate of force application of the pair of the two pistons is not controlled by any digital system. Instead, imposing the pair of forces requires an operator who uses a lever to increase the required torque. The lever is circled in Figure 3.1. It must be noted that, in this way, the rate of torque application is not constant, since it is imposed by the human hand through the lever. This is clearly reflected in the response diagrams that will be presented in section 3.3. The stroke of the pistons can reach 15 cm, allowing, therefore, the free end to rotate up to 52 degrees approximately, a number sufficient to meet the requirements of the current experiments.

The measurement of the applied torque in each experiment was done using a load cell placed at a suitable distance at the fixed end as shown in Figure 3.2. Due to the fact that the load cell records only the force, the torque was calculated by the product of the distance times the force recorded by the measuring system. The rotation angle was measured using an angle sensor at the free end, shown in Figure 3.3.

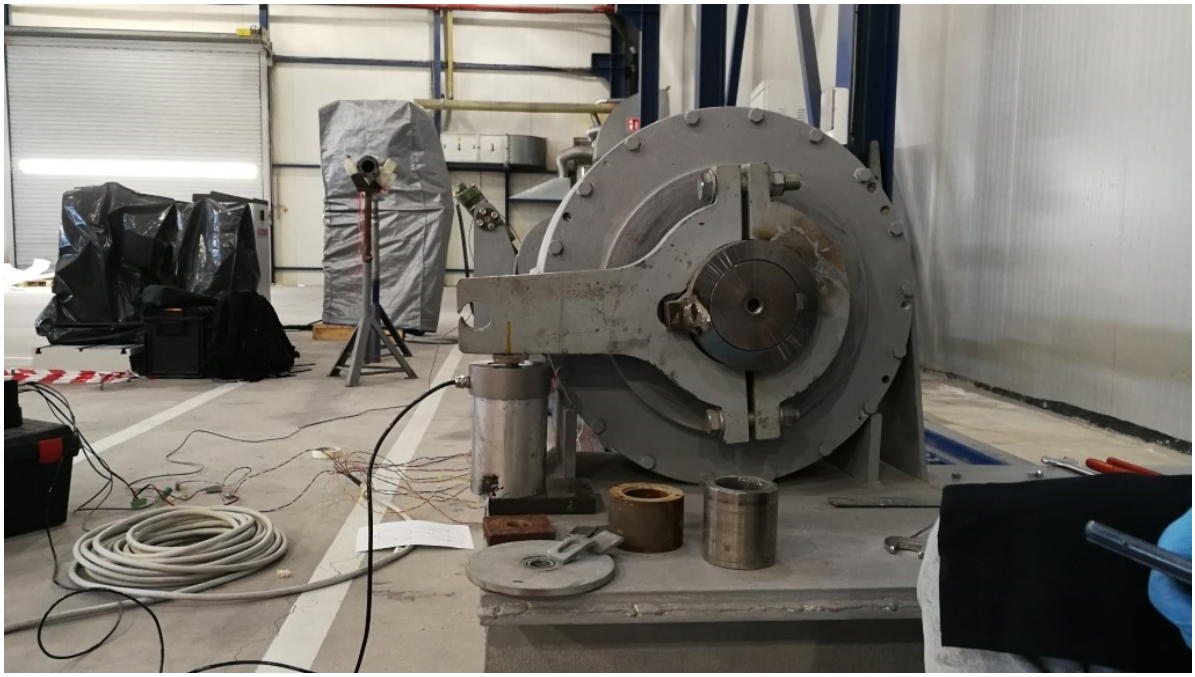

Figure 3.2: Load cell

Figure 3.3: Angle measuring sensor (clinometer)

On the CFRP shafts tested, strain gages were bonded at the distance of L/2 and 3L/4 from the fixed end, as shown in Figure 3.4.

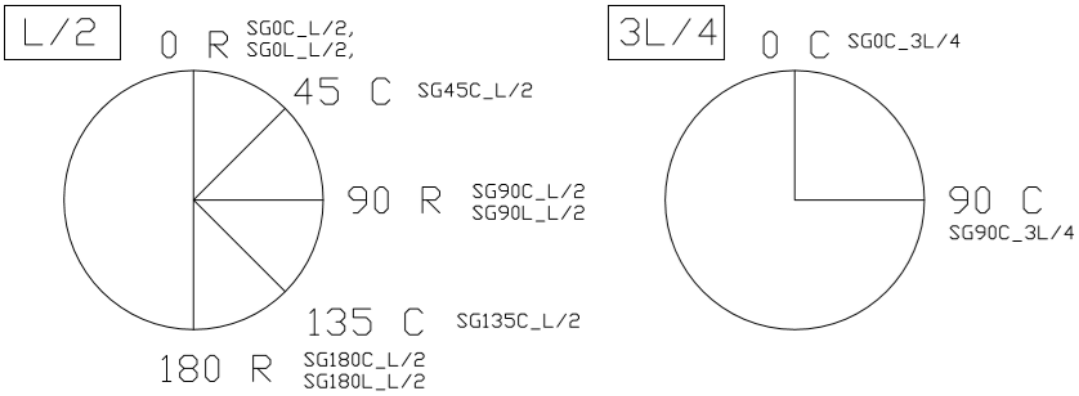

Figure 3.4: Drawing design of strain gages

The nomenclature of the strain gages is easy to understand. For example: SG0C_L / 2:

- SG: Abbreviation of the term Strain Gage
- 0: The circumferential position of the strain gage (here it is at 0 degrees)

- C: Circumferential, shows the direction of the measured deformation (L, Longitudinal and C, circumferential)
- L/2: The longitudinal position of the Strain Gage (here it is at a distance of L/2 from the fixed end, in the middle of the shaft)

Strain gages of rosette type were used at 0, 90 and 180 degrees, for the simultaneous measurement of the circumferential and longitudinal strains. The shafts with the bonded strain gages are shown in Figure 3.5.

Figure 3.5: Installation of strain gages on the shafts

For all the tests the sampling frequency was 5 Hz for all strain gages, the load cell and the clinometer. All the measuring devices (strain gages, clinometer and load cell) were connected to the same measuring system ("Spider") which was connected to a computer where the experimental data were transmitted real-time, as shown in Figure 3.6.

Figure 3.6: Test arrangement and data acquisition system

3.2 Shaft principal dimensions

Three CFRP shafts were tested in torsion (tests explained in section 3.3). They were all manufactured by B&T Composites. The manufacturer provided us with the following data: Two of them (shafts 1A and 1B) have the same lay-up [± 12° / ± 12° / ± 80° / ± 12° / ±12°] and layer thickness: ± 12 = 0.95 mm, ± 80 = 0.32 mm, while, the outer layer thickness is: ±12= 0.52 mm. The geometric dimensions are shown in table 3.1.

Table 3.1: Shaft 1.A & 1.B geometric data

Length (without end fittings) (measured) (m)	External diam (measured) (m)	Internal diam (calculated) (m)	Thickness (calculated) (m)
1.355	118	0.11062	0.00369

The test was performed twice for both shafts 1A and 1B. The first time, there was a failure in the bonding between the composite and the metal flange before any failure in the composite material. For this reason, bolts were placed around the two ends of the flanges, in an effort to additionally support the bonding between the composite and the metal and to achieve greater torque, thus better understanding of the mechanical behavior of the shaft. Eight bolts per flange were installed in two different ways as shown in Figures 3.7 and 3.8.

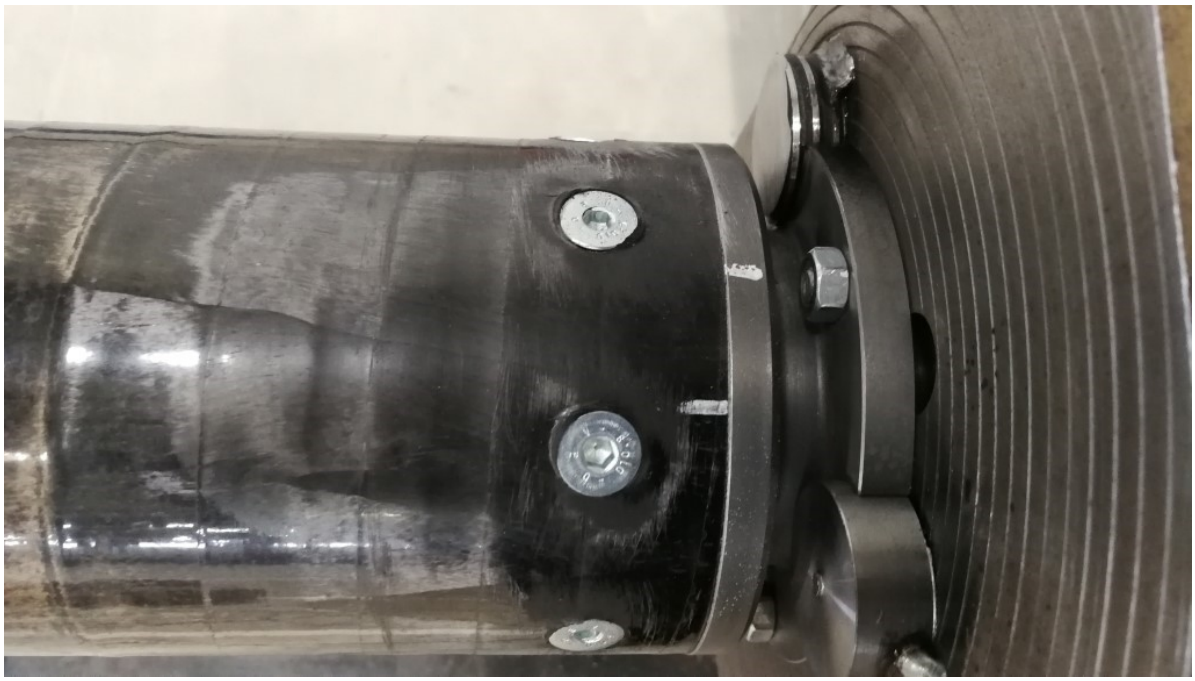

Figure 3.7: One bolt per 45 degrees (Shaft 1A)

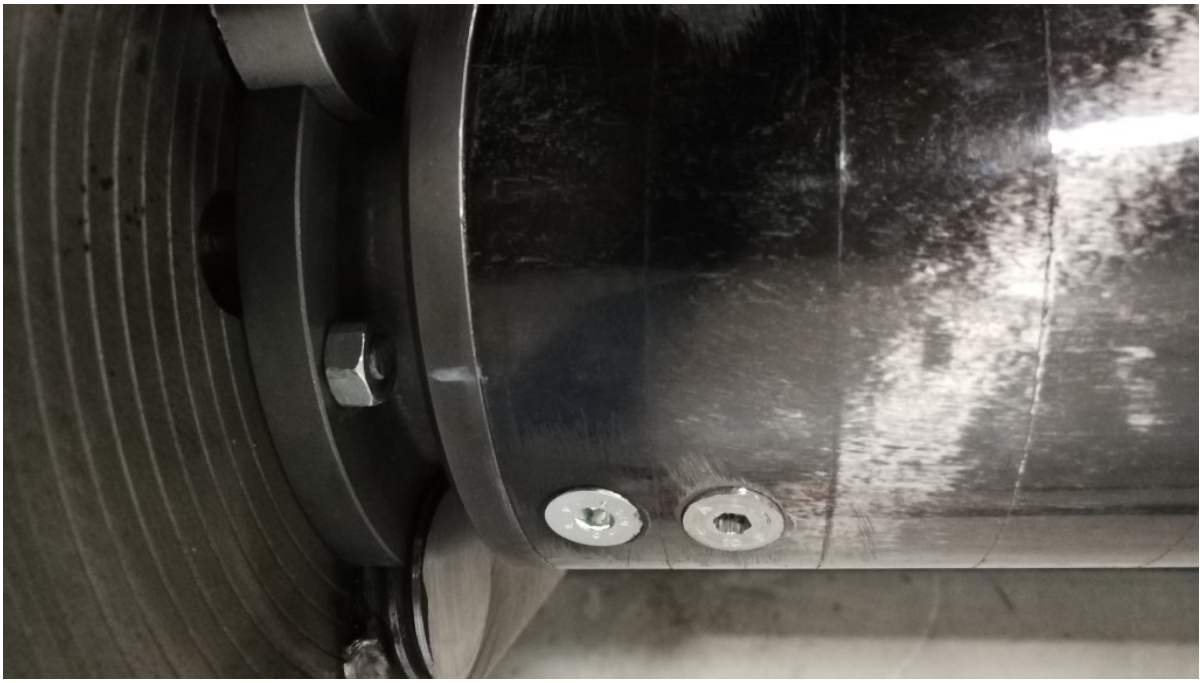

Figure 3.8: Two bolts per 90 degrees (Shaft 1B)

In the first case (Shaft 1.A), the eight bolts were placed per 45 degrees in the same longitudinal position, as shown in Figure 3.7, while in the second case (Shaft 1B), the eight bolts were placed as pairs of two in the same peripheral position per 90 degrees, in a close longitudinal position as shown in Figure 3.8 (Bolt Type: Flat Socket Cap Screw 90° / DIN 7991, bolt diameter: M8) .

Figure 3.9 is a schematic top view of the shafts, demonstrating the composite active length in each case of bolting.

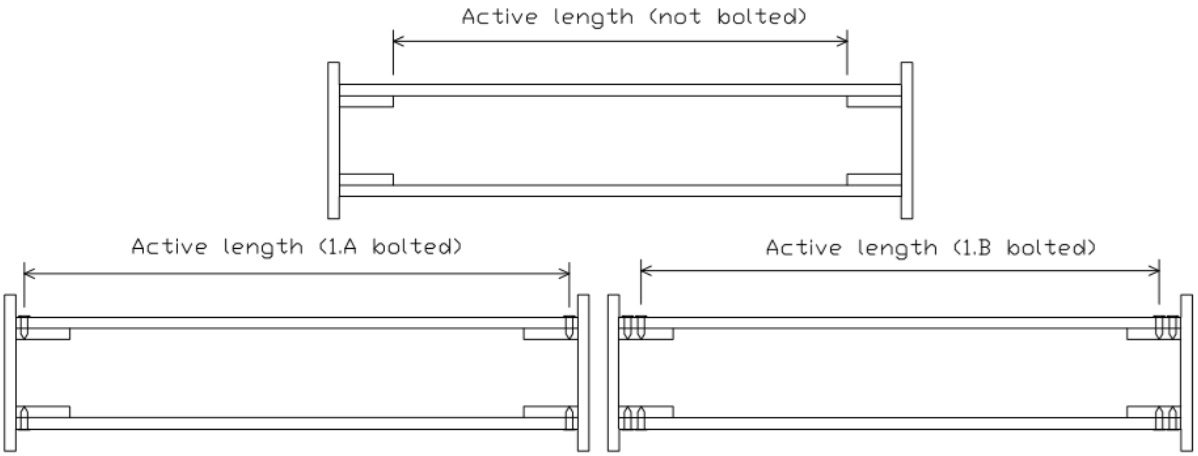

Figure 3.9: The effect of the bolts on the active length

The active length of the shafts 1.A and 1.B at the not bolted experiment is **1.255 m** (measured). After the placement of the bolts the active length of shaft 1.A is **1.305 m** (measured). The active length of shaft 1.B is **1.291 m** (measured) after the bolts placement.

The lay up of the third shaft (Shaft 2) is: $[\pm 12^{o}/+85^{o}/\mp 12^{o}_{2}/-85^{o}/\pm 12^{o}_{2}/+85^{o}/\mp 12^{o}_{2}/-85^{o}/\pm 12^{o}_{2}/+85^{o}/\mp 12^{o}_{2}]$ with the geometric features demonstrated in Table 3.2:

Table 3.2: Shaft 2 geometric data

Length (end fittings included) (m)	External diam (m)	Internal diam (m)	Thickness (m)
3	0.210	0.200	0.0055

The manufacturer provided us also, with the flange drawing of shaft 2, shown in Figure 3.10.

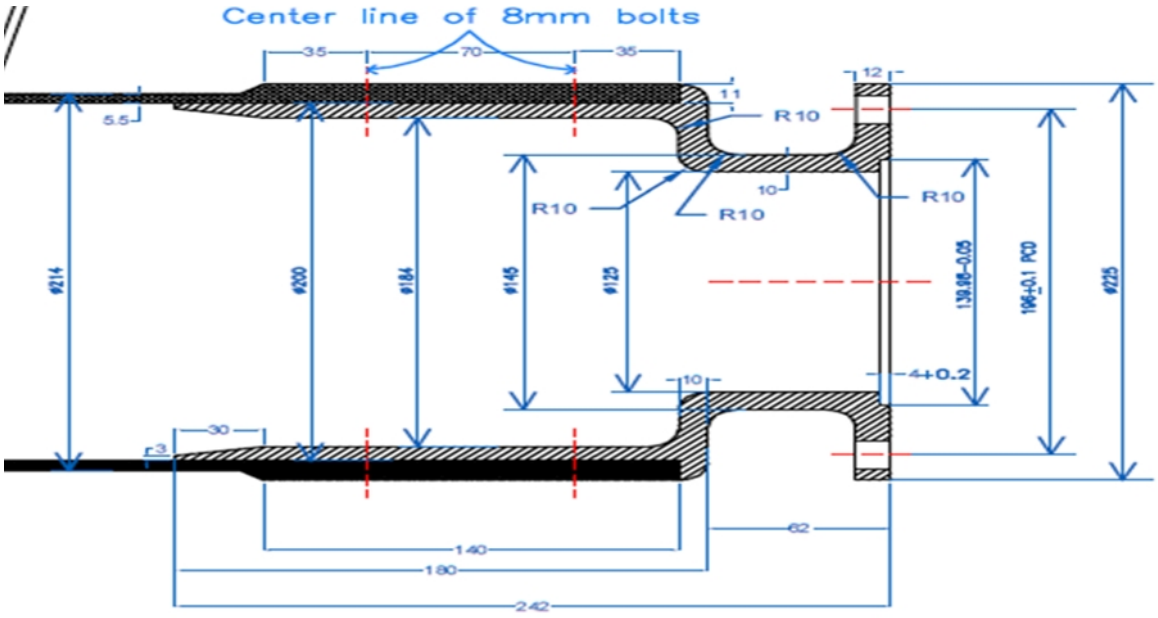

Figure 3.10 : Shaft 2 flange drawing

The length of shaft 2 without the end fitting flange can be calculated by using the geometrical data in Figure 3.10:

Length= 3 – 2(0.062 + 0.010) = 2.856 m

The active length is:

Active length= 3 – 0.062 – 2(0.062 + 0.010 + 0.035 + 0.070) = 2.646 m

3.3 Torsion experiments

In the next sections the diagrams of Torque-Time, Angle-Time, Torque-Angle, Strains-Time and Strains-Torque of the shafts are presented, extracted from the data recorded during the tests. For the shafts 1.A and 1.B, a comparative study of the results is made before and after the placement of the bolts,. Note that in the diagrams that follow, in some Strain Gages, an attempt was made to clear any noise effects due to the operation of the pump which moved the hydraulic pistons.

3.3.1 Shaft 1.A experimental data analysis

3.3.1.1 Shaft 1.A non-bolted test

For shaft 1A the following torque-time and angle-time diagrams are presented. They will be compared to the strain-time diagrams. The main goal is to find out, if the strains and the rotation angle follow the same path as the torque, as a function of time.

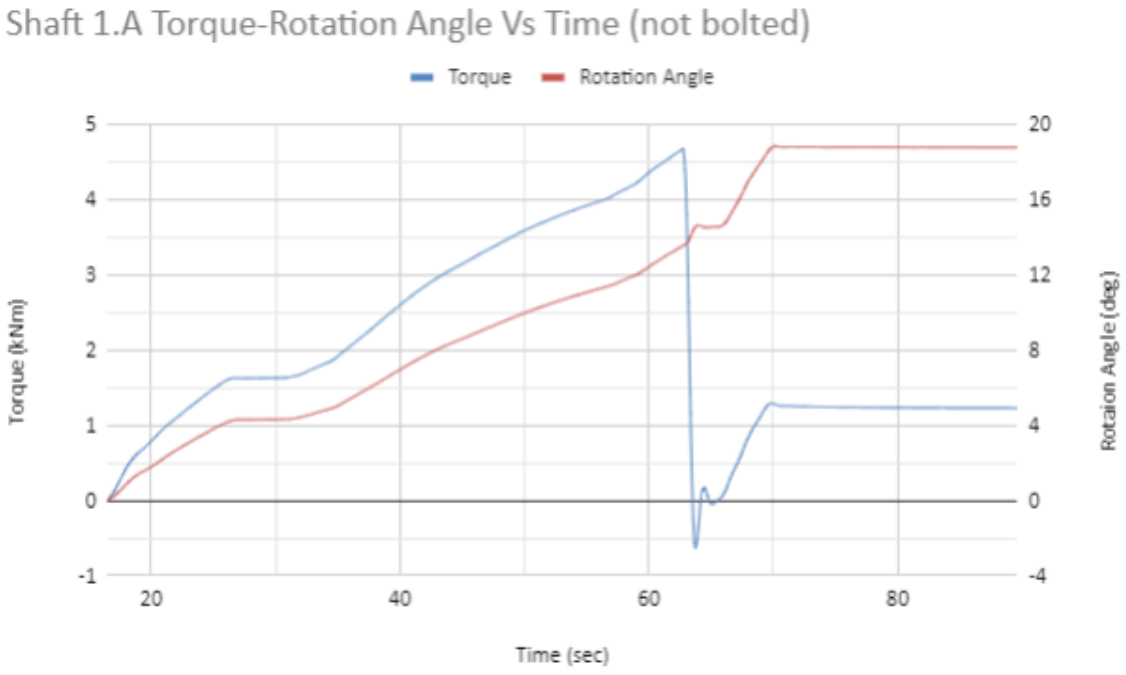

Figure 3.11: Shaft 1.A comparative diagram of Torque-Time & Rotation Angle-Time (not bolted)

In Figure 3.11 a comparative diagram of torque and rotation angle vs Time is shown. It can be seen that the angle behaves exactly like the torque versus time for shaft 1.A. A critical point is the failure of the connection between the flange and the composite at time t_{1ANB}=62.6 sec. At this time, the torque reaches the maximum value T_{1ANB}= 4.659 kNm and the angle of rotation reaches the value of R_{1ANB}= 13.50 deg.

In Figures 3.12 and 3.13 the circumferential and longitudinal strains versus time diagrams are demonstrated. It can be seen, that in both diagrams, the strains exhibit the same behaviour as the torque, with respect to time.

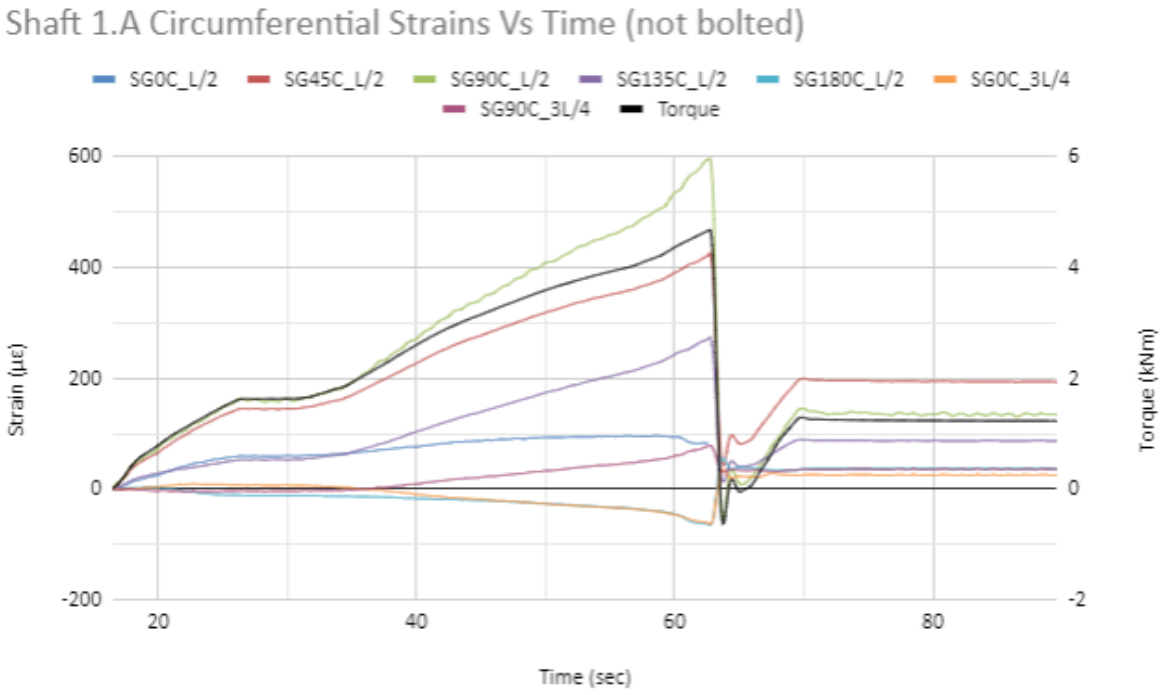

Figure 3.12: Shaft 1.A diagram Circumferential Strains-Time (not bolted)

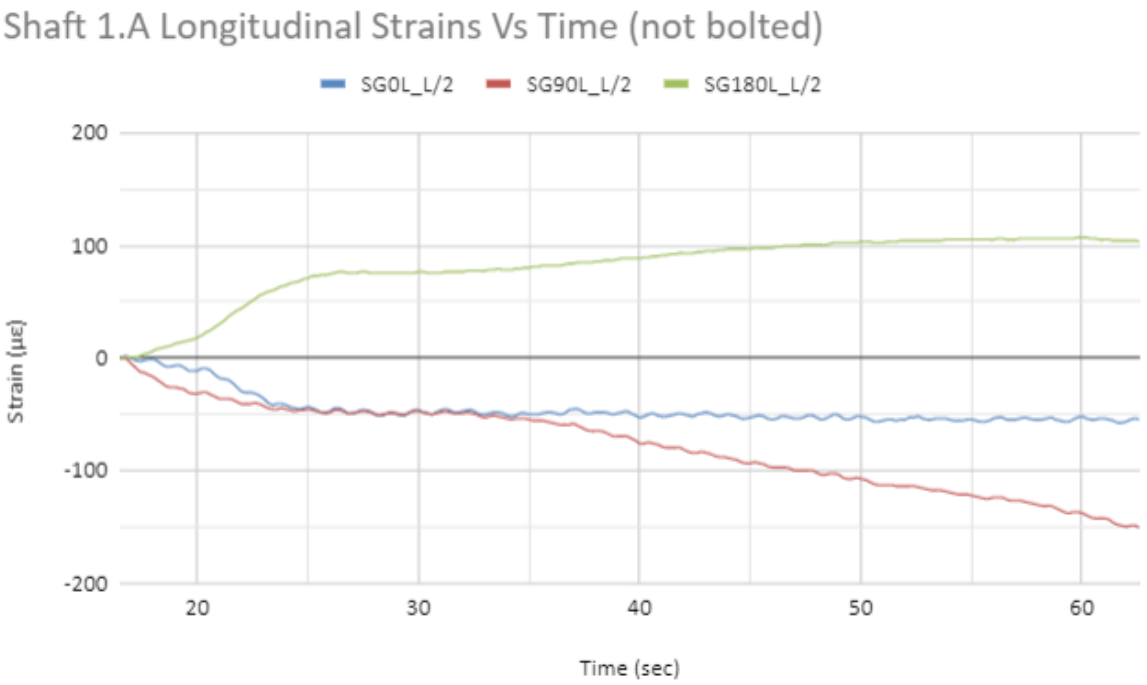

Figure 3.13: Shaft 1.A diagram Longitudinal Strains-Time (not bolted)

Useful information can be obtained from the diagrams of torque versus angle and strain versus torque that are demonstrated next.

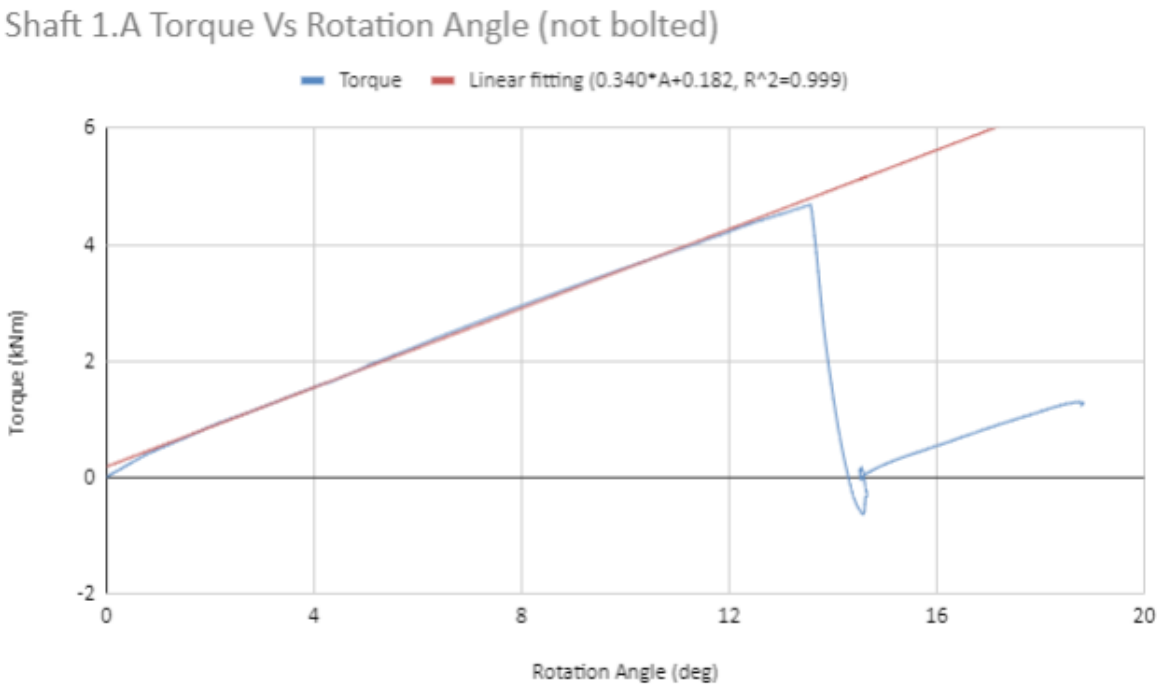

Figure 3.14: Shaft 1.A diagram Torque-Rotation Angle (not bolted)

In Figure 3.14 the torque versus rotation diagam is demonstrated. The perfect linear correlation between torque and angle of rotation (R^2= 0.999), can be seen. From the results of

the not bolted test we can obtain the average torsional stiffness of TS_{1ANB}= 0,340 kNm/deg (Linear fitting equation: T=0.340*A +0.182).

In figures 3.15 and 3.16 the circumferential strains versus torque are demonstrated.

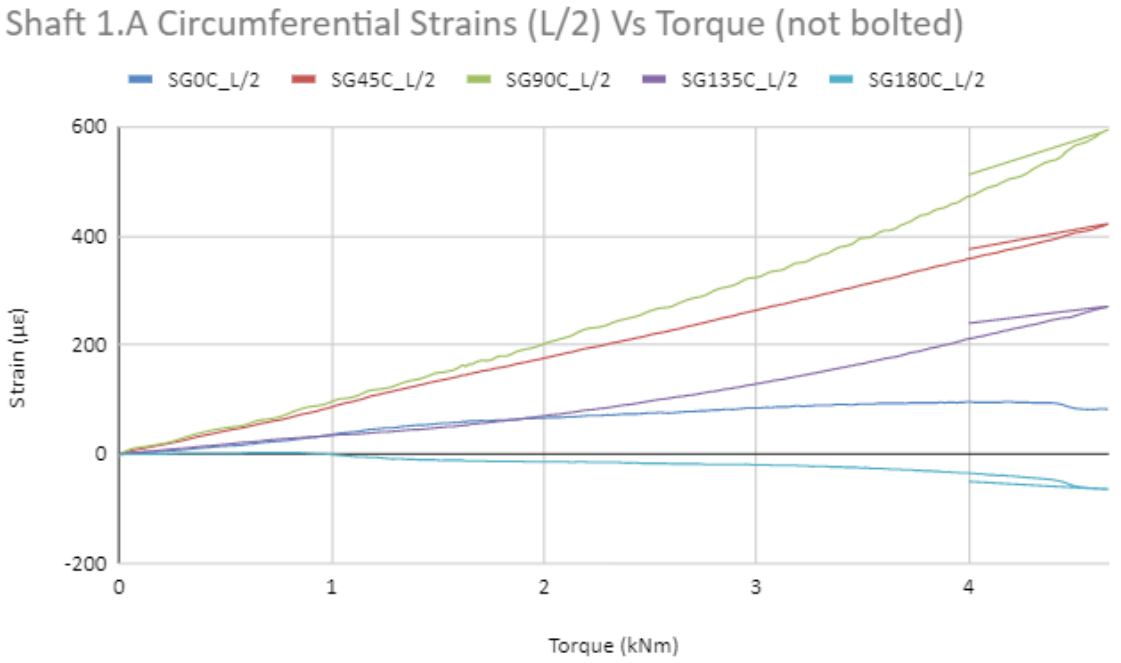

Figure 3.15: Shaft 1.A diagram of Circumferential Strains (L/2)-Torque (not bolted)

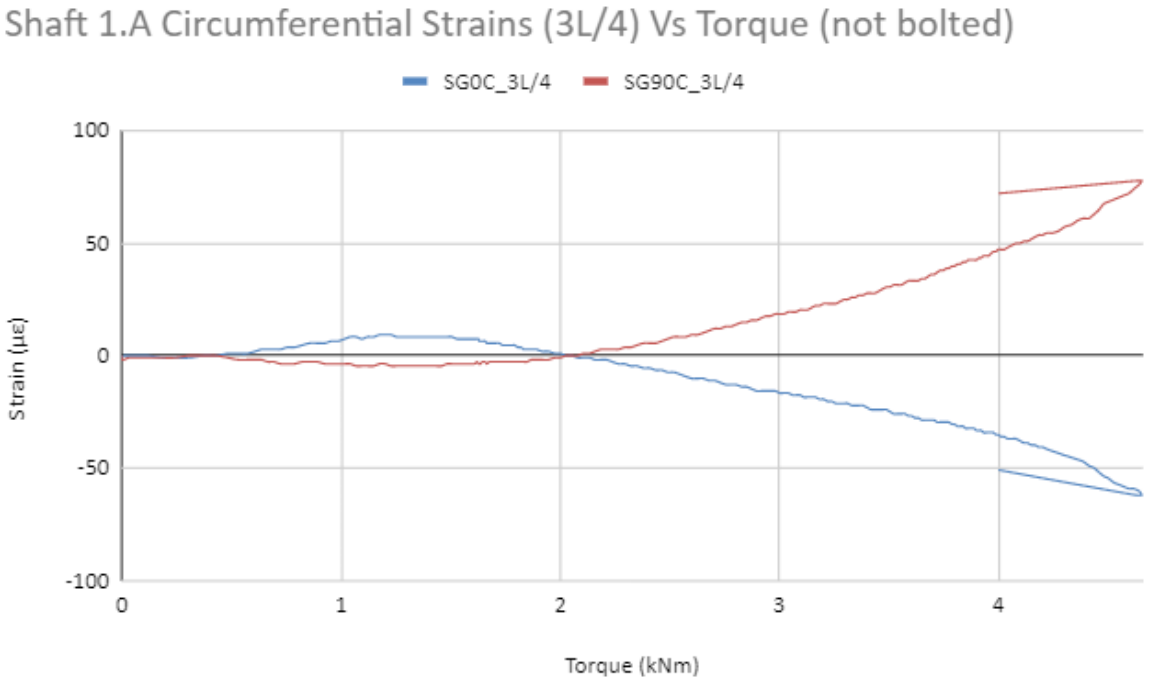

Figure 3.16: Shaft 1.A diagram of Circumferential Strains (3L/4)-Torque (not bolted)

It is obvious that the circumferential strains are tensile to the points of 0, 45, 90, and 135 degrees in the mid-section of the shaft. The same applies to the point of 90 degrees at 3L/4

position. On the other hand, the strains are compressive at the point of 180 degrees in mid-section and at the point of 0 degrees at 3L/4 position. The maximum value is recorded by the SG90C_L/2 strain gage and it is approximately equal to 600 με, while the minimum is recorded by SG180C_L/2 approximately equal to -60 με.

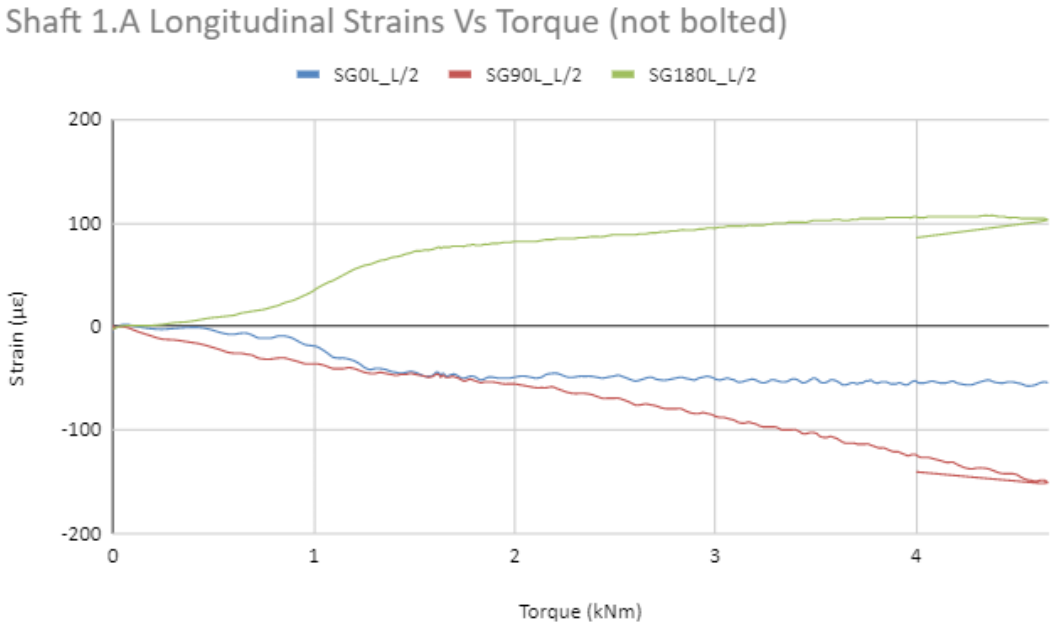

Figure 3.17: Shaft 1.A diagram of Longitudinal Strains-Torque (not bolted)

In Figure 3.17 the longitudinal strains versus torque are shown. It can be seen that they are compressive at 0 and 90 degrees, while, the recorded strains are tensile at 180 degrees. The maximum strain is recorded by strain gage SG180L_L/2, and it is approximately equal to 100 με, while the minimum strain is recorded by SG90L_L/2, approximately equal to -150 με.

3.3.1.2 Shaft 1.A bolted test

Next the corresponding diagrams of shaft 1.A after the placement of the bolts are depicted.

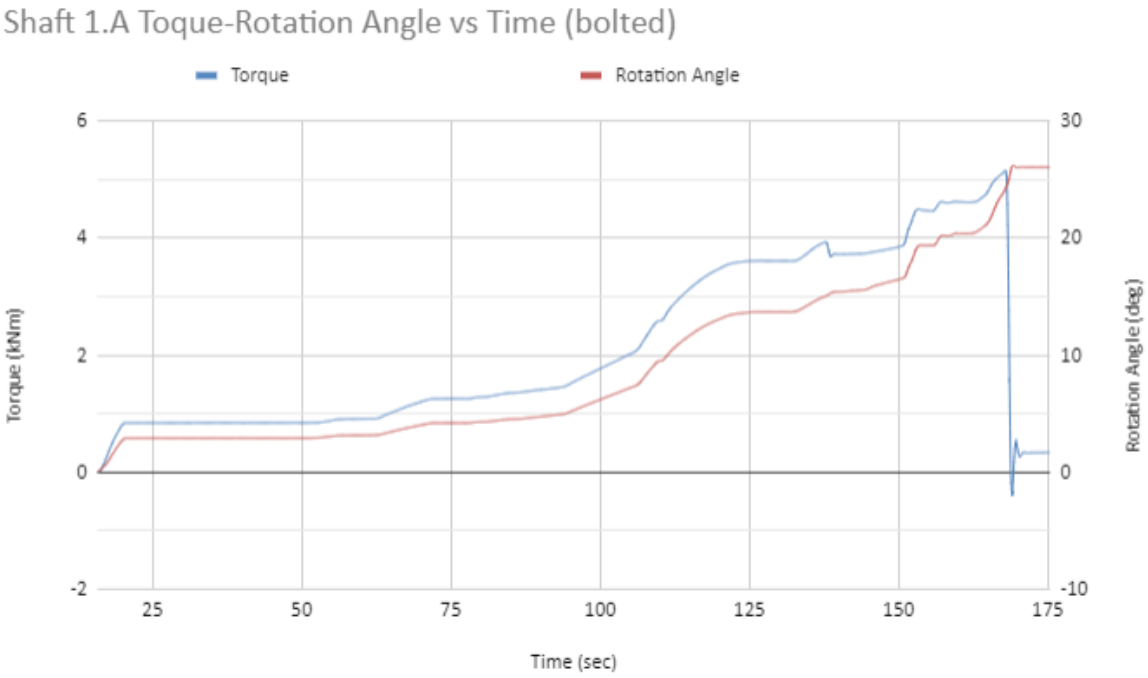

Figure 3.18: Shaft 1.A comparative diagram of Torque-Time and Rotation Angle-Time (bolted)

In Figure 3.18 the comparative diagram of torque and rotation angle versus time is shown. We notice that the angle behaves similarly to the torque in the test of shaft 1.A after placing the bolts. Two critical points must be noted: The first is at time t_{1AB}'= 137.8 sec and it is when a first partial failure occurs. This is reflected on the diagram. The torque value at this point is T_{1AB}'= 3,937 kNm and the angle value is R_{1AB}'= 15.040 deg. The point can be distinguished more easily in the diagrams that are presented later on. However, even after that point, we can notice that the angle follows the path of the torque satisfactorily. The second critical point is that of the final failure of the connection, at time t_{1B}= 168.0 sec. This is when the torque reaches the maximum value of T_{1AB}= 5.154 kNm just like the angle of rotation does, R_{1AB}= 24.307 deg.

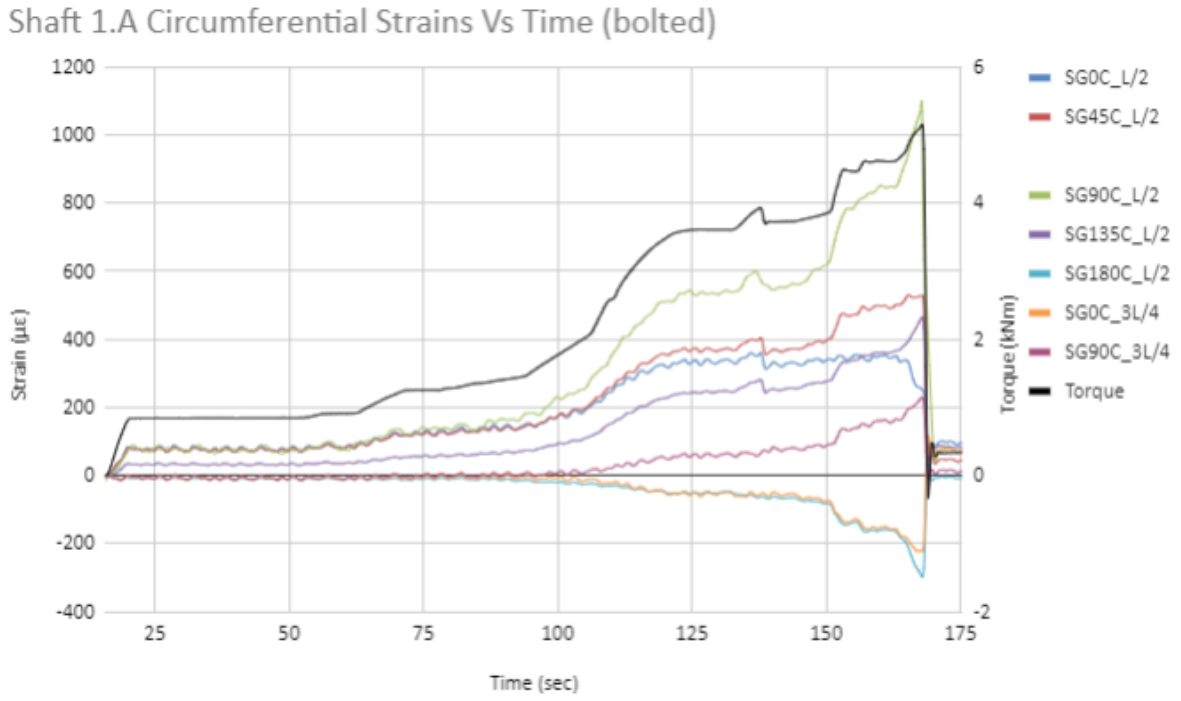

Figure 3.19: Shaft 1.A diagram of Circumferential Strains-Time (bolted)

In Figures 3.19 and 3.20, the circumferential and longitudinal strains versus time diagrams are demonstrated. We can notice that they follow the same path as the torque with respect to time and the point of partial failure, mentioned earlier, is clearly reflected.

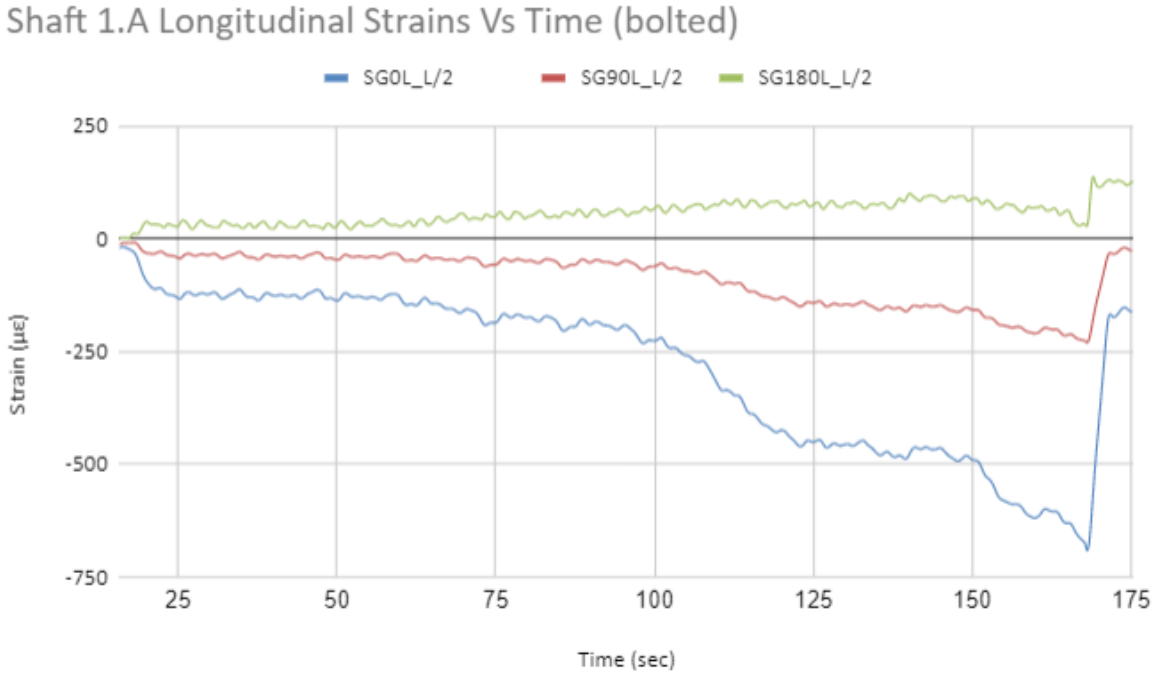

Figure 3.20: Shaft 1.A diagram of Longitudinal Strains-Time (bolted)

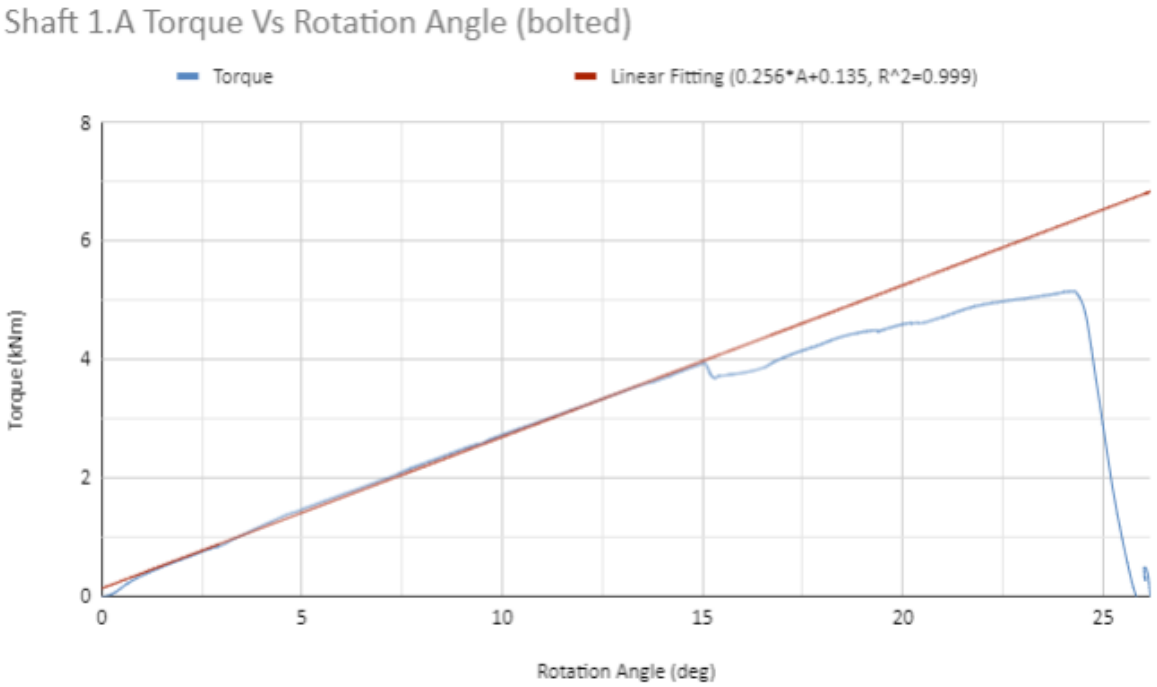

Figure 3.21: Shaft 1.A diagram of Torque-Rotation Angle (bolted)

In Figure 3.21 the diagram of torque versus rotation angle is shown. The point of partial failure, mentioned earlier, can be noticed. We can also see the perfect linear correlation between torque and rotation (R^2= 0.999). From the results of shaft 1.A bolted test we can extract an average torsional stiffness of TS_{1B}= 0.256 kNm/deg (Linear fitting equation: T= 0.256*A+ 0.135).

The circumferential strains vs torque are demonstrated in Figures 3.22 and 3.23.

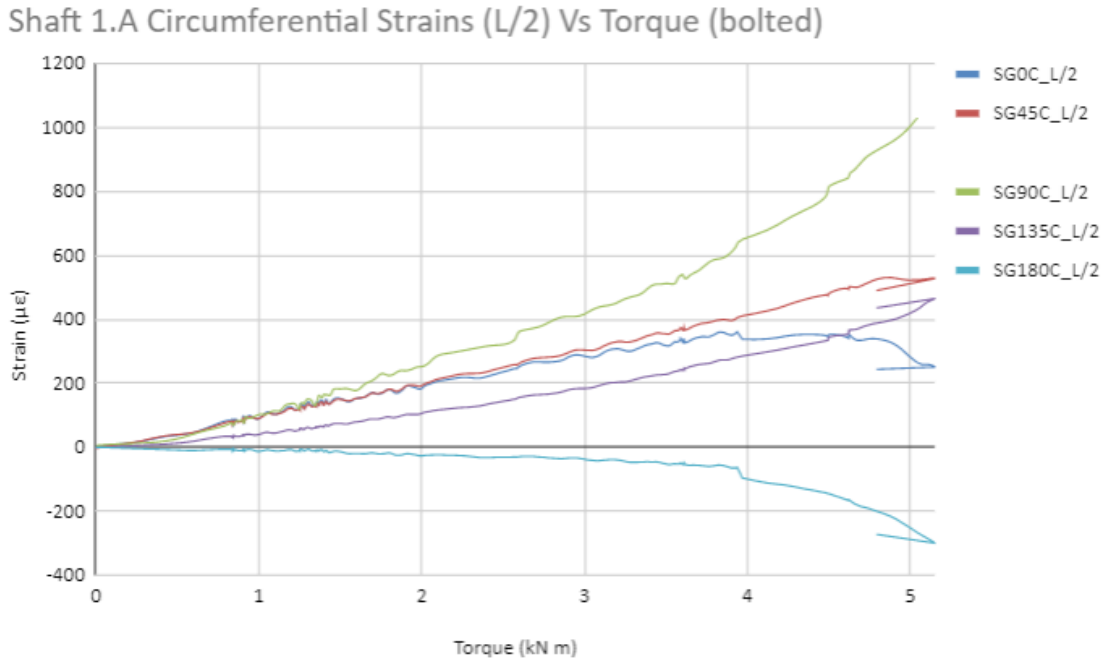

Figure 3.22: Shaft 1.A diagram of Circumferential Strains-Torque (bolted)

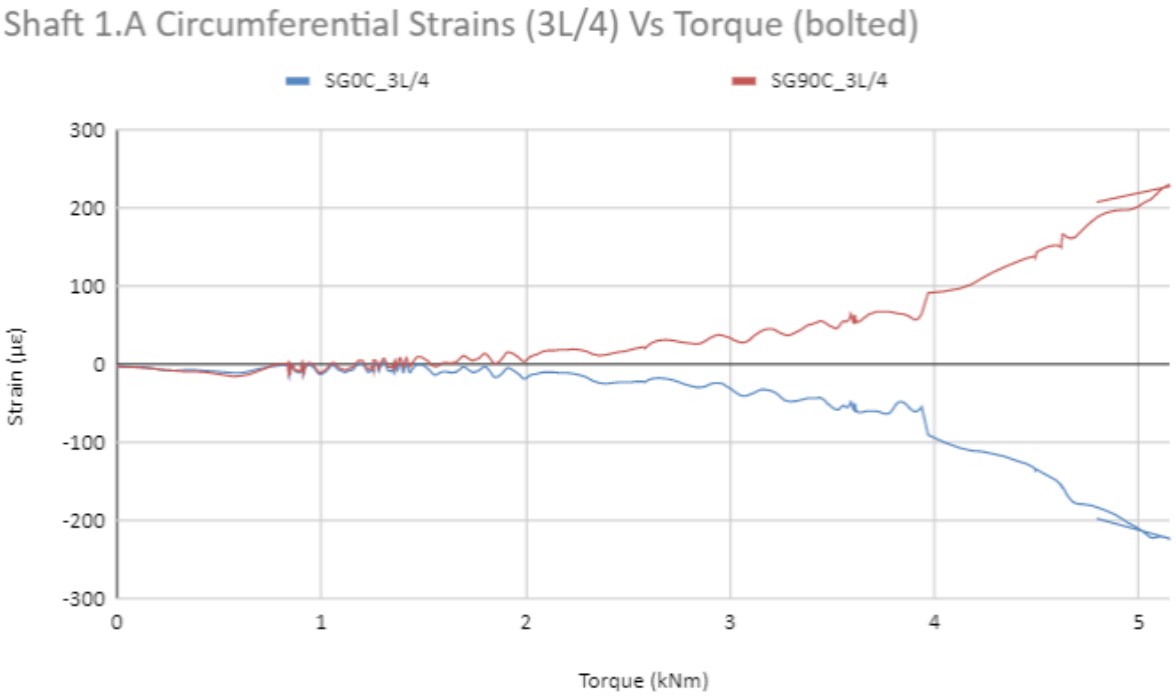

Figure 3.23: Shaft 1.A diagram of Circumferential Strains (3L/4)- Torque

In the diagrams is obvious that the strains are tensile at the points of 0, 45, 90, and 135 degrees at the mid-section of the shaft. The same applies to the point of 90 degrees in position 3L/4. On the other hand, the strains are compressive at the point of 180 degrees in mid-section and also, at 0 degrees at 3L/4. The maximum value is recorded by strain gage SG90C_L/2, reaching approximately 1100 με, while the minimum value is recorded by SG180C_L/2, approximately equal to -300 με.

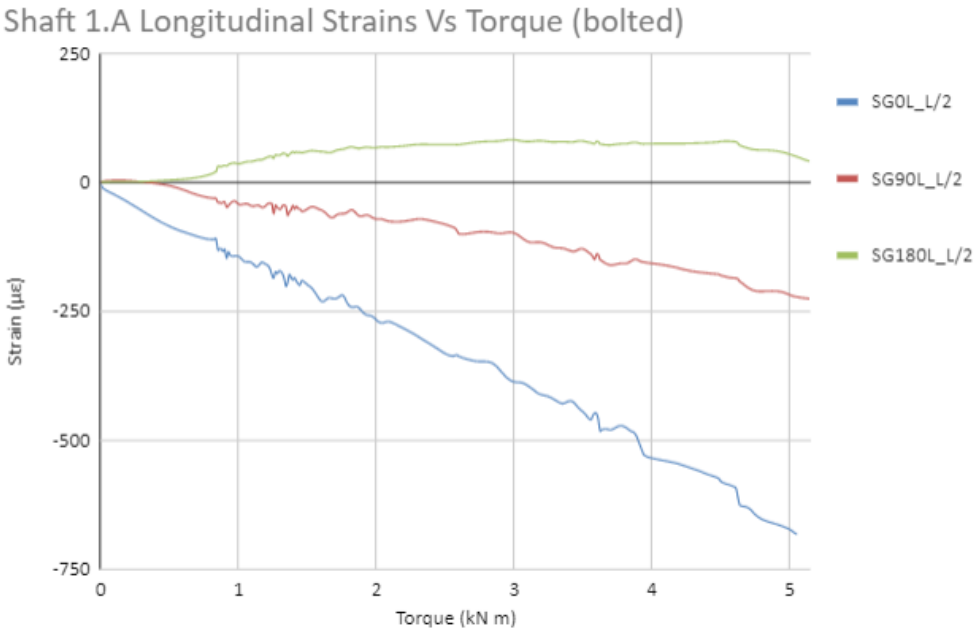

Figure 3.24: Shaft 1.A diagram of Longitudinal Strains-Torque (bolted)

In Figure 3.24 the diagram of longitudinal strains versus torque is presented. It can be seen that the longitudinal strains are tensile at the point of 180 degrees. On the other hand, the strains are compressive at the points of 0 and 90 degrees. The maximum strain is recorded by strain gage SG180L_L/2 almost exceeding the value of 100 με, while the minimum is recorded by SG90L_L/2 approximately equal to -700 με.

3.3.1.3 Shaft 1.A comparative study and modeshape estimation

In a first attempt of a comparative study of the measurements before and after the installation of the bolts, the paths of the torque versus time of both tests are presented in the same diagram. In Table 3.3 the maximum absolute values of strains are presented as recorded on both experiments of shaft 1.A. The minus demonstrates that the specific strain is compressive.

Table 3.3: Maximum strain values for both experiments of shaft 1.A

Strain (με)	Circ.	SG0C_L/2	SG45C_L/2	SG90C_L/2	SG135C_L/2	SG180C_L/2
	Bolted	360.923	530.769	1112.308	465.231	-0.923
	Not bolted	96.000	421.846	594.462	270.462	-63.692
	Long.	SG0L_L/2		SG90L_L/2		SG180L_L/2
	Bolted	8.308		13.846		87.692
	Not bolted	-57.231		-151.385		107.077
	3L/4	SG0C_3L/4		SG90C_3L/4		
	Bolted	2.769		229.846		
	Not Bolted	-61.846		77.538		

Figure 3.25: Shaft 1.A comparative diagram of Torque-Rotation

Some interesting comparative observations can be made from the previous analysis and the diagram in Figure 3.25 (Torque vs Rotation comparison). Most importantly, in the case of shaft 1.A the placement of the bolts doesn't help much to achieve a higher level of torque. On the other hand, it leads to higher levels of strains and maximum angle of rotation. The placement of the bolts resulted in increasing the active length of shaft 1.A almost 4%. An increase to the active length leads to a reduce to the torsional stiffness. Due to this fact, there has been a 24.7% torsional stiffness reduction due to the installation of the bolts. The shaft before and after mounting the bolts is subjected to the same type of deformation at the same points. We conclude this from the fact that the sensors that were initially recording tensile strains they do so after the shaft bolting. The same applies to those that were compressed. Furthermore the Strain Gages that initially recorded the highest strains, they also do so after the bolts fitting. Note that, in the bolted test, the end that failed was not the one that failed before the installation of the bolts.

The shaft demonstrated on both tests a perfect linear behaviour. The first indication that the recorded strains give, is that the shaft is probably going to buckle in type-2 modeshape, i.e formation of two crests and two troughs around the circumference. More specifically, from the diagram of shaft 1.A in Figure 3.15 we notice that SG90C_L/2 strain gage records the maximum strains (tensile strains) with an increasing tendency. This is an indication that this strain gage is close to a crest. On the other hand, the strain gages at 0 and 180 degrees in mid-section present particular interest. The 0 degrees line is tensile and the 180 degrees compressive, however, they both record low values of strains. Furthermore, both lines have a compressive tendency (both lines are curved downwards). This indicates that both gages are in the areas of troughs. For the gages SG45C_L/2 and SG135C_L/2 we notice that both record tensile strains with increasing tensile tendency (curved upwards), while, the gage at 45 degrees is recording higher values than the gage at 135 degrees, which indicates that they are

both located in a crest area, not that close as SG90C_L/2. The next figure is a schematic view of the cross section at the middle of the shaft, suggesting the location of each strain gage with respect to a type-2 buckling modeshape of shaft 1.A. In Figure 3.26 the red circle indicates the cross section at the middle of the shaft before buckling occurs.

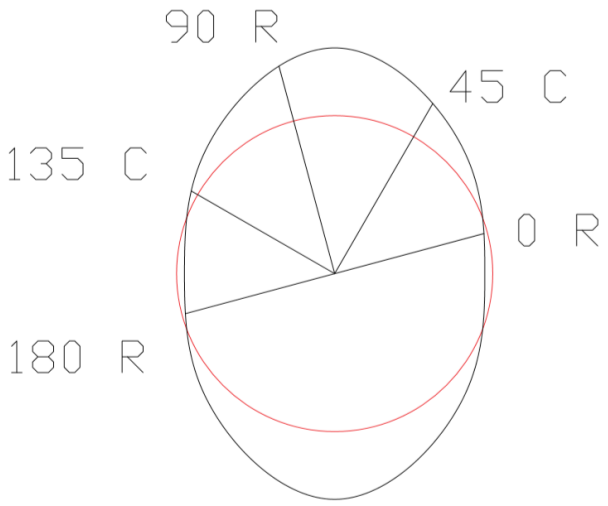

Figure 3.26: Modeshape 2 of shaft 1.A

3.3.2 Shaft 1.B experimental data analysis

3.3.2.1 Shaft 1.B non-bolted test

The same course of study is followed for shaft 1.B. In Figure 3.26 a comparative diagram of the torque and rotation with respect to time is presented.

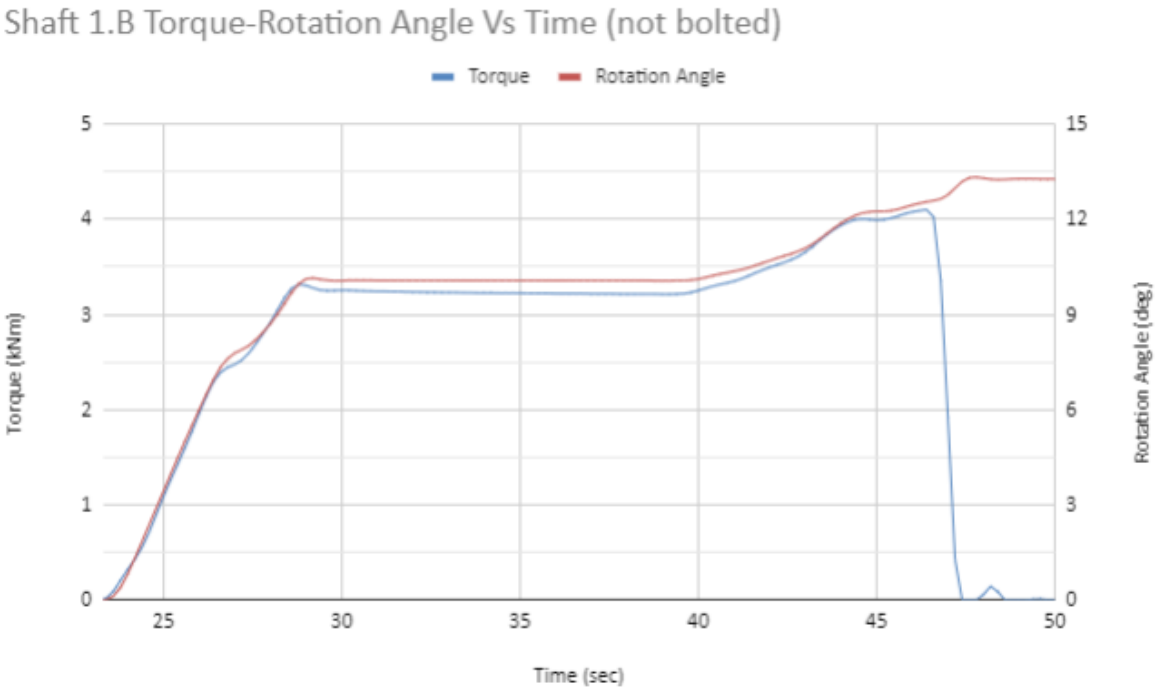

Figure 3.27: Shaft 1.B comparative diagram of Torque-Time & Rotation Angle-Time (not bolted)

In Figure 3.27 we can easily notice that the rotation angle exhibits the same behaviour as the torque versus time during the not bolted test. The critical point in this diagram is the failure point between the flange and the composite at time t_{1BNB}= 46.4 sec. The torque reaches the maximum value of T_{1BNB}= 4.101 kNm and the angle value is R_{1BNB}= 12.549 deg.

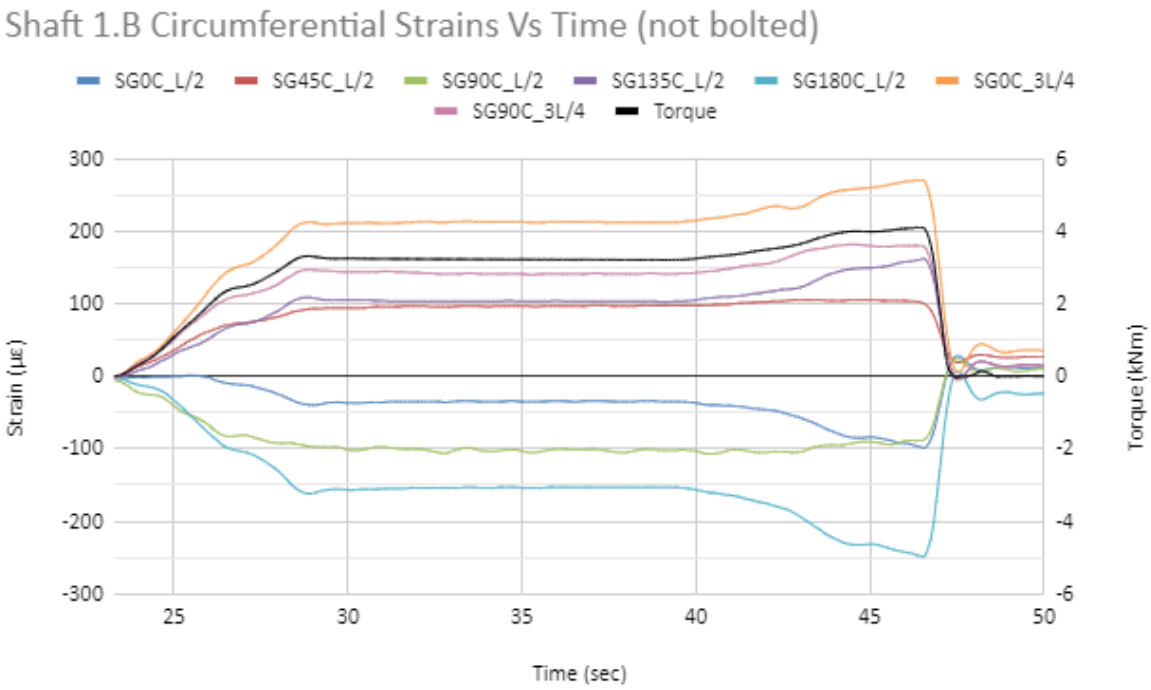

Figure 3.28: Shaft 1.B diagram of Circumferential Strains-Time

In figures 3.28 and 3.29 the diagrams of the circumferential and longitudinal strains versus time are presented. They all follow the same path as the torque, as a function of time.

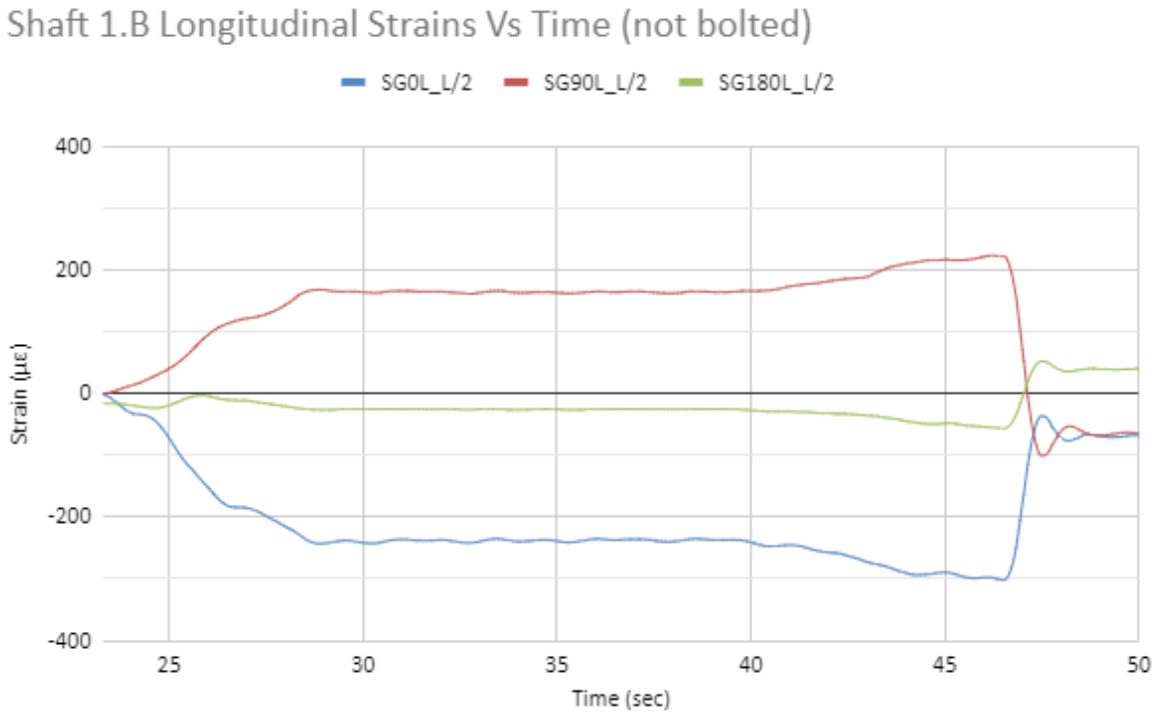

Figure 3.29: Shaft 1.B diagram of Longitudinal Strains- Time (not bolted)

Next, the diagrams of torque versus rotation and strains versus torque are demonstrated.

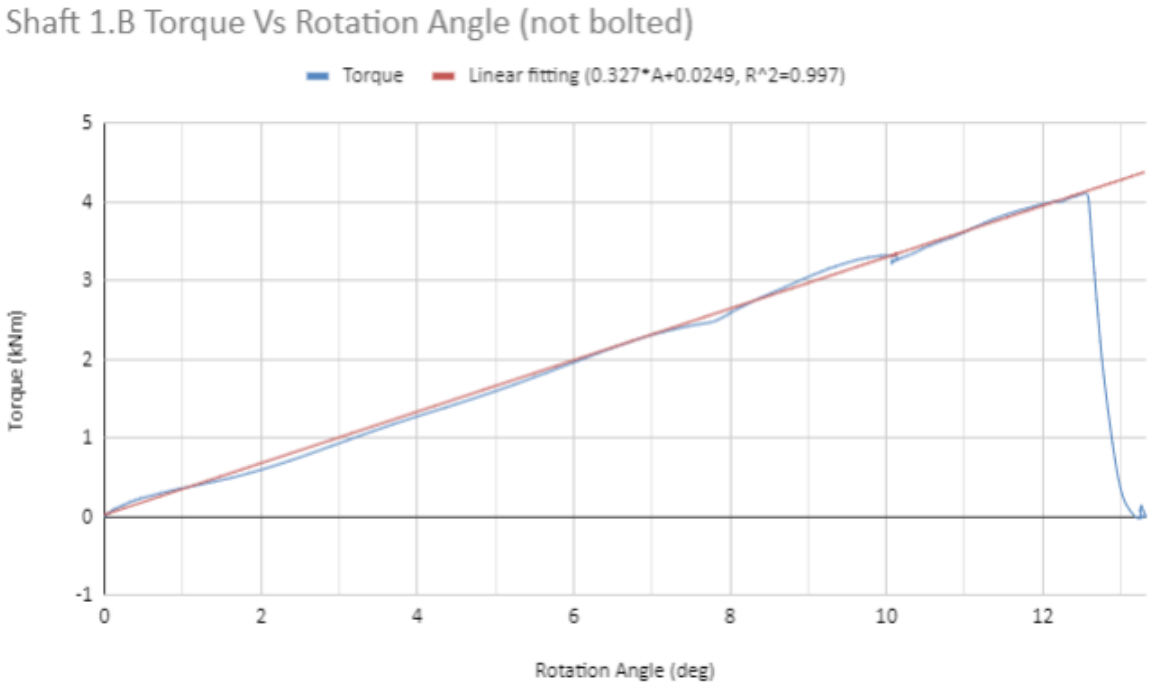

Figure 3.30: Shaft 1.B diagram of Torque-Rotation (not bolted)

In Figure 3.30 the diagram of torque versus rotation angle is presented. We can notice the perfect linear correlation between the torque and the angle of rotation (R^2=0.997). From the

data of the not bolted test of shaft 1.B we can obtain the average torsional stiffness of TS_{1BNB}= 0,327 kNm/deg (Linear Fitting equation: T= 0.327*A+0.0249).

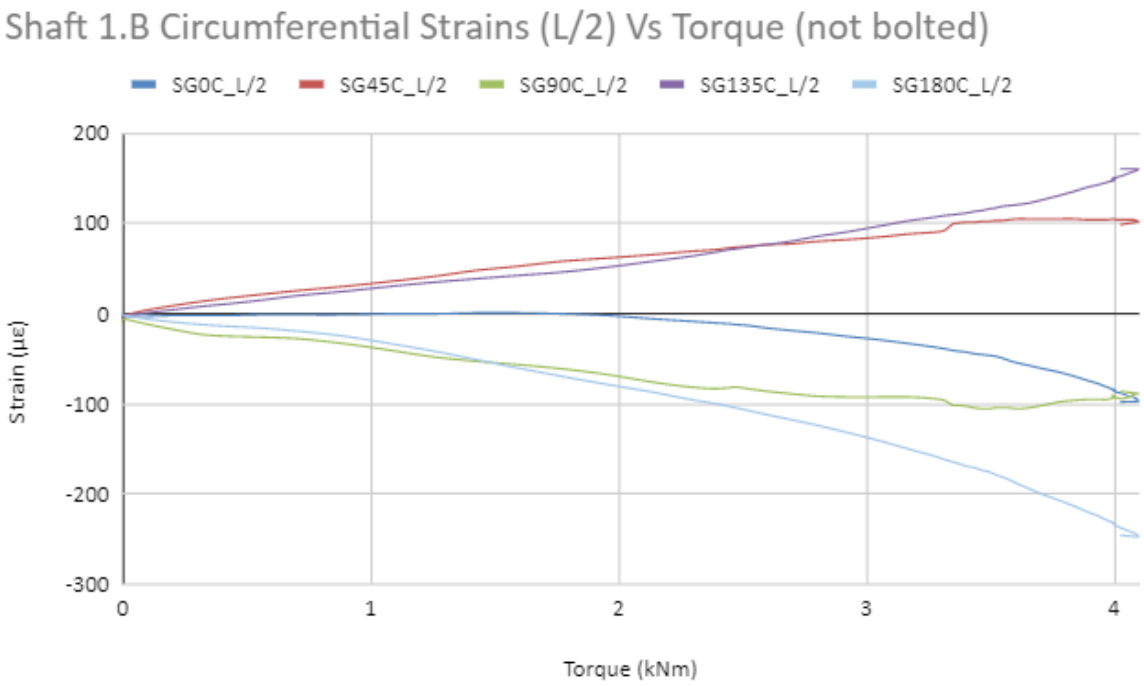

Figure 3.31: Shaft 1.B diagram of Circumferential Strains-Torque (not bolted)

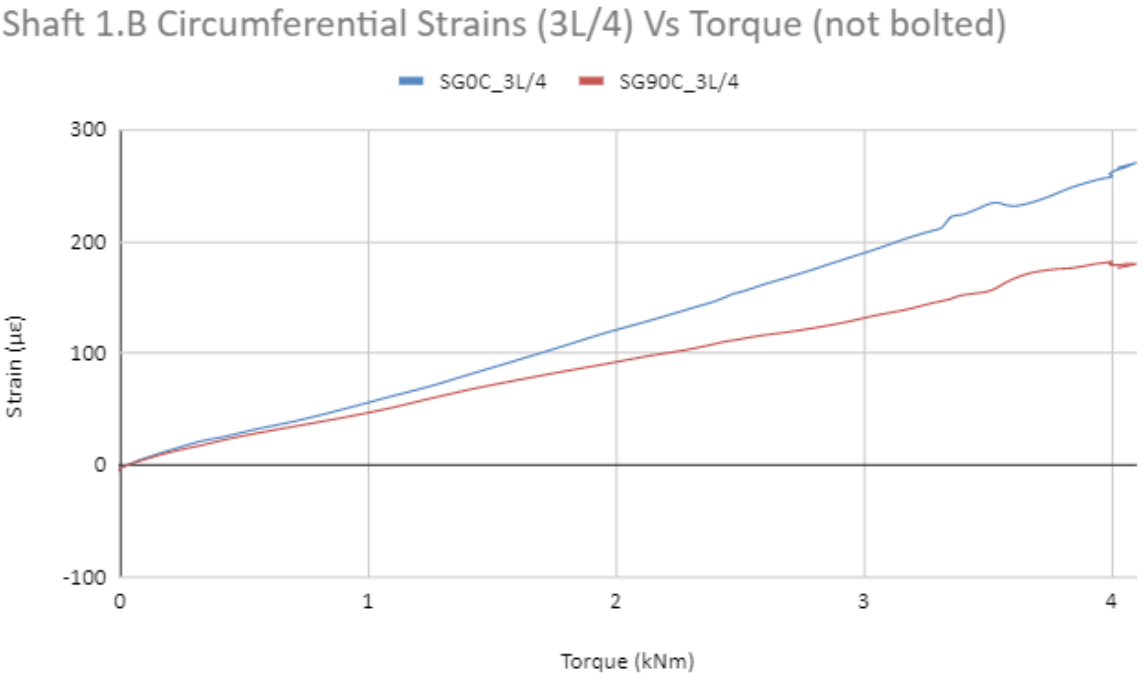

Figure 3.32: Shaft 1.B diagram of Circumferential Strains Vs Torque (not bolted)

In Figures 3.31 and 3.32 the diagrams of circumferential strains versus torque are demonstrated. It is shown that the recorded strains are tensile at the points of 135 and 45 degrees at L/2 position just like at the points of 0 and 90 degrees at 3L/4 position. On the

other hand, the circumferential strains are compressive at the points of 0, 90 and 180 degrees at L/2 position. The maximum value is recorded by strain gage SG0C_3L/4 and it exceeds 250 με, while the minimum value is recorded by SG180C_L/2 and it is approximately equal to -250 με.

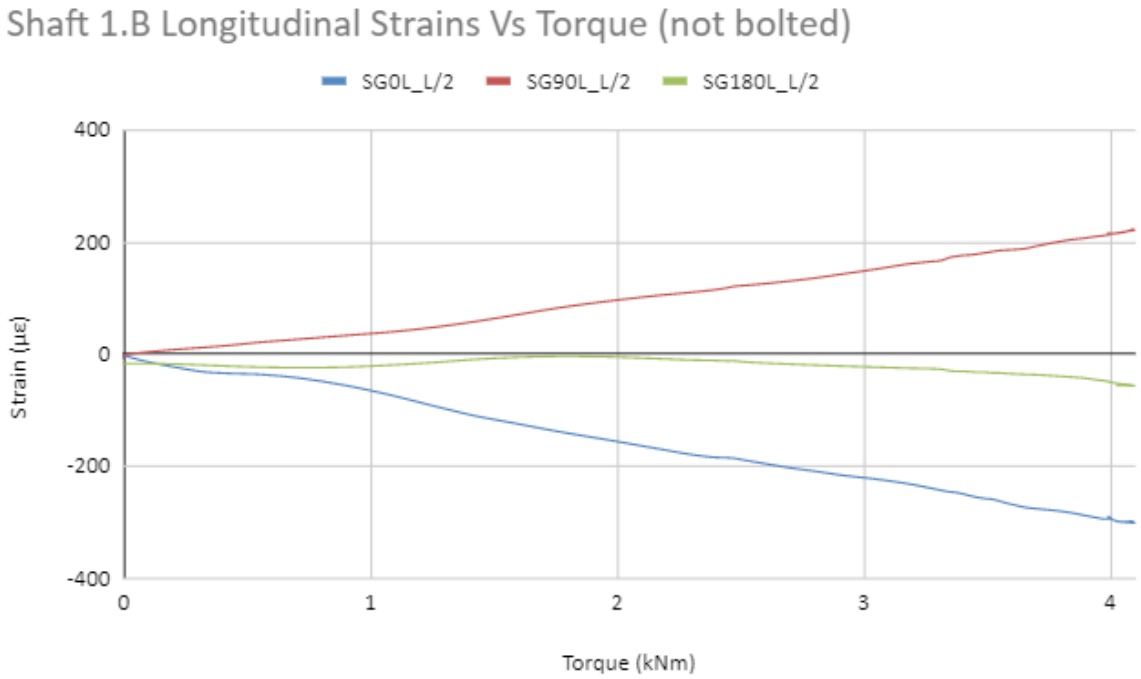

Figure 3.33: Shaft 1.B diagram of Longitudinal Strains-Torque (not bolted)

In Figure 3.33 the diagram of longitudinal strains versus torque is demonstrated. It shows that the recorded strains are tensile at the point of 90 degrees and compressive at the points of 0 and 180 degrees in the mid-section of shaft 1.B. The maximum value is recorded by strain gage SG90L_L/2 exceeding 200 με, while the minimum is recorded by SG0L_L/2 and it is approximately equal to -300 με.

3.3.2.2 Shaft 1.B bolted test

Next, the diagrams of shaft 1.B after the bolts fitting are presented.

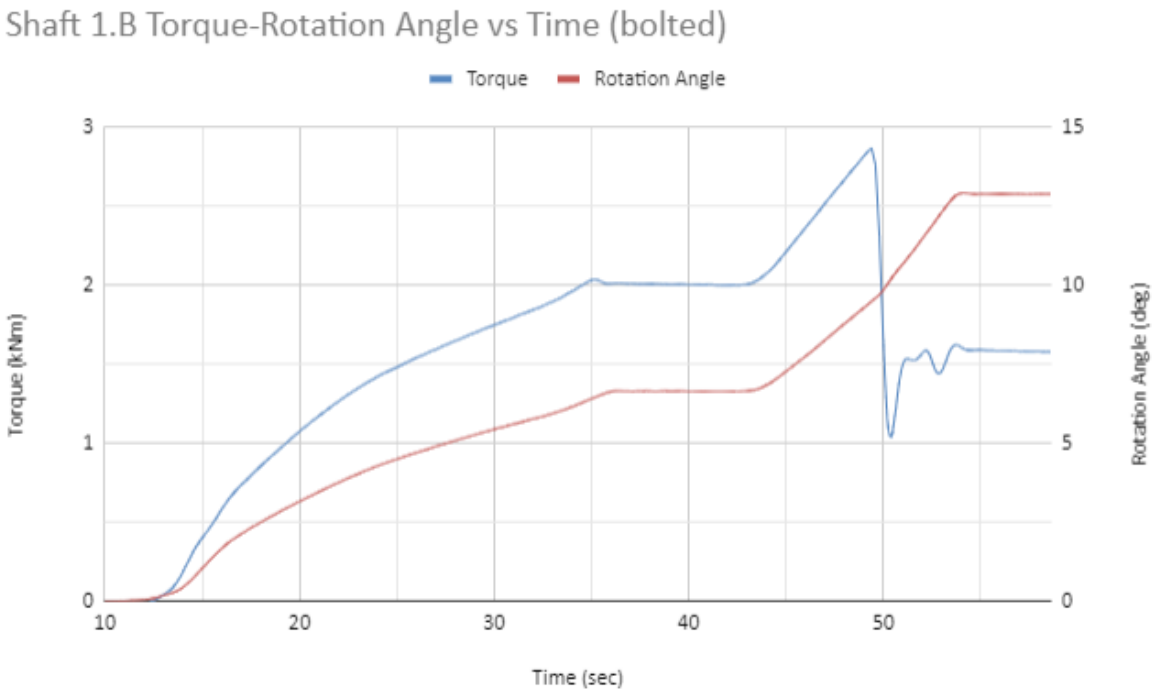

Figure 3.34: Shaft 1.B comparative diagram of Torque-Time & Rotation Angle-Time (bolted)

In Figure 3.34 the comparative diagram of torque and rotation angle versus time is illustrated. It shows that the angle follows the same path as the torque as a function of time for shaft 1.B bolted experiment. Two critical points are noticed on this test: The first is found at time t_{1BB}'= 35.2 sec when a first partial failure of the bonding, between the flange and the composite, occurs and it is reflected in the diagram. The torque value at this point is T_{1BB}'= 2.033 kNm and the rotation angle value is R_{2B}'= 6.453 deg. This point is easier to notice in the next diagrams. However, even after that point we can notice that the angle exhibits the same behaviour as the torque satisfactorily. The second point is the final breakdown of the connection at time t_{1BB}= 49.4 sec. It is when the torque reaches the maximum value of T_{1BB}= 2.864 kNm, while the angle reaches the value of R_{1BB}= 9.480 deg.

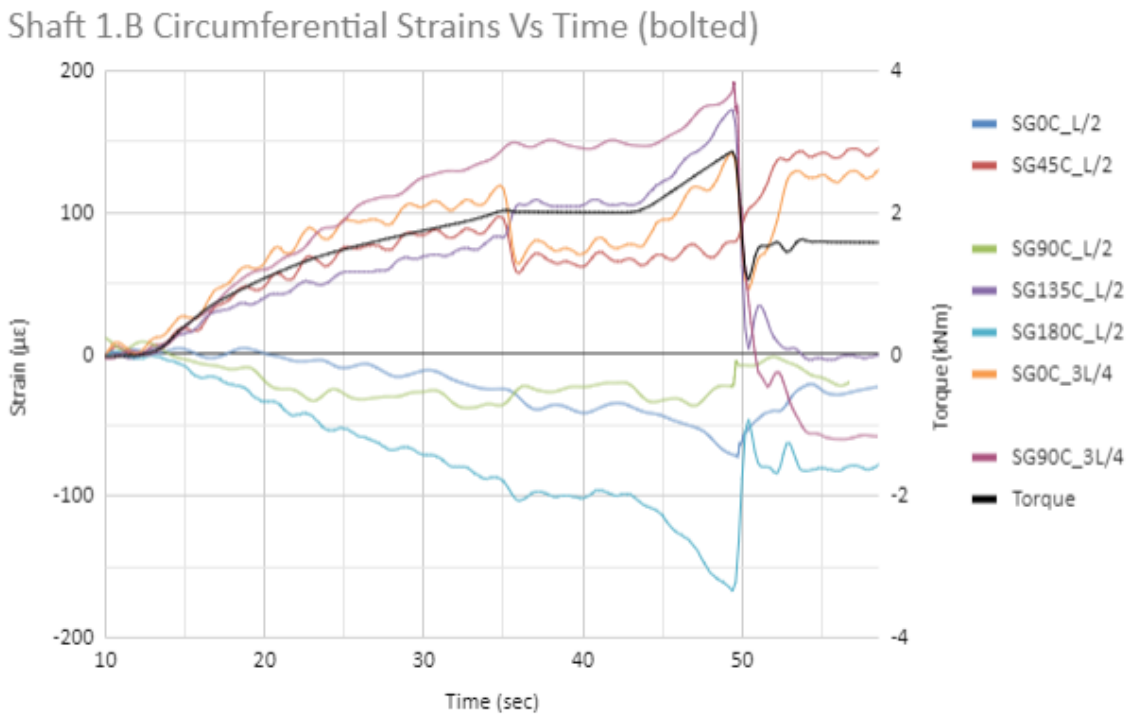

Figure 3.35: Shaft 1.B diagram of Circumferential Strains-Time (bolted)

In Figure 3.35 we can see the course of the circumferential strains versus time. We can notice that they follow the course of the applied torque and the point of partial failure, mentioned earlier, is clearly reflected. This is also evident in the diagram of the longitudinal deformations, as shown in Figure 3.36. It must be noted that in this case the diagrams are more "wavy" than the previous diagrams due to the fact that they were not cleared from the noise as much as the previously. They were not cleared enough, in order to make the point of the partial failure more perspicuous.

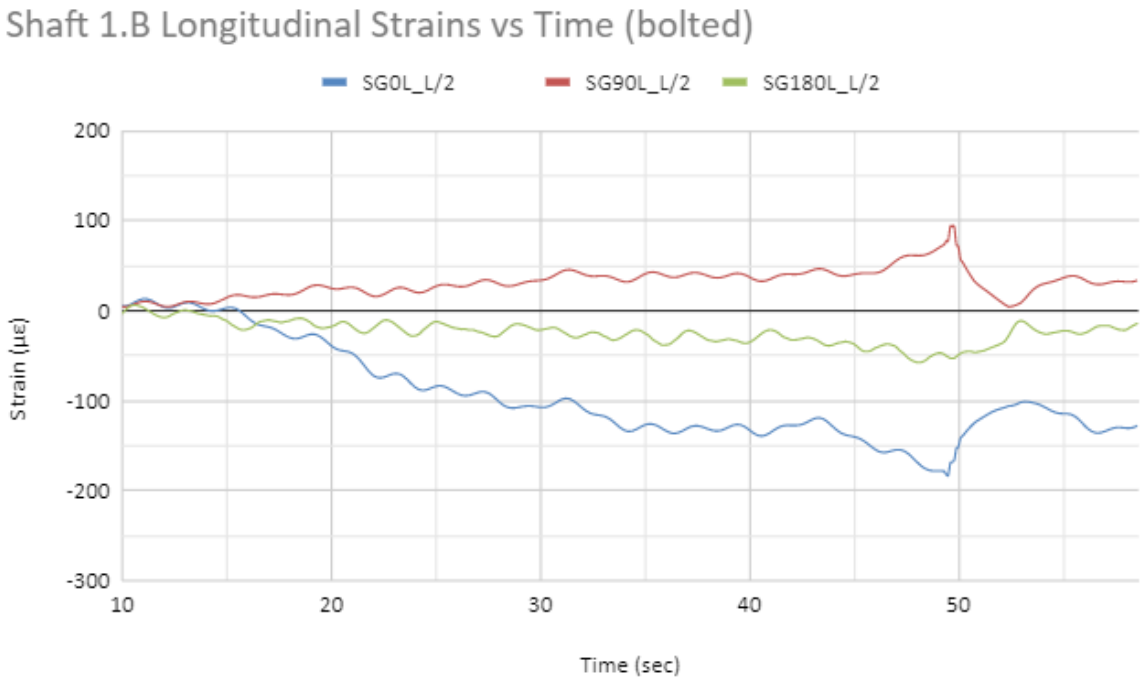

Figure 3.36: Shaft 1.B diagram of Longitudinal Strains -Time (bolted)

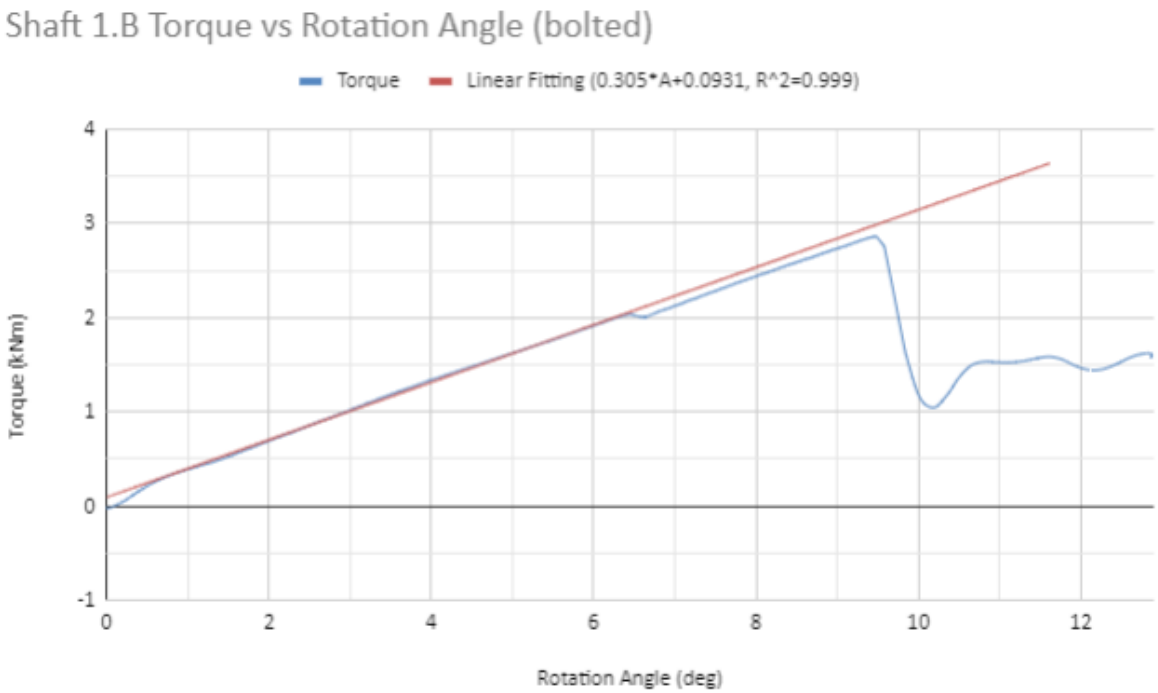

Figure 3.37: Shaft 1.B diagram of Torque-Rotation (bolted)

In Figure 3.37 the diagram of torque versus rotation is demonstrated. The point of the partial failure, we mentioned earlier, is clearly reflected. The diagram shows the perfect linear correlation between the torque and angle (R^2= 0.999) even after the point of the first failure of the connection. From the results of the bolted test we can obtain an average torsional stiffness of TS_{1BB}= 0.305 kNm/deg. (linear fitting equation: T= 0.305*A+0.0931).

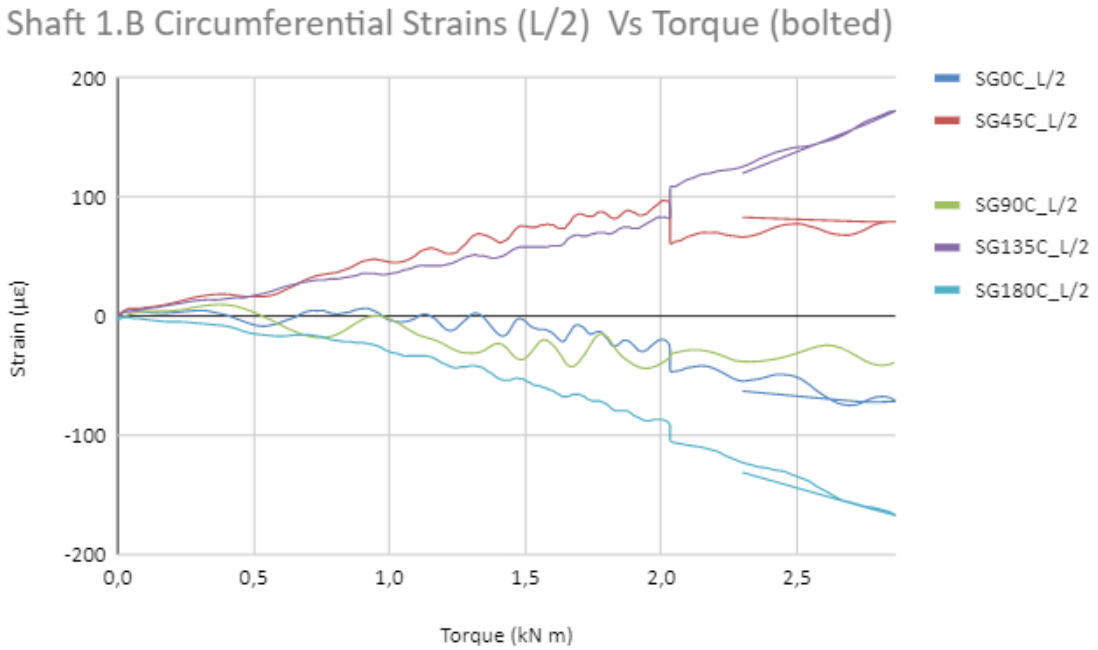

Figure 3.38: Shaft 1.B diagram of Circumferential Strains-Time (bolted)

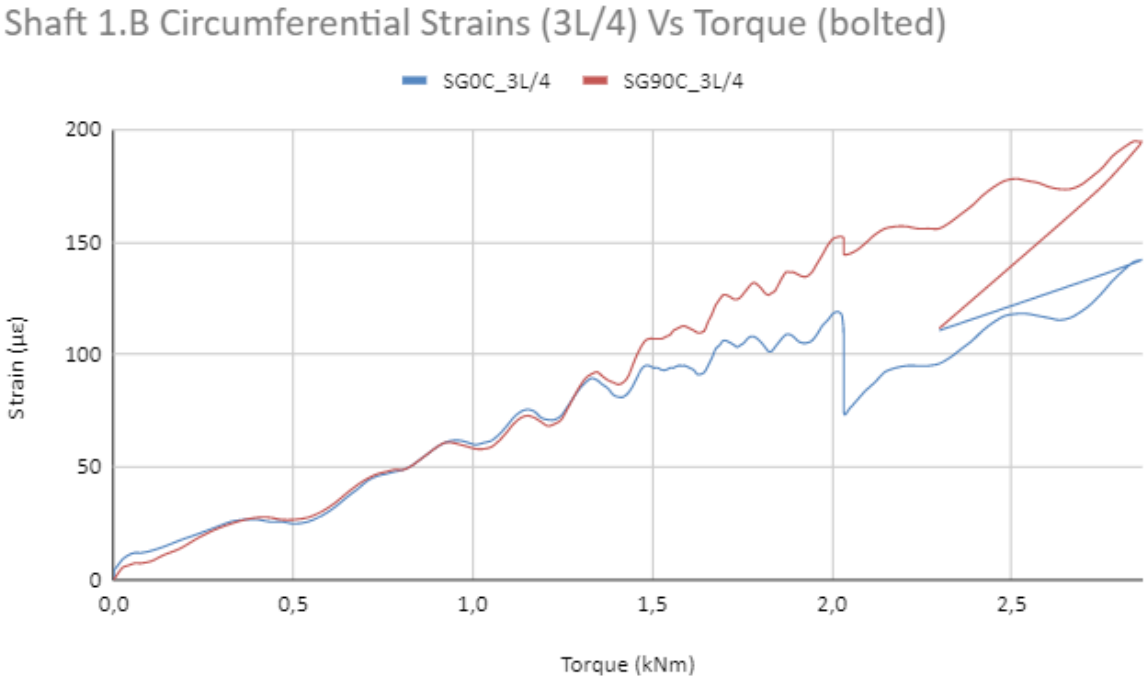

Figure 3.39: Shaft 1.B diagram of Circumferential Strains (3L/4)-Torque (bolted)

In Figures 3.38 and 3.39 the circumferential strains versus torque diagrams are presented. The strains are tensile at the points of 135 and 45 degrees in mid-section and at 0 and 90 degrees at 3L/2 position. On the other hand, the strains are compressive at 0, 90 and 180 degrees in mid-section. The maximum value is recorded by Strain Gage SG0C_3L/4 and it is almost equal to 150 με, at the partial failure and almost 200 με, at the final failure. The minimum

value is recorded by SG180C_L/2 approximately equal to -100 με, at the point of the partial failure, and exceeds -150 με in total failure.

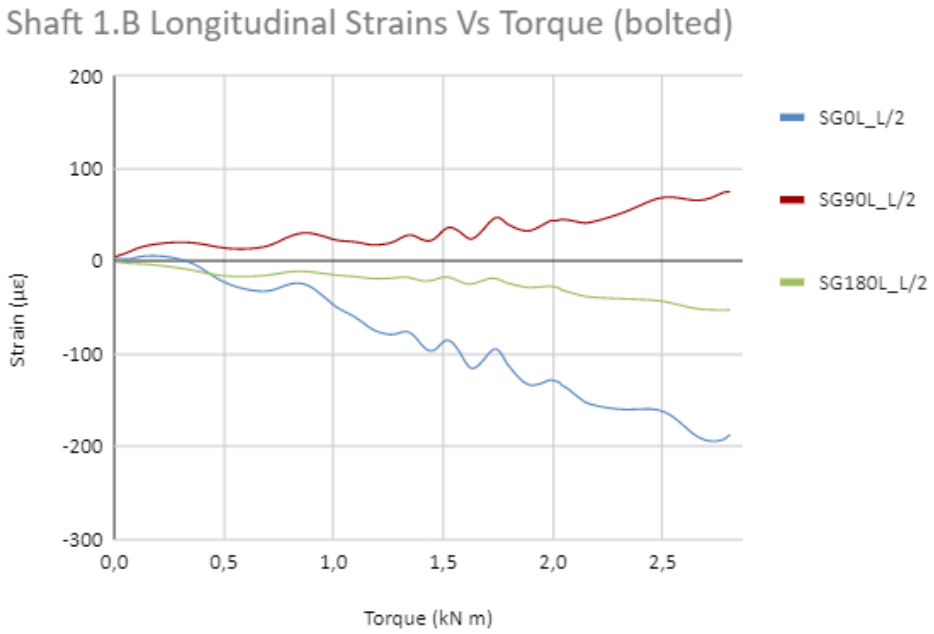

Figure 3.40: Shaft 1.B diagram of Longitudinal Strains-Torque (bolted)

In Figure 3.40 the longitudinal strain versus torque diagram is shown. The strains are tensile at the point of 90 degrees and compressive at the points of 0 and 180 degrees in mid-section of the shaft. The maximum strain is recorded by SG90L_L/2 exceeding 50 με, while the minimum is recorded by SG0L_L/2 approximately equal to -200 με.

3.3.2.3 Shaft 1.B comparative study and modeshape estimation

From the previous analysis and the diagram in Figure 3.41 we can make some comparative observations. In table 3.4 the maximum strains are presented, as recorded on both experiments of shaft 1.B. The minus demonstrates that the strain is compressive.

Table 3.4: Maximum strain values for both experiments of shaft 1.B

Strain (με)	Circ.	SG0C_L/2	SG45C_L/2	SG90C_L/2	SG135C_L/2	SG180C_L/2
	Bolted	-74.769	96.923	-68.308	172.615	-167.077
	Not bolted	-97.846	105.231	-105.231	160.615	-247.385
	Long.	SG0L_L/2		SG90L_L/2		SG180L_L/2
	Bolted	220.615		104.308		-57.231
	Not bolted	-300.923		222.462		-56.308
	3L/4	SG0C_3L/4			SG90C_3L/4	
	Bolted	142.154			194.769	
	Not Bolted	270.462			181.846	

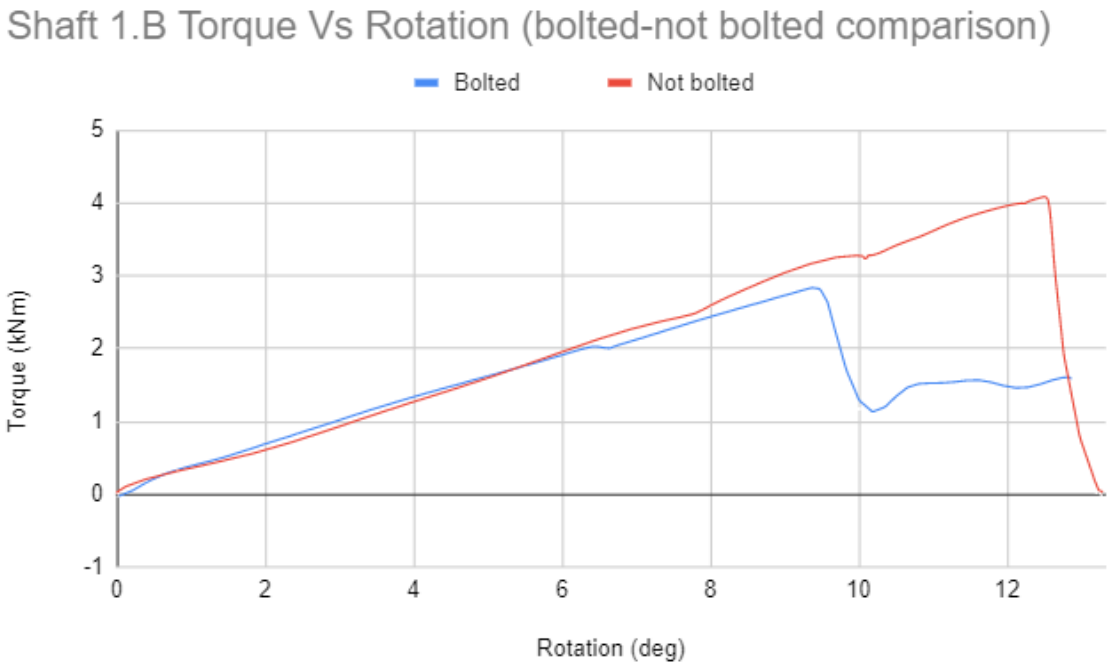

Figure 3.41: Shaft 1.B comparative diagram of Torque-Angle

In Figure 3.41 the torque versus rotation diagram is shown for shaft 1.B in both bolted and not bolted tests. The most important conclusion is that the placement of the bolts does not help at all the flange-metal connection to achieve a higher level of torque. Also, it significantly reduces the values of the total strains. The same applies to the final maximum torque and rotation angle of failure. The way the bolts were placed "weakened" the material locally, reducing, therefore, the strength of the connection in torsion. In the case of shaft 1.B the bolts placement resulted in a 6.7% torsional stiffness reduction while the active length

increased almost 2.9%. However, the shaft before and after mounting the bolts is deformed in the same way, i.e. the sensors that initially recorded tension, they still do so after the bolts fitting. The same applies to those which recorded compressive strains. At the same time, the Strain Gages that initially recorded the highest strains, they still record the highest strains after the placement of the bolts.

As we notice, from the analysis we did on both tests, shaft 1.B exhibits a perfectly linear behaviour. The first indication, the recorded strains give, is that the shaft is probably going to buckl in type-2 modeshape. By exploiting the information from the diagrams of both tests of 1.B shaft, we can end up to certain conclusions and a suggestion for the location of the strain gages, on the modeshape of the shaft. We can notice that we did not manage to put any strain gage close to an area of trough or crest. On both bolted and not bolted tests the strains recorded by the strain gages at 0, 90 and 180 degrees are overall compressive. However, there is a difference on the course each line takes versus torque. Both gages at 0 and 180 degrees record strains with compressive tendency (lines curved downwards). On the other hand, at 90 degrees the recorded strain line has a tensile tendency (line curved upwards), with low values of recorded strains. Although the 90 degrees gage records higher absolute values of strain than 0 and 180 degrees at the beginning of the test, it ends up recording lower absolute values of strain. The indication given by these facts is that 0 and 180 degrees are on the wider trough area of the type-2 modeshape and the gage of the 90 degrees is on a wider crest area and a bit closer to the area where the deformation changes from trough to crest. An exactly opposite indication is given by the 45 degrees gage. The strains recorded by this gage are overall tensile but the line has a compressive tendency (line curved downwards). The 45 degrees gage records higher strains than 135 gage, but it ends up recording lower strains. This fact indicates that the 45 degrees gage is on the wider trough area close to the area where the deformation changes from crest to trough. Lastly, the 135 degrees line is overall tensile with an increasing tendency (line curved upwards) with strain values close to 45 degrees gage. This indicates that the 135 is on a wider crest area. In Figure 3.42, is a schematic view of the cross section at the middle of the shaft and suggests the location of each strain gage on the type-2 buckling modeshape of shaft 1.B.

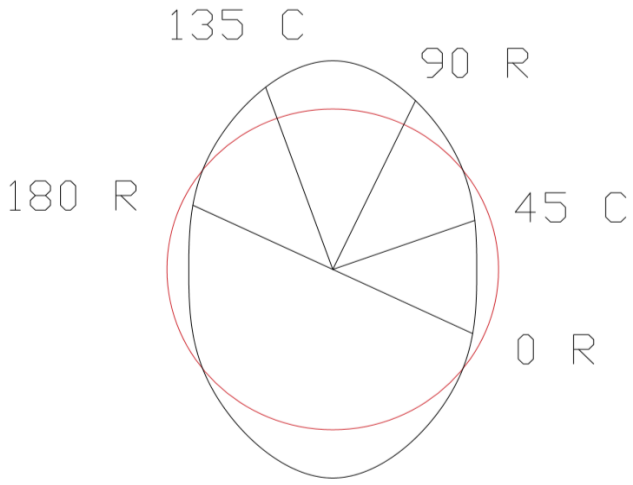

Figure 3.42: Modeshape 2 of shaft 1.B

3.3.3 Shaft 1.A & 1.B data summary and conclusions

In table 3.5 there is a summary table that includes all the important data recorded from the tests. The magnitude T demonstrates the torque, the magnitude R demonstrates the angle of rotation, while TS demonstrates the torsional stiffness. The magnitudes T′ and R′ are the points of partial failure of the connection after the placement of the bolts.

Table 3.5: Summary table for shafts 1.A & 1.B

Shaft	Not bolted			Bolted				
	T (kNm)	R (deg)	TS (kNm/deg)	T′ (kNm)	T (kNm)	R′ (deg)	R (deg)	TS (kNm/deg)
1.A	4.659	13.500	0.340	3.937	5.154	15.040	24.307	0.256
1.B	4.101	12.549	0.327	2.033	2.864	6.453	9.480	0.305

Shaft 1.A is nominally identical to 1.B in every aspect (lay-up diagram, geometrical dimensions, end fitting configuration). However, as it is shown in table 3.5 at the not bolted experiments, shaft 1.B failed at 4.101 kNm, a value almost 12 % lower than the torque reached by shaft 1.A. On the other hand, the torsional stiffness reached in shaft 1.B experiment is 3.8 % lower than the torsional stiffness of shaft 1.A which is a much lower deviation. This shows that the composite parts of the shafts behave almost the same in torque. Taking into consideration that they both failed in flange area in addition with the aforementioned torque deviation, it can be concluded that the initial adhesive bonding between metal and composite was of dubious quality and inadequate. The strain values cannot be compared between the two shafts, due to the fact that the strain gages were not bonded at the same circumferential position with respect to the buckling modeshape. In Figure 3.43 the torque versus rotation comparison of the two unbolted shafts, is shown in the same diagram.

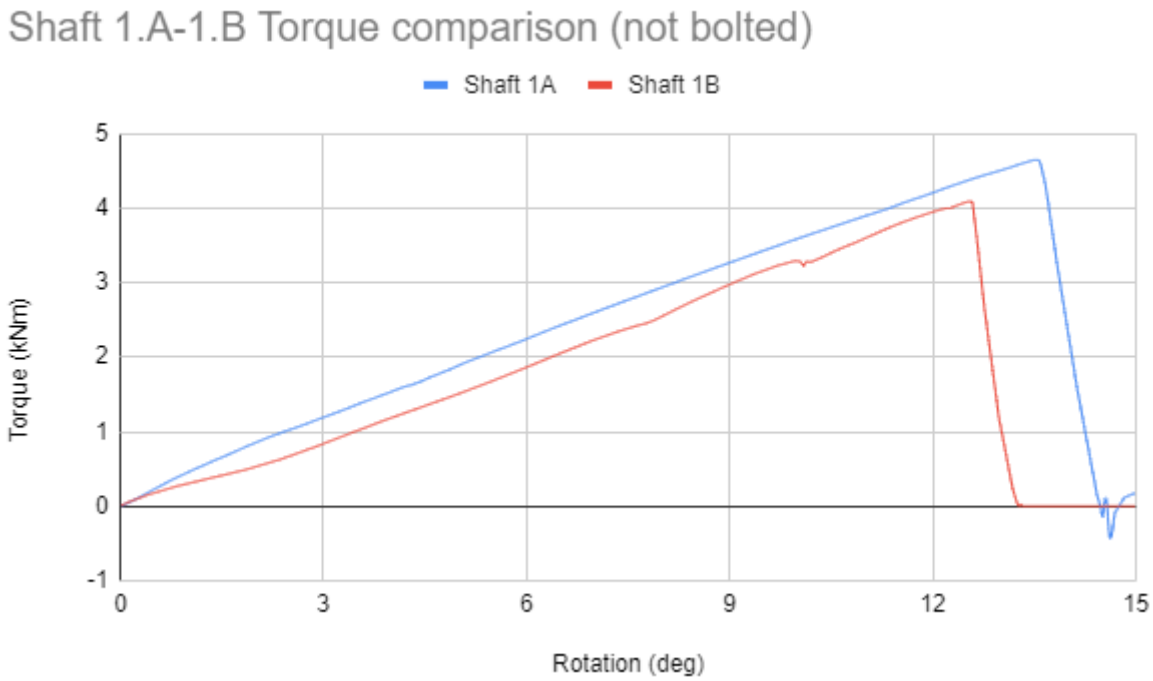

Figure 3.43: Shaft 1.A and 1.B torque comparison (not bolted)

For both shafts, the installation of the bolts contributed in reducing the torsional stiffness, as shown in table 3.5. The reason is that the active length of the shafts is increased because of the bolts. The bond of the flange is considered broken after the bolt placement, so, the distance between the closest connection points between the cylinder and the flange are the bolts. The longer active length results in less torsional stiffness. This is the main reason why the torsional stiffness is reduced more in shaft 1.A than 1.B.

Both shafts, as shown in the previous analysis, demonstrated a perfect linear behaviour. The failure of each shaft occurred in the flange area, which can be seen in the following figures for the bolting tests. In figures 3.44 and 3.45 the difference of the failure due to the chosen way of placing the bolts, between the flange and the composite, is shown. In shaft 1.B the way the bolts were installed, resulted in "weakening" locally the composite. This led to the gradual penetration of the bolt heads inside the layers of the composite. That was the main reason why the connection at shaft 1.B failed in much lower torque than for shaft 1.A which failed almost instantly by forming a rupture image between the composite layers.

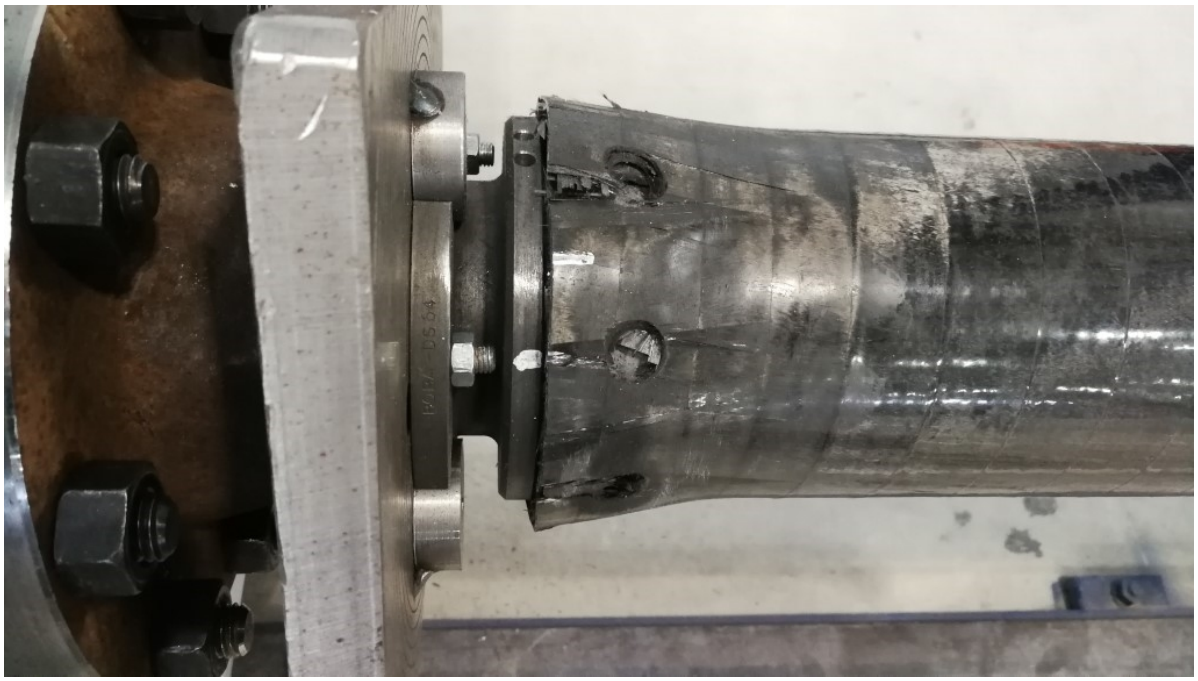

Figure 3.44: Shaft 1.A failure

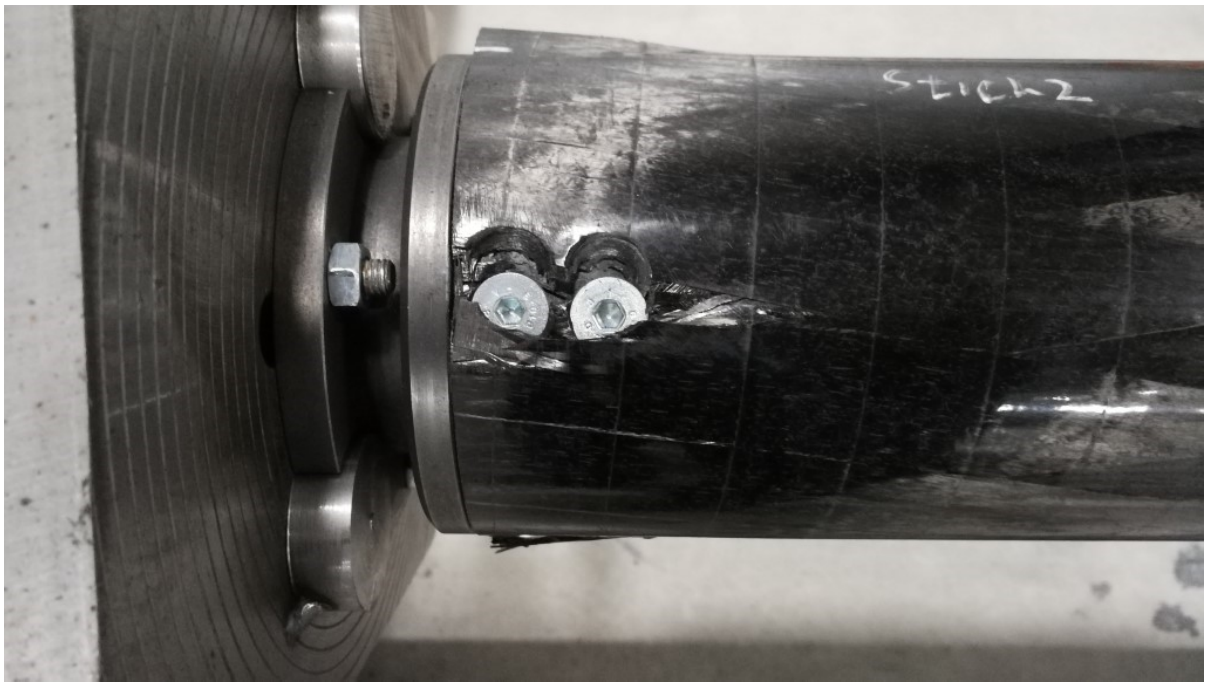

Figure 3.45: Shaft 1.B failure, bolt penetration into the composite layers

3.3.4 Shaft 2 experimental data analysis

3.3.4.1 Shaft 2 test

For shaft 2, the experiment was performed once until failure. Once more, the connection between the composite and the flange failed. As it can be seen in Figure 3.46, the flange-composite connection is tougher than the previous shafts, by using bolts and additional composite material thickness at the connection area.

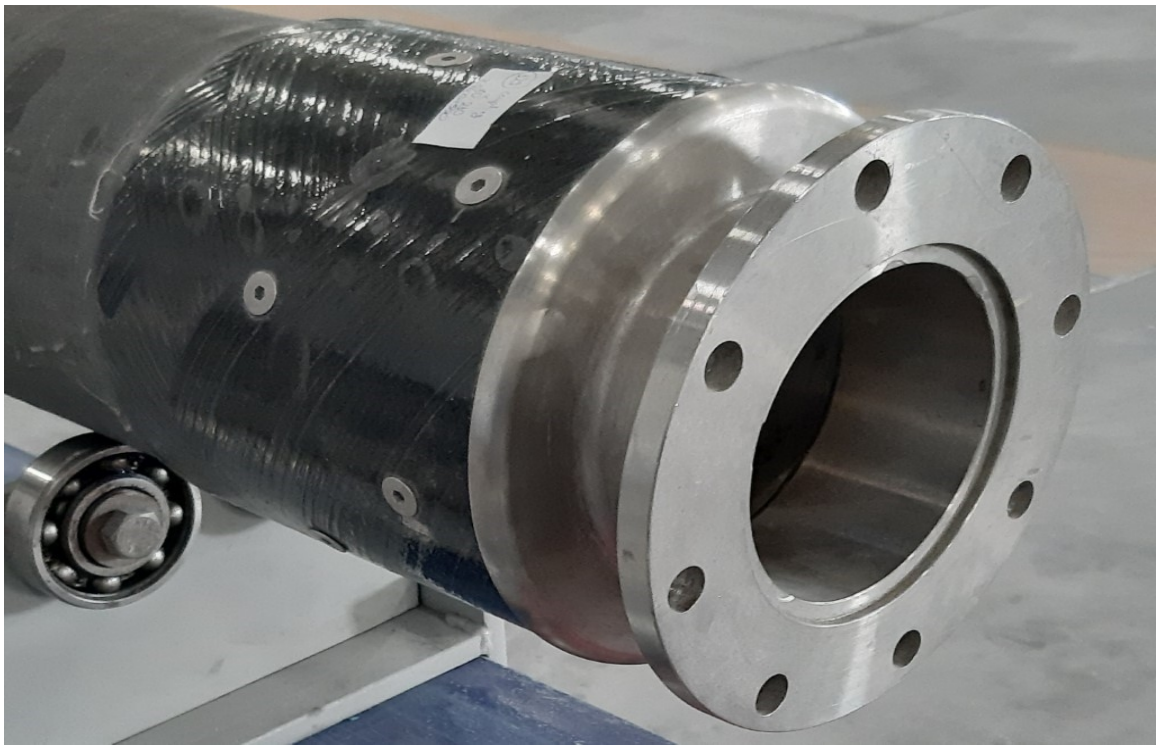

Figure 3.46: The flange connection (end fitting) with the composite shaft

As we can see in Figure 3.46, the bolts are mounted in the best possible way in the case of Shaft 2. Each bolt is put in a different longitudinal position than the previous one, so that they are as far as possible from each other, resulting in the best possible avoidance of local "weakening" of the fibers.

In Figure 3.47, the diagram of torque and rotation versus time is demonstrated. It shows that the rotation anle follows the same path as the torque during the test of shaft 2. The critical point is when the connection fails in time t_3= 92.8.4 sec. This is when the torque reaches the maximum value of T_3= 21.379 kNm while the rotation angle reaches the value of R_3=14.887 deg.

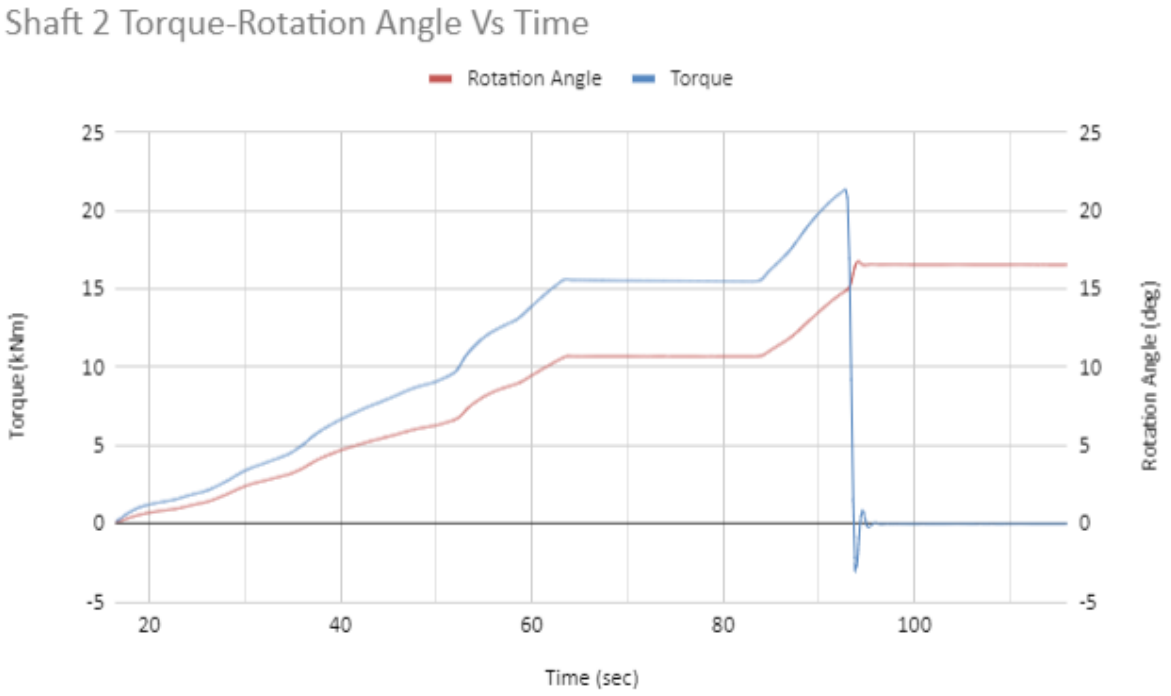

Figure 3.47: Shaft 2 comparative diagram of Torque-Time & Rotation Angle-Time

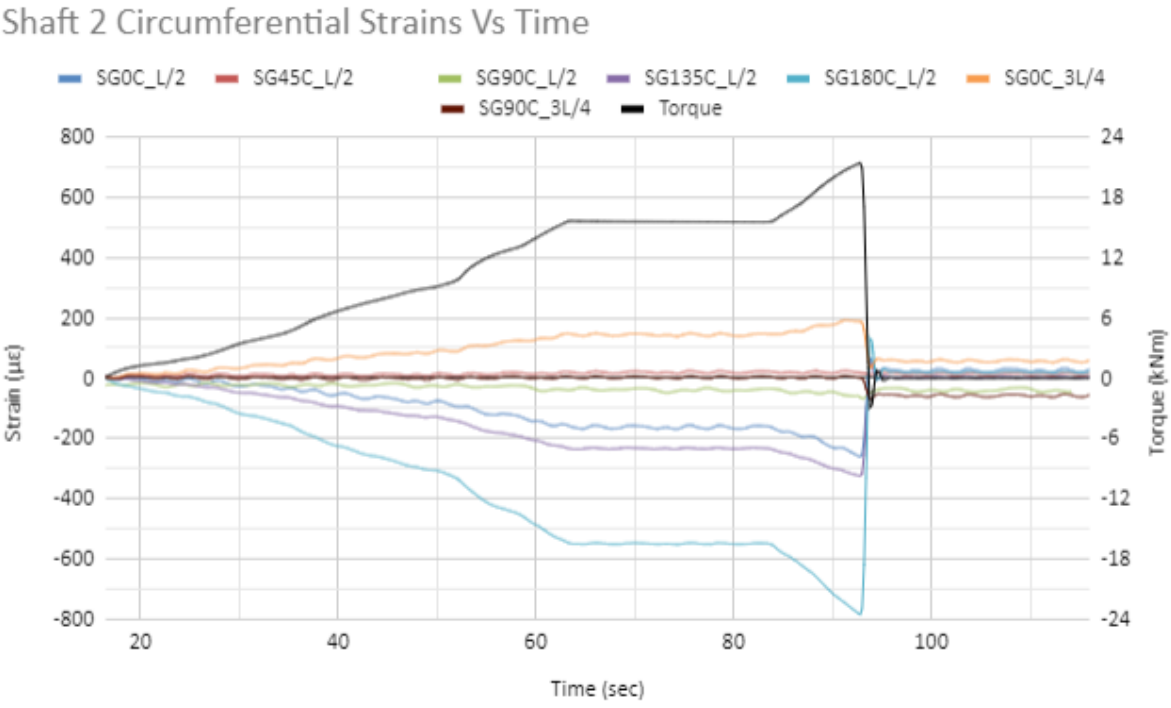

Figure 3.48: Shaft 2 diagram of Circumferential Strains-Time

The similarity between strain and torque lines can be seen in the diagram of the circumferential strains in Figure 3.48, too. Also, this can be noticed in the diagram of the longitudinal strains in Figure 3.49.

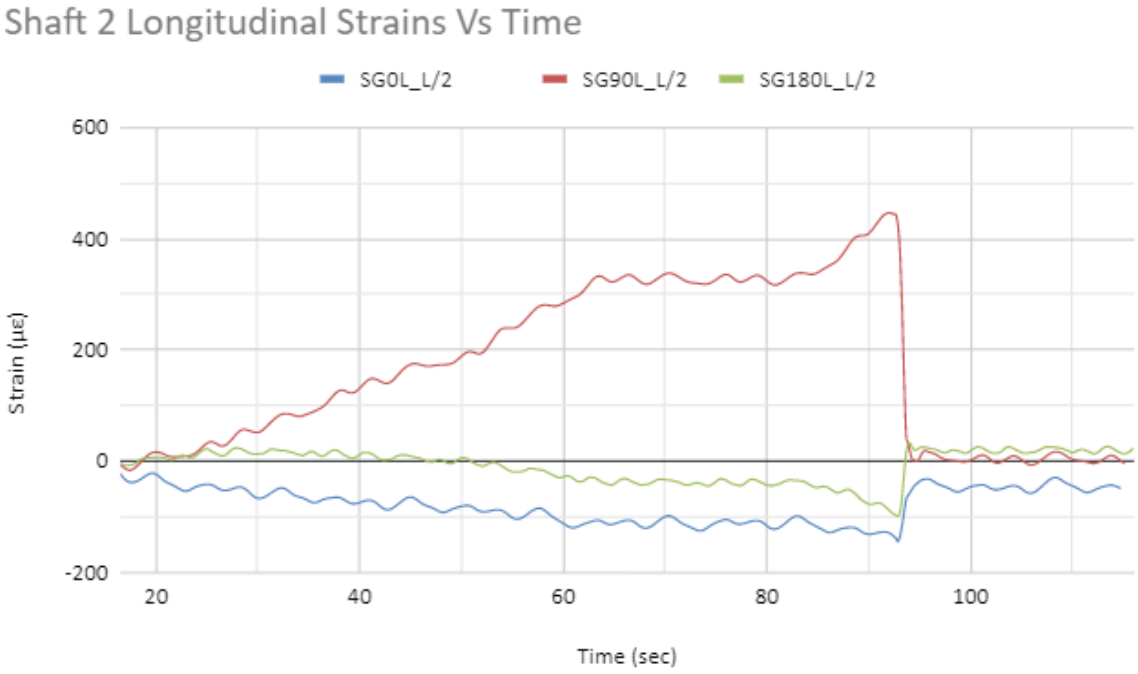

Figure 3.49: Shaft 2 diagram of Longitudinal Strains-Time

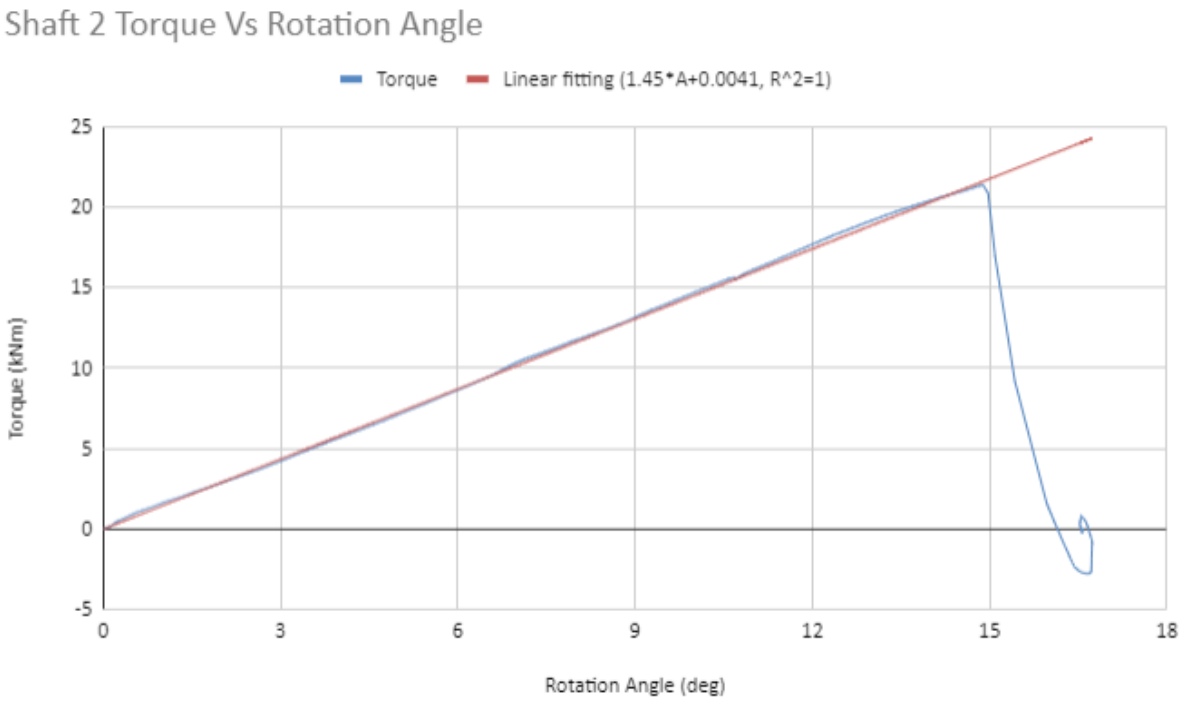

Figure 3.50: Shaft 2 diagram of Torque-Rotation Angle

In the diagram of torque versus rotation angle demonstrated in Figure 3.50, the perfect linear correlation between the torque and the angle of rotation (R^2= 1) can be noticed. The shaft 2 operates in the linear region. From the test results we can extract the average torsional stiffness of TS_2= 1.450 kNm/deg (Linear Fitting equation: T=1.45*A+0.0041).

In Figures 3.51 and 3.52 the circumferential strains diagrams are presented. The strains are tensile at the point of 0 degrees at 3L/4 position, while, low values of strains are recorded by the gage of 45 degrees in mid-section. Furthermore, low values of compressive and tensile strains are recorded by strain gage SG90C_3L/4. On the other hand, compressive strains are recorded at the points of 0, 90, 135 and 180 degrees in the mid-section of the shaft 2. The maximum value is recorded by SG0C_3L/4 and it is almost equal to 200 με, while the minimum value is recorded by SG180C_L/2, approximately equal to -800 με.

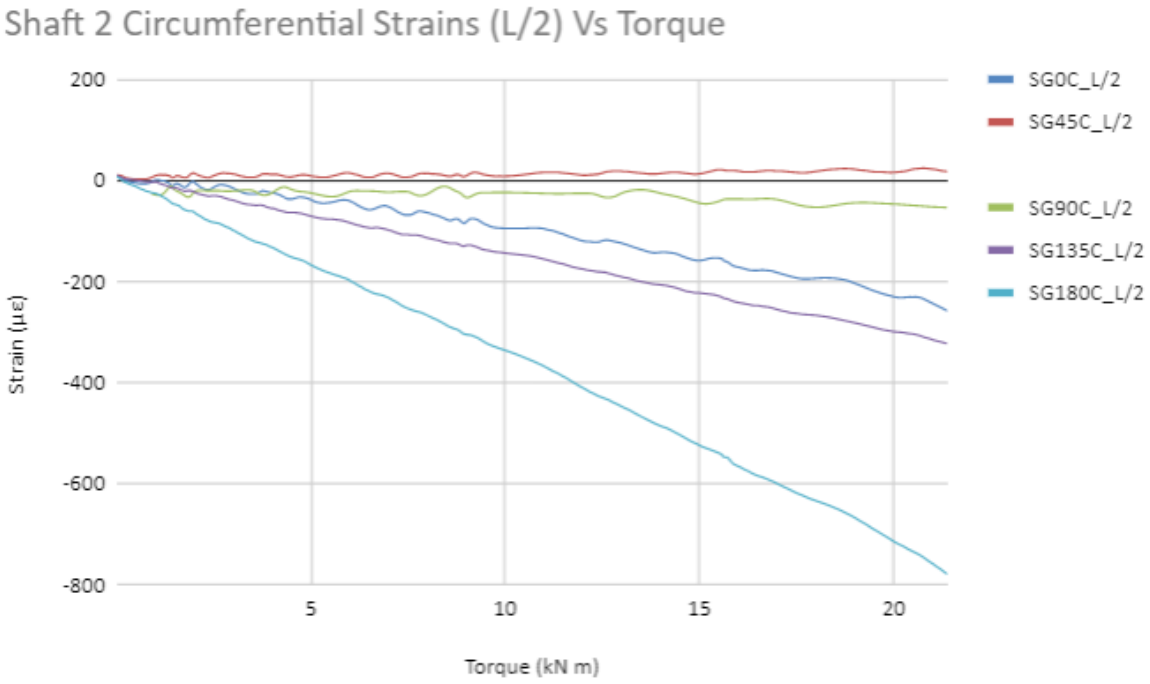

Figure 3.51: Shaft 2 diagram of Circumferential Strains-Torque

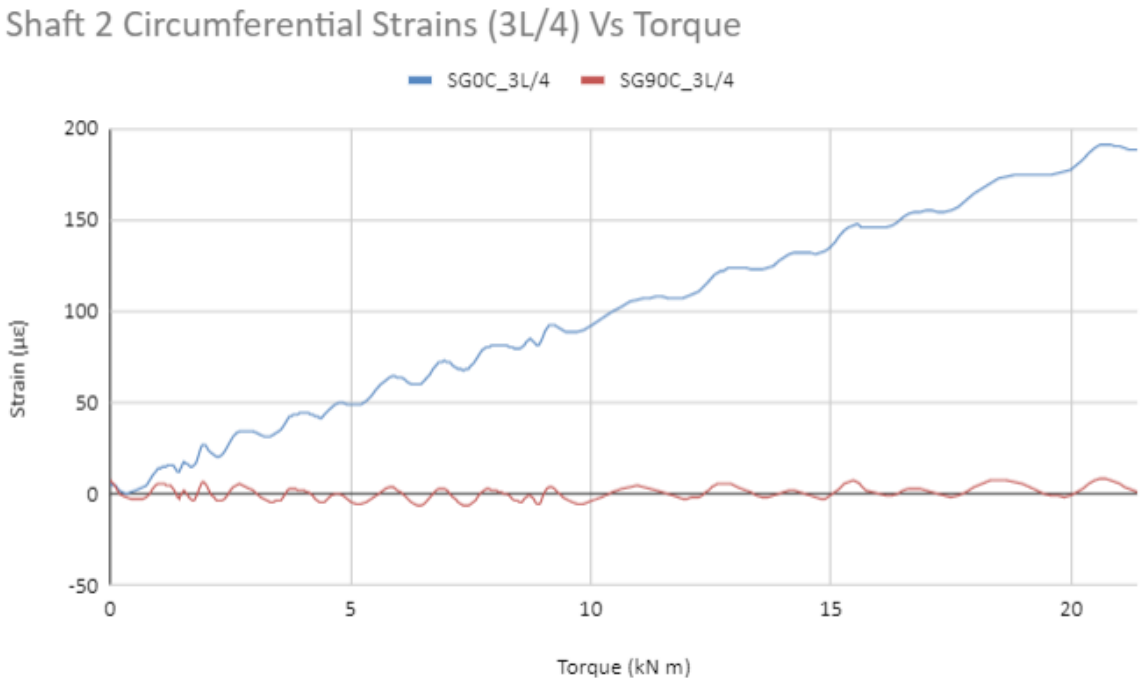

Figure 3.52: Shaft 2 diagram of Circumferential Strains-Torque

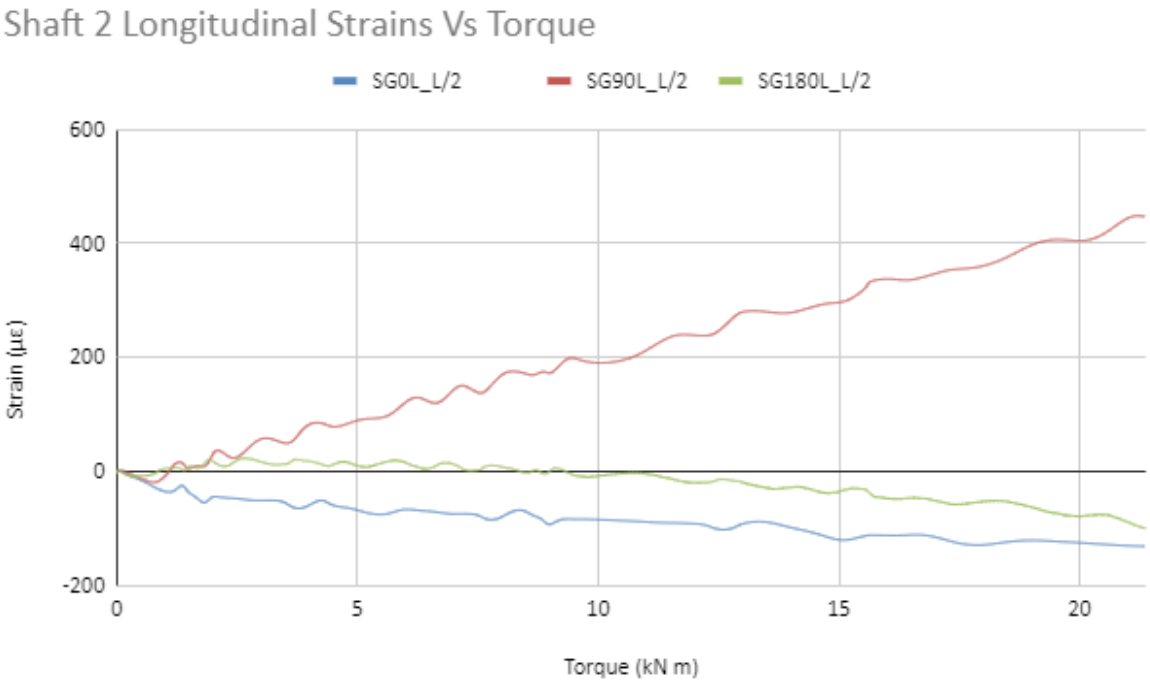

Figure 3.53: Shaft 2 diagram of Longitudinal Strains-Torque

The longitudinal strains diagram demonstrated in Figure 3.53, shows that the strains at the point of 90 degrees of the L/2 position are tensile while at the point of 0 degrees of the position L/2 are compressive. At 180 degrees point we notice that the strains are tensile at first but they become compressive at the end of the experiment. The maximum strain is

recorded by SG90L_L/2 exceeding 400 με, while the minimum strain is recorded by SG0L_L/2, exceeding 100 με.

3.3.4.2 Shaft 2 modeshape estimation and fail mechanism

It is already clear, from the previous analysis, that the shaft exhibits a linear behaviour in torsion. Some indications can be made by studying the circumferential strain diagrams, shown previously. The first indication given by the recorded strains is that the shaft is probably going to buckle in type-2 buckling modeshape.. In figure 3.51, we can notice that the strains recorded at 45 and 90 degrees are low. Furthermore, these lines are almost linear without any curvature which could help us indicate the position they were glued on the shaft 2 modeshape. A good indication is given by the gages at 0, 135 and 180 degrees. These strain lines are compressive with a compressive tendency. This indicates that they all were glued close to a trough region. In Figure 3.54, there is a schematic view of the suggested position of the gages on the buckling modeshape of shaft 2. In table 3.6 the maximum strains are presented, as recorded in experiments of the shaft 2.

Table 3.6: Maximum strain values for both experiments of shaft 1.B

Strain (με)	SG0C_L/2	SG45C_L/2	SG90C_L/2	SG135C_L/2	SG180C_L/2
	260.308	24.000	-75.692	-324.000	-783.692
	SG0L_L/2		SG90L_L/2		SG180L_L/2
	-151.385		453.231		-98.769
	SG0C_3L/4			SG90C_3L/4	
	191.077			8.308	

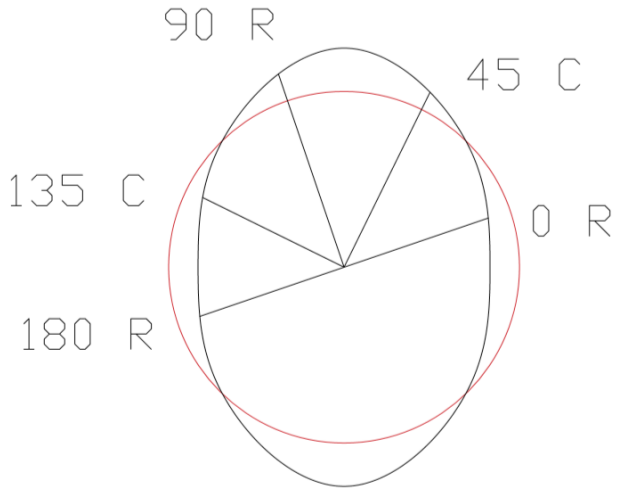

Figure 3.54: Shaft 2 modeshape 2

As shown in figure 3.55 there is no visible evidence of the failure of the bonded and bolted joint between the composite cylinder and the metallic flange, a fact indicating that, any such failure took place internally, between the cylinder and flange. The failure is perceptible due to the fact that the white marker line, which was initially drawn from the metal of the flange and crossed the composite material of the shaft continuously, has shifted to the side of the shaft. The failure occurred due to the interior breaking of the bolts that supported the connection.

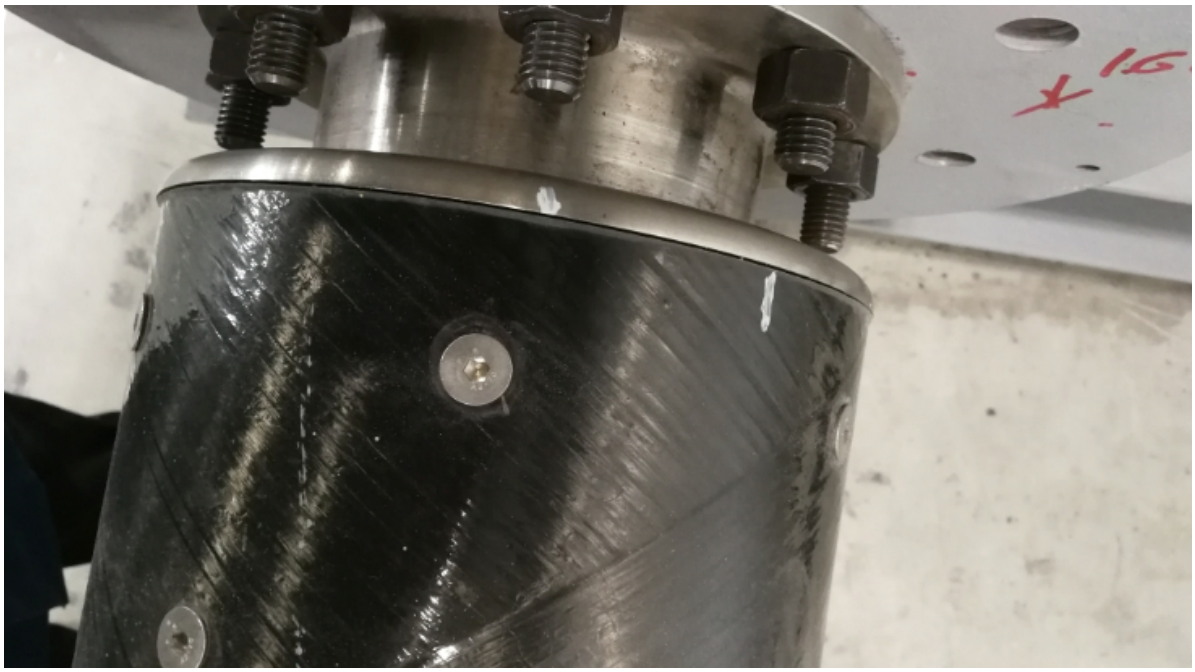

Figure 3.55: Shaft 2 connection fail

3.4 Conclusions

The previous experimental study has led to many valuable conclusions. First and foremost, the strains showed that the failure, which occurred in the end fitting area of the shafts, took place while the shafts operated in the linear region. This shows that the torque capacity of the composite part of the shaft, was beyond the torque reached in the experiments. The connection between metal flange and composite is an area of critical importance for a composite driveshaft configuration.

The way the bolts were installed, changed the shafts mechanical properties. The failure of the adhesive joint and the installation of the bolts resulted in increasing the active length of the shafts 1.A and 1.B which contributed in reducing the overall torsional stiffness in each shaft. In shaft 1.A, there has been a 24.7% torsional stiffness reduction due to the installation of the bolts, while, for shaft 1.B, the torsional stiffness reduction was almost 6.7% with 4% and 2.9% active length increase respectively. Furthermore, the bolts didn't contribute in reaching a much higher torsional load in the case of shaft 1.A. In the case of shaft 1.B the bolt fitting was destructive for the material and its mechanical properties so it reached an even lower maximum load. A significant parameter is the bolting distance. Placing the bolts too close will result in "hurting" the composite locally.

Any assumption on the modeshape cannot rely only on the values of the strain. At the graphs is imprinted the tendency of each strain. The curvature of each line is a good indication that states whether the shaft is going to form a crest or a trough on the point that the strain is recorded. The suggestion made by the present thesis is that all the shafts, form type-2 buckling modeshape but this remains an uncertain suggestion which relies only on the indications described previously.

3.5 Suggestions for improvement of the test fixture

In this section, some suggestions are made in order to improve the torsion test machine for future experiments.

The first problem encountered, was the non-controlled torque application rate. The motor that moved the hydraulic pistons, was manually controlled by pushing a lever. This was the main reason why, the torsion application rate wasn't constant. Furthermore, in this way, the experiment deviated from a static load type testing, which demands certain low rate values of the applied loading. The rate must be controlled. The manual application of torque does not permit a steady rate, except if the lever is pushed in full throttle, but in that way, the torsion pace becomes too fast.

An improvement can be made without changing the lever configuration. A pressure valve can be installed after the lever by which the oil flow, that moves the pistons, can be controlled. In this way, the push of the lever, in full throttle, will impose the torque with a satisfying and low rate. In figure 3.56, a pressure valve is shown (model V152). This valve is used in order to regulate the oil flow or the system's pressure. It limits the pressure developed by the pump in the hydraulic circuit, thus limiting the force imposed on other components (the pistons in this application). The valve opens whenever the preset pressure is reached. To increase pressure setting, the handle is manually turned clockwise.

Figure 3.56: V152 Pressure Relief Valve

Also, a better and more precise way to measure the torque is suggested. Instead of using the load cell and calculate the torque as described in section 3.1, a flange type static torque

transducer can be used. In figure 3.57 an example of the aforementioned device is demonstrated.

Figure 3.57: Flange type static torque transducer, Model DTD-F

The DTD-F series of static / reaction torque transducers have end flanges for bolting between machinery where a direct drive is required. Including applications are the testing of automotive drives, aircraft actuator and industrial robots, with offshore and marine submersible device versions available.

The product is designed with the following characteristics:

- Capacities: 0-10Nm to 0-50kNm
- 2mV/V Output (1.5mV/V on 20kNm+)
- Environmental Protection: IP65
- Accuracy: <±0.25%/Rated Capacity
- Custom Capacities to 200kNm+

The design of the DTD-F lends itself readily to customisation, allowing the manufacturer to offer custom flange sizes and fixing configurations, as well as versions for applications where operating conditions are particularly harsh or involve total submersion.

Another problem was that the movable end of the fixture, lifted from one of the rails (while leaning on the other) after exceeding 10 kNm of torsional torque. Figure 3.58 shows the free end's position on the rails, while Figure 3.59 shows the lift the bed gets during the experimental process.

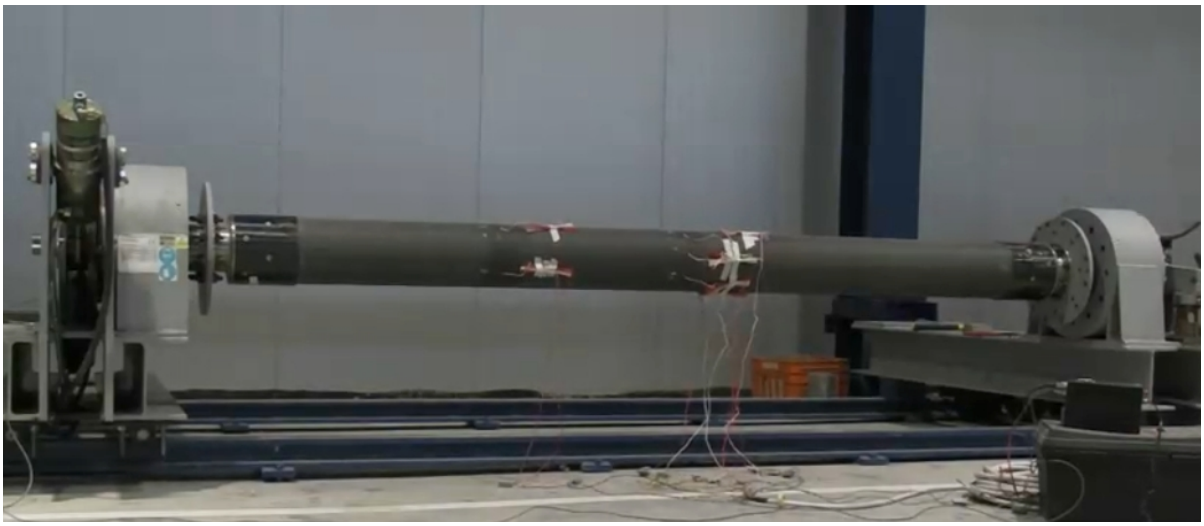

Figure 3.58: The free end of the test fixture (on the left) in its normal horizontal position

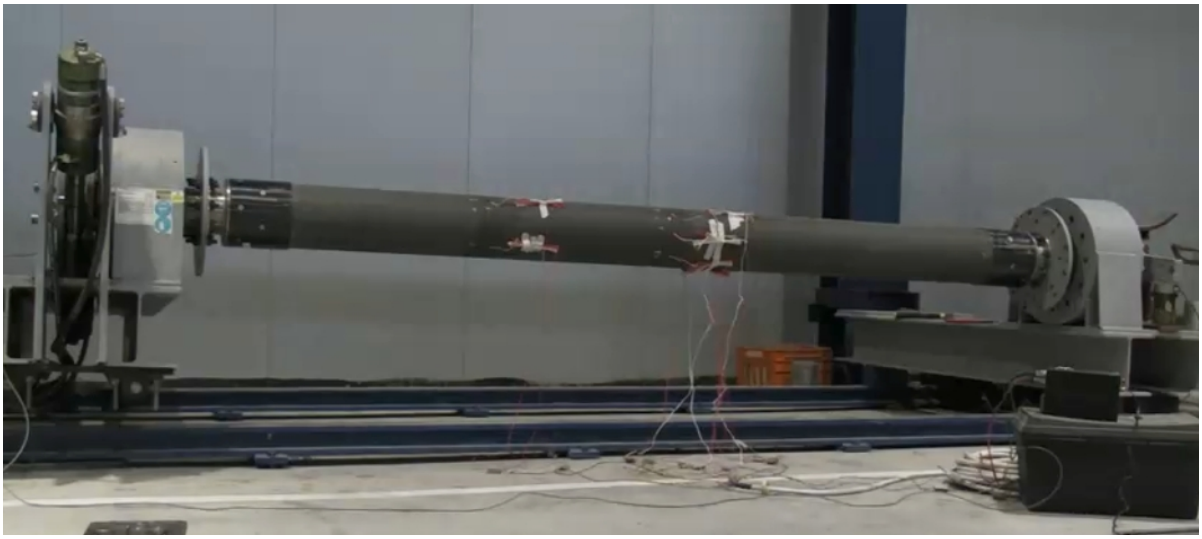

Figure 3.59: The free end lifted after the application of a certain amount of load

In order to fix the free end on the rail and reach higher torque values the patent configuration shown in figure 3.60 was established. A small plate is put under the rail. Over the rail a cylinder is placed and over the cylinder a metal component is placed, which leans on both the cylinder and the movable end (the metal component is pointed in Figure 3.60). A second small plate is put over the metal component and two screws are bolted through the two small plates as shown in the figure. In this way the metal component is bonded at the horizontal position, shown in Figure 3.60, preventing, in that way, the movable end from lifting. The patent worked perfectly, so, it is suggested for future experiments.

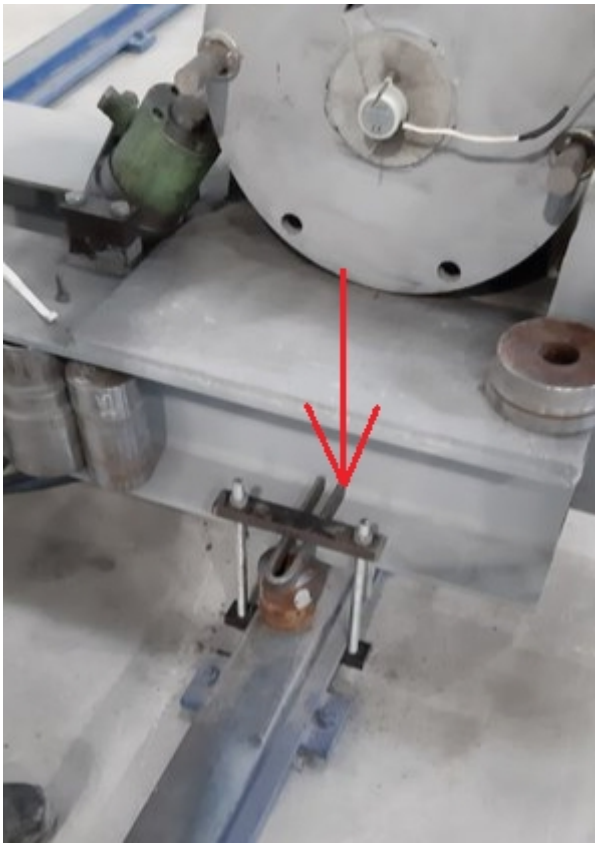

Figure 3.60: Fixing the free end in horizontal plane

Due to the fact that the clinometer used in the experiments wasn't very accurate and reliable, another way to measure the rotation is suggested. The rotation can be calculated by measuring the stroke of the hydraulic piston. In Figure 3.61 the free end is demonstrated and in Figure 3.62 a sketch of the free end is drawn. Figure 3.63 demonstrates a geometrical solution of the rotation angle formula with respect to the piston stroke.

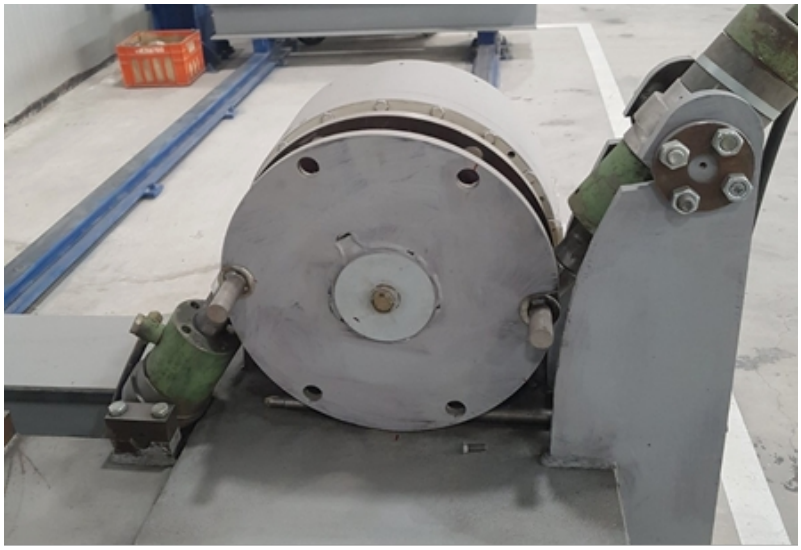

Figure 3.61: The free end

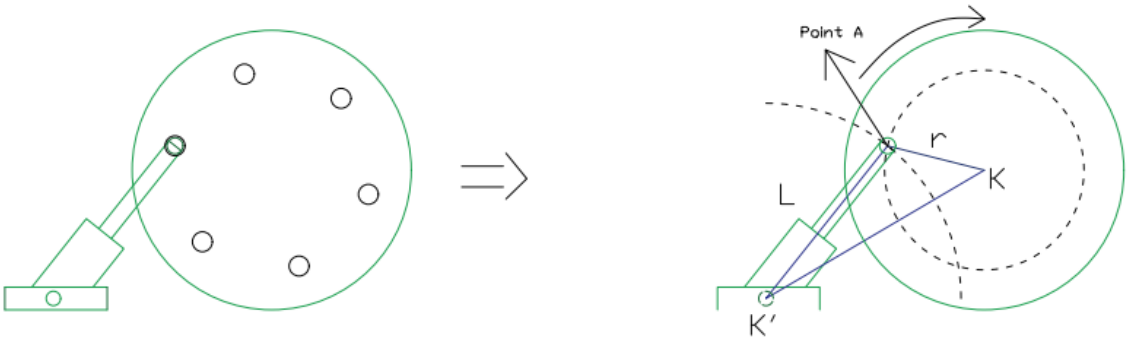

Figure 3.62: Free end sketch

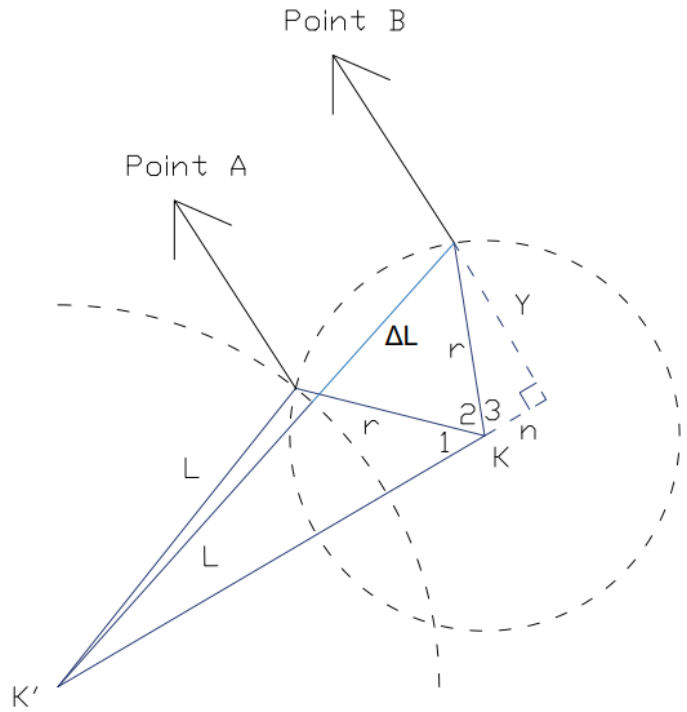

Figure 3.63: Geometry of the free end

In figures 3.61 to 3.63 the point K' is where the piston's joint is fixed. The piston can rotate around that point. The point K is the centre of rotation. The point A is the starting point of the piston. In that position the piston is not extended (piston's length= L, it can be measured easily). At point B is the position the extended piston when it imposes a random value of force, in order to rotate the free end (piston's stroke= ΔL). The parameter "r" is the radius of the threaded hole, in which the piston is fixed in order to impose the force, from the centre of rotation. The parameter "Y" refers to the distance of the point B from the straight line (K'K). The angle K_2 must be calculated with respect to the extension of the piston. The geometrical solution is given next:

$$(L+\Delta L)^2 = Y^2 + ((KK')+n)^2 \Rightarrow$$
$$\Rightarrow Y^2 = (L+\Delta L)^2 - ((KK')+n)^2 \qquad (3.1)$$
$$r^2 = Y^2 + n^2 \Rightarrow$$

$$Y^2 = r^2 - n^2 \quad (3.2)$$

$$(1),(2) \Rightarrow (L+\Delta L)^2 - ((KK')+n)^2 = r^2 - n^2 \quad (3.3)$$

$$\cos\left(\widehat{K_3}\right) = \frac{n}{r} \Rightarrow$$

$$n = \cos\left(\widehat{K_3}\right) * r = -r * \cos\left(\widehat{K_1} + \widehat{K_2}\right) \quad (3.4)$$

$$(3.3),(3.4) \Rightarrow \widehat{K_2} = \left(\cos^{-1}\frac{(K'K)^2 + (r)^2 - (L+\Delta L)^2}{2((K'K)r)}\right) - \widehat{K_1}$$

All the above parameters can be measured. For measuring ΔL an LVDT displacement transducer can be used. The suggested design is the one demonstrated in Figure 3.64.

Figure 3.64: LVDT transducer

On the piston two small braces can be attached. In figure 3.65, a simple schematic view of the piston is shown with the braces on it. It is a suggestion on how the LVDT can be placed on the piston. To the braces the two ends of the transducer will be placed. In this way it will be able to measure the elongation of the piston and, therefore, the angle of rotation.

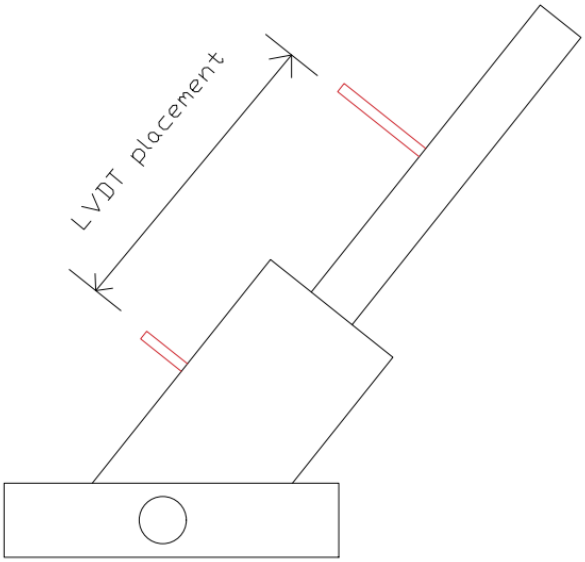

Figure 3.65: Schematic view of the piston with the braces

Last but not least, the block where the hydraulic pump is placed must be disconnected from the beam of the free end. The operation of the pump transmitted vibrations to the free end and to the shaft which were recorded by the strain gages. That was the reason why, there was noise in strain diagrams demonstrated in section 3.3.

CHAPTER 4

CONCLUSIONS AND RECOMMENDATIONS FOR FUTURE WORK

4.1 Conclusions

A summary of the present thesis conclusions is made in this section.

- There is a range of shaft dimensions that can be tested at the torsion test machine located at the Strength of Materials Laboratory, that can comply with the rules and standards of the Class Program of the DNV-GL register.
- All the tested shafts failed at the end fitting area. They all operated in the elastic region. The placement of the bolts did not contribute in reaching higher torque levels. The tests showed that in both shafts 1.A and 1.B, the torsional stiffness reduced dramatically after the placement of the bolts due to the fact that the active length increased in each occasion.
- The indications given by the recorded strains is that a type-2 buckling modeshape is the most probable to occur to all the shafts tested. Of course, the results should be confirmed by conducting a destructive experiment of the composite part of the driveshaft.
- The torsion test device in B&T Composites facility can receive some improvements. These are the pressure relief valve, the static torque transducer, the LVDT transducer and the patent shown in Figure 3.60 The cost-effective suggestions given in the present thesis will lead to an easier conduction of more accurate experiments in the future.

4.2 Recommendations for future work

On this chapter, suggestions for further future research are made.

- From the experimental analysis, a big interest is presented on the torsional buckling phenomenon. On the experiments, all the shafts demonstrated a perfect linear behaviour until the maximum torque. An experimental study on which the shafts will demonstrate, also, a nonlinear buckling behaviour is recommended. This will lead to higher levels of deformation magnitudes, leading, therefore, to a better understanding of the way the torsional buckling evolves on a composite shaft.
- In the present thesis the importance of the end fitting is outlined. The connection between composite and metal flange seems to be a very interesting objective of a future thesis. A FEM analysis model could be developed in order to study the way the bolted connection, between flange and composite, affects the mechanical properties of the driveshaft.
- An experimental and numerical study of the composite to metal adhesive joint at the end fitting area of a driveshaft is strongly recommended.

- A bibliographic study is suggested, to the ISO and DIN standards of various flange models that could be used as end fittings in composite shafting systems aiming at developing a finite element analysis model of these flange models.
- The Shipbuilding Technology Laboratory has the need of a torsion test device. The design of a torsion test machine or the improvement of the present experimental set up with the aim to conduct torque-controlled and displacement-controlled torsion tests in various shafts is suggested.

Literature

Badie, M., Mahdi, E., & Hamouda, A. (2011). An investigation into hybrid carbon/glass fiber reinforced epoxy composite automotive drive shaft. *Materials & Design*, 32(3), 1485-1500. https://doi.org/10.1016/j.matdes.2010.08.042

Barbero, E. J. (2010). *Introduction to Composite Materials Design, Second Edition.* http://doi.org/10.1017/CBO9781107415324.004

Bilalis E. (2016). Experimental and Numerical Study of Composite Shafts

Ghatage K.D., Hargude N.V., (2012). OPTIMUM DESIGN OF AUTOMOTIVE COMPOSITE DRIVE SHAFTWITH GENETIC ALGORITHM AS OPTIMIZATION TOOL. *International Journal of Mechanical Engineering and Technology (IJMET),* 3(3), (pp. 438-449)

Hao, W., Huang, Z., Zhang, L., Zhao, G., & Luo, Y. (2019). Study on the torsion behavior of 3-D braided composite shafts. *Composite Structures*, 229(1), ["111384"]. http://doi.org/10.1016/j.compstruct.2019.111384

Hao, W., Huang, Z., Xu, Y., Zhao, G., Chen, H., & Fang, D. (2020). Acoustic emission characterization of tensile damage in 3D braiding composite shafts. *Polymer Testing*, 81(13, Part 3), ["106176"]. https://doi.org/10.1016/j.polymertesting.2019.106176

Hao, W., Yuan, Z., Tang, C., Zhang, L., Zhao, G., & Luo, Y. (2019). Acoustic emission monitoring of damage progression in 3D braiding composite shafts during torsional tests. *Composite Structures*, 208(1), 141-149.

Jaure, (2017). Carbon Fibre Shaftlines JCFS. Retrieved from https://www.regalbeloit.com/-/media/Files/Literature/Industries/Marine/Marine-Literature-Jaure-Form-9517E-June-4-2017.pdf

Kaviprakash, G., Lawrence, D.I., Kannan, R.C., Regan, P.A., (2014). Design and Analysis of Composite Drive Shaft for Automotive Application. *International Journal of Engineering Research & Technology (IJERT),* 3(11), 429-436

Lee, D. G., Kim, H. S., Kim, J. W., & Kim, J. K. (2004). Design and manufacture of an automotive hybrid aluminum/composite drive shaft. Composite Structures, 63(1), 87-99. https://doi.org/10.1016/S0263-8223(03)00136-3

Leslie, J. C., Truong, L., Ii, J. C. L., Blank, B., & Frick, G. (1996). Composite Driveshafts : Technology and Experience. http://doi.org/10.4271/962209

Nadeem, S. S., Giridhara, G., & Rangavittal, H. (2018). A Review on the design and analysis of composite drive shaft. *Materials Today: Proceedings*, 5(1, Part 3), 2738-2741.

Prasad, A. S., Ramakrishna, S., & Madhavi, M. (2018). Experimental Investigations on Static and Dynamic Parameters of Steel and Composite Propeller Shafts with an Integrated Metallic Joints. *Materials Today: Proceedings*, 5(13, Part 3), 26925-26933.

Rompicharla, R. P. K., & Rambabu, K. (2012). Design and Optimization of Drive Shaft with Composite Materials. *International Journal of Modern Engineering Research*, 2(5), 3422–3428.

Tong, L., Mouritz, A. P., & Bannister, M. K. (2002). Chapter 2 - Manufacture of 3D Fibre Preforms. In L. Tong, A. P. Mouritz, & M. K. Bannister (Eds.), *3D Fibre Reinforced Polymer Composites* (pp. 13-46). Oxford: Elsevier Science.

Tsouvalis, N. (1998). *Analysis and Design of Composite Material Crafts.*

Zhao, G., Zhang, L., Tang, C., Zhou, Y., Hao, W., & Luo, Y. (2018). Experimental study on the torsion behavior of a 3D 4-directionally braided composite shaft using DIC and AE. *Polymer Testing*, 72(1), 122-131. https://doi.org/10.1016/j.polymertesting.2018.10.016